Report No. 6276
Copy No.

SEISMIC HOLOGRAPHY FOR UNDERGROUND VIEWING

(11)

FINAL REPORT

July 1972

Contract No: H0210032
Amount of Contract: $48,839
Effective: April 30, 1971
Terminates: May 31, 1972

Principal Investigator:

R. F. Steinberg (313) 352-7985
Bendix Research Laboratories
Southfield, Michigan 48076

Project Engineer:

Gerald L. Fitzpatrick

Sponsored by:

Advanced Research Projects Agency
ARPA Order No. 1579, Amend. 2
Program Code 1F10

DISCLAIMER NOTICE

THIS DOCUMENT IS THE BEST QUALITY AVAILABLE.

COPY FURNISHED CONTAINED A SIGNIFICANT NUMBER OF PAGES WHICH DO NOT REPRODUCE LEGIBLY.

UNCLASSIFIED

Security Classification

DOCUMENT CONTROL DATA - R&D

(Security classification of title, body of abstract and indexing annotation must be entered when the overall report is classified)

1. ORIGINATING ACTIVITY (Corporate author) Bendix Research Laboratories Bendix Center Southfield, Michigan 48076	2a. REPORT SECURITY CLASSIFICATION Unclassified 2b GROUP

3. REPORT TITLE

Seismic Holography for Underground Viewing

4. DESCRIPTIVE NOTES (Type of report and inclusive dates)

Final Technical Report, April 30, 1971 - May 31, 1972

5. AUTHOR(S) (Last name, first name, initial)

Steinberg, Ronald F.
Thuren, John B.

6. REPORT DATE June 1972	7a. TOTAL NO. OF PAGES 83	7b. NO. OF REFS 28
8a. CONTRACT OR GRANT NO. H0210032 b. PROJECT NO. ARPA Order 1579 Amend. 2 c. Program 1F10 d.	9a. ORIGINATOR'S REPORT NUMBER(S) 6276 9b. OTHER REPORT NO(S) (Any other numbers that may be assigned this report)	

10. AVAILABILITY/LIMITATION NOTICES

11. SUPPLEMENTARY NOTES BRL Project 2411	12. SPONSORING MILITARY ACTIVITY Advanced Research Projects Agency

13. ABSTRACT

The objective of this research program was to define a preliminary underground viewing system, based on acoustic holography principles, which is capable of detecting and imaging underground anomalies associated with a selected field test site. System requirements based on the geology of the selected site were specified and a proposed field test was designed. In addition, studies to develop a holographic weak signal enhancement technique were made.

DD FORM 1 JAN 64 1473

UNCLASSIFIED

14. KEY WORDS	LINK A		LINK B		LINK C	
	ROLE	WT	ROLE	WT	ROLE	WT
Seismic Holography Underground Viewing Weak Signal Enhancement						

INSTRUCTIONS

1. **ORIGINATING ACTIVITY:** Enter the name and address of the contractor, subcontractor, grantee, Department of Defense activity or other organization *(corporate author)* issuing the report.

2a. **REPORT SECURITY CLASSIFICATION:** Enter the overall security classification of the report. Indicate whether "Restricted Data" is included. Marking is to be in accordance with appropriate security regulations.

2b. **GROUP:** Automatic downgrading is specified in DoD Directive 5200.10 and Armed Forces Industrial Manual. Enter the group number. Also, when applicable, show that optional markings have been used for Group 3 and Group 4 as authorized.

3. **REPORT TITLE:** Enter the complete report title in all capital letters. Titles in all cases should be unclassified. If a meaningful title cannot be selected without classification, show title classification in all capitals in parenthesis immediately following the title.

4. **DESCRIPTIVE NOTES:** If appropriate, enter the type of report, e.g., interim, progress, summary, annual, or final. Give the inclusive dates when a specific reporting period is covered.

5. **AUTHOR(S):** Enter the name(s) of author(s) as shown on or in the report. Enter last name, first name, middle initial. If military, show rank and branch of service. The name of the principal author is an absolute minimum requirement.

6. **REPORT DATE:** Enter the date of the report as day, month, year, or month, year. If more than one date appears on the report, use date of publication.

7a. **TOTAL NUMBER OF PAGES:** The total page count should follow normal pagination procedures, i.e., enter the number of pages containing information.

7b. **NUMBER OF REFERENCES:** Enter the total number of references cited in the report.

8a. **CONTRACT OR GRANT NUMBER:** If appropriate, enter the applicable number of the contract or grant under which the report was written.

8b, 8c, & 8d. **PROJECT NUMBER:** Enter the appropriate military department identification, such as project number, subproject number, system numbers, task number, etc.

9a. **ORIGINATOR'S REPORT NUMBER(S):** Enter the official report number by which the document will be identified and controlled by the originating activity. This number must be unique to this report.

9b. **OTHER REPORT NUMBER(S):** If the report has been assigned any other report numbers *(either by the originator or by the sponsor)*, also enter this number(s).

10. **AVAILABILITY/LIMITATION NOTICES:** Enter any limitations on further dissemination of the report, other than those imposed by security classification, using standard statements such as:

(1) "Qualified requesters may obtain copies of this report from DDC."

(2) "Foreign announcement and dissemination of this report by DDC is not authorized."

(3) "U. S. Government agencies may obtain copies of this report directly from DDC. Other qualified DDC users shall request through _____."

(4) "U. S. military agencies may obtain copies of this report directly from DDC. Other qualified users shall request through _____."

(5) "All distribution of this report is controlled. Qualified DDC users shall request through _____."

If the report has been furnished to the Office of Technical Services, Department of Commerce, for sale to the public, indicate this fact and enter the price, if known.

11. **SUPPLEMENTARY NOTES:** Use for additional explanatory notes.

12. **SPONSORING MILITARY ACTIVITY:** Enter the name of the departmental project office or laboratory sponsoring *(paying for)* the research and development. Include address.

13. **ABSTRACT:** Enter an abstract giving a brief and factual summary of the document indicative of the report, even though it may also appear elsewhere in the body of the technical report. If additional space is required, a continuation sheet shall be attached.

It is highly desirable that the abstract of classified reports be unclassified. Each paragraph of the abstract shall end with an indication of the military security classification of the information in the paragraph, represented as *(TS)*, *(S)*, *(C)*, or *(U)*.

There is no limitation on the length of the abstract. However, the suggested length is from 150 to 225 words.

14. **KEY WORDS:** Key words are technically meaningful terms or short phrases that characterize a report and may be used as index entries for cataloging the report. Key words must be selected so that no security classification is required. Identifiers, such as equipment model designation, trade name, military project code name, geographic location, may be used as key words but will be followed by an indication of technical context. The assignment of links, rules, and weights is optional.

Report No. 6276

SEISMIC HOLOGRAPHY FOR UNDERGROUND VIEWING

ic

TABLE OF CONTENTS

		Page
SECTION 1 - TECHNICAL REPORT SUMMARY		1-1
1.1	General	1-1
1.2	Selection of Field Test Site	1-2
1.3	Analysis of Field Test Site to Determine System Requirements	1-2
1.4	Preliminary Design of Underground Viewing System - Seismic Holography Experiment	1-3
1.5	Evaluation of Seismic Energy Sources and Detectors	1-5
	1.5.1 Seismic Energy Sources	1-5
	1.5.2 Seismic Detectors - Geophones	1-6
1.6	Holographic Weak Signal Enhancement Studies	1-6
SECTION 2 - SELECTION OF FIELD TEST SITE		2-1
2.1	Criteria Used for Site Selection	2-1
2.2	Potential Sites Evaluated	2-1
	2.2.1 Climax Stock, U.S.A.E.C. Nevada Test Range, Nye County, Nevada	2-2
	2.2.2 Batholith of Southern California	2-3
	2.2.3 Pikes Peak Area, Colorado	2-4
	2.2.4 Guadalupe Mountains Area, New Mexico and Texas	2-5
	2.2.5 Victorio Peak Area, Texas	2-6
	2.2.6 Big Bend Area, Texas and Mexico	2-6
	2.2.7 Winnfield Salt Dome, Winn Parish, Louisiana	2-7
SECTION 3 - ANALYSIS OF VIEWING SYSTEM REQUIREMENTS BASED ON GEOLOGY OF FIELD TEST SITE		3-1
3.1	Topographic and Geologic Features of the Climax Stock, Area 15, Nevada Test Site, Nevada	3-1
3.2	Compilation of Geophysical Information Climax Stock, Area 15	3-4
3.3	Evaluation of Shear Wave Velocities and Poisson's Ratio for all Zones at Nevada Test Site	3-8
3.4	Attenuation	3-9
3.5	Reflection and Transmission Coefficients for Layering at the Nevada Test Site	3-14
3.6	Model of Tunnel Response	3-15
3.7	Surface Rayleigh Waves	3-21
3.8	Tunnel Destressed Zone and Other Factors Affecting Signal Transmission	3-22
SECTION 4 - DESIGN OF UNDERGROUND VIEWING SYSTEM - SEISMIC HOLOGRAPHY EXPERIMENT		4-1

		Page
4.1	Calculated Amplitudes of Received Signals Based Upon the Composite Model of the Nevada Test Site	4-1
4.2	Holographic Aperture Design	4-10
4.3	Holographic Data Acquisition	4-13
4.3.1	Monofrequency CW	4-13
4.3.2	Pulsed Monofrequency CW	4-14
4.3.3	Impulsive (Explosive) Sources	4-15
4.3.4	Frequency Modulated (Chirp Pulses)	4-16
4.3.5	Detection of Chimney Formed by Nuclear Explosion	4-16
4.4	Auxiliary Experiments	4-17
4.4.1	Refraction Survey	4-17
4.4.2	Reflection Experiments	4-17
4.5	Equipment Requirements for Holographic Field Experiment	4-18
4.5.1	Vibrator Source for Holographic Surveys	4-18
4.5.2	Geophones for Holographic Surveys	4-18
4.5.3	Amplifier and Recording System for Holographic Surveys	4-19
4.6	Summary of Experiments	4-19
SECTION 5 - EVALUATION OF SEISMIC ENERGY SOURCES AND DETECTORS		5-1
5.1	Seismic Energy Sources	5-1
5.2	Seismic Detectors - Geophones	5-2
SECTION 6 - HOLOGRAPHIC WEAK SIGNAL ENHANCEMENT STUDIES		6-1
SECTION 7 - RELEVANT LITERATURE		7-1
7.1	References	7-1
7.2	Supplementary Bibliography	7-3
SECTION 8 - INVENTION DISCLOSURE		8-1
APPENDIX A - HOLOGRAPHIC WEAK SIGNAL ENHANCEMENT TECHNIQUE		A-1

LIST OF ILLUSTRATIONS

Figure No.	Title	Page
3-1	Map Showing Location of Piledriver Tunnels Area 15, Nevada Test Site, Nevada	3-2
3-2	Fault Zone Plunge Section	3-3
3-3	Map of Climax Stock Area	3-5
3-4	Lollipop NXVP Line No. 1	3-6
3-5	Uphole Time Depth Curves	3-7
3-6	Attenuation Plots for Lollipop Refraction Line No. 1	3-10
3-7	Generalized Cross Section of 1500 Tunnel Showing Relation of Tunnel to Shot Point	3-24
3-8	Generalized Map of 1500 Tunnel Showing Crushed and Collapsed Zones Due to the U 15a Explosion	3-24
4-1	Hard Hat Site, Ray Paths for Sample Calculation	4-2
4-2	Piledriver Site, Ray Paths for Sample Calculation	4-8
4-3	Map Showing Location of Holographic Aperture With Respect to Nevada Test Site	4-11
4-4	Determination of Number of Fringes	4-12
4-5	Holographic Data Acquisition of Continuous Monofrequency Waves	4-14
4-6	Holographic Data Acquisition of Pulsed Monofrequency Waves	4-15
6-1	Layout in the Computer Simulation Model	6-2
6-2	Conventional Holographic Reconstruction of $(S_1 + S_2)$ in Image Plane of S_2. S_2 is Not Visible.	6-3
6-3	Conventional Holographic Reconstruction of $(S_1 + S_2)$ in Image Plane of S_1. S_2 is Not Observable.	6-4
6-4	Weak Signal Enhancement Reconstruction in the Image Plane of S_2. S_2 is Much Larger Than S_1 After Enhancement.	6-5
6-5	Computer Simulation Model	6-6
6-6	Reconstruction of $(S_1 + S_2)$ in Image Plane of S_2. S_2 is Not Visible.	6-7
6-7	Weak Signal Enhancement Reconstruction of a Single Scatterer in Image Plane of S_2. Only Scattered P-Waves are Allowed.	6-8
6-8	Weak Signal Enhancement Reconstruction of a Single Scatterer in Image Plane of S_2. Random Scattering Targets are Included in the Model.	6-9
6-9	Weak Signal Enhancement Reconstruction of a Single Scatterer in Image Plane of S_2. Both Scattered P- and S-Waves are Allowed.	6-10

Figure No.	Title	Page
6-10	Weak Signal Enhancement Reconstruction of Extended Scatterers in the Image Plane of S_2. Only Scattered P-Waves are Allowed.	6-12
6-11	Weak Signal Enhancement Reconstruction of Extended Scatterer (4λ) in Image Plane of S_2. Random Scattering.	6-13
6-12	Weak Signal Enhancement Reconstruction of an Extended Scatterer (4λ) in Image Plane of S_2. Both Scattered P- and S-Waves are Allowed.	6-14
6-13	Weak Signal Enhancement Reconstruction of an Extended Scatterer (4λ) in Image Plane of S_2. Scattered S-Wave Attenuated by a Factor of 2.	6-15
6-14	Weak Signal Enhancement Reconstruction of an Extended Scatterer in Image Plane of S_2. Scattered S-Waves Attenuated by a Factor of 4.	6-16
6-15	Weak Signal Enhancement Reconstruction of an Extended Scatterer in Image Plane of S_2. Scattered S-Waves Attenuated by a Factor of 8.	6-17

SECTION 1

TECHNICAL REPORT SUMMARY

1.1 GENERAL

The objective of this research program was to define the preliminary underground viewing system, based on acoustic holography principles, which is capable of detecting and imaging underground anomalies associated with a selected field test site. System requirements based on the geology of the selected site were specified and a proposed field test was designed. In addition, studies to develop a holographic weak signal enhancement technique were made.

The potential benefits to be gained from the development of an underground viewing system are many. For the first time, a method would be available to "look" into the ground and "see" targets, thereby defining such anomalies as tunnels, mines, bunkers, and other voids or water-filled cavities. It would be a valuable tool for surveying the earth ahead of, or prior to, excavations to determine potential hazards, for defining certain fractures, or crushed zones in the earth such as those which exist after a nuclear underground explosion, and for locating underground bunkers and supply stores.

Specific tasks to be accomplished during this program are given below.

1. Select a suitable field test site at which a future field test experiment could be performed.
2. Perform a theoretical analysis to determine system requirements based on the geology of the selected test site.
3. Design a preliminary underground viewing system based on the system requirements determined from 2 above.
4. Perform an evaluation of presently available seismic energy sources and detectors to determine if their characteristics are consistent with system requirements. Recommend modifications of present systems, or new designs, if available equipment characteristics are not adequate.
5. Investigate holographic reconstruction techniques appropriate for the display of seismic holograms, with emphasis on the development of image enhancement techniques.

The results of these tasks are summarized in the following subsections. Detailed discussions are presented in subsequent sections of this report.

1.2 SELECTION OF FIELD TEST SITE

The selection of a specific field test site is a deviation of the original program plan. Initially, Bendix scientists and the Contracting Agent's Project Engineer were to jointly identify the types of targets (tunnels, miners, bunkers, etc.) of greatest interest to the government. The types of hard rock in which the targets might exist along with typical target depths were also to be specified. At the first meeting between Bendix personnel and the Contracting Agent's Project Engineer, Mr. Gerald L. Fitzpatrick, on 18 June 1971, it became apparent that a more practical approach would be to identify the specific field test site at which known and well-defined targets exist and where the geologic conditions of the area were known and documented.

With this modification of the program plan, a search for a potential site was begun. Some of the criteria used for site selection included the degree of surface weathering, the type of earth material at the site ("hard" or crystalline rock was the principal geologic medium of interest as specified in the contract), targets (tunnels, caves, bunkers, etc.) associated with the site, surface topography, and access to the area. Potential sites that were evaluated included:

- Climax Stock, U.S.A.E.C. Nevada Test Range, Nye County, Nevada
- Batholith of Southern California
- Pikes Peak area, Colorado
- Guadalupe Mountains area, New Mexico and Texas
- Victorio Peak area, Texas
- Big Bend area, Texas and Mexico
- Winnfield Salt Dome, Winn Parish, Louisiana

A description of these sites was given in the Semiannual Technical Report, and is also included in Section 2 of this report for completeness.

The site selected was the "Piledriver" site in the Climax Stock on the U.S.A.E.C. test range in Nevada. Tentative selection was made in a meeting on September 13, 1971, with Bendix scientists and consultants and the Contracting Agent's Project Engineer. The site was then visited and inspected on September 14, 1971. During this visit, A.E.C. personnel indicated that there would be no problem in arranging to use the site for a future experiment. They also indicated they are very interested in this project, since it may provide a means to resolve fracture zones caused by nuclear explosions.

1.3 ANALYSIS OF FIELD TEST SITE TO DETERMINE SYSTEM REQUIREMENTS

The geology of the "Piledriver" site is well documented. The rock material consists of two petrological types, granodiorite and quartz monzonite. The two materials are similar in both physical and acoustic properties. Velocity logs made at drill holes in the area also documented

this geology. Targets associated with the site include a vertical shaft extending down to two tunnel complexes, one at a depth of 780 feet, the other at 1400 feet, and chimneys (fracture zones) caused by the nuclear explosions. A plan view of the test site is shown in Figure 3-1.

A model of the test site area was derived based on known geological information and the results of a refraction survey made in that area in 1961. The model includes three layers above a half-space. Both tunnels and chimneys formed by the nuclear explosion are located in the half-space. The characteristics of these layers are summarized below.

- Near-surface or sub-weathering layer. Highly weathered granodiorite, compressional wave velocity 2150 ft/sec, approximate depth zero to 20 feet.
- Weathered layer. Weathered granodiorite, compressional wave velocity 3600 ft/sec, approximate depth 20 to 100 feet.
- Alteration zone. Altered or fractured granodiorite, compressional wave velocity 12,000 to 13,000 ft/sec, approximate depth 100 to 300 feet.
- Half-space. Unaltered granodiorite, compressional wave velocity 17,000 to 23,000 ft/sec. Note: In some cases, this half-space apparently starts fairly close to the surface.

Based on this model of the test site, computer programs were written to calculate ray paths in the medium, to determine the maximum operating frequencies that can be used, and to determine the reflection from and mode conversions at the various interfaces. The results from these calculations were then used in the design of the seismic holographic experiment.

1.4 PRELIMINARY DESIGN OF UNDERGROUND VIEWING SYSTEM - SEISMIC HOLOGRAPHY EXPERIMENT

The results of the analysis of the field test site were used to specify the equipment required for a seismic holographic experiment and to define the types of seismic energy excitation, excitation frequencies, location of the energy sources, and location of and spacing of detectors (geophones) in the holographic array. Several constraints were adhered to in this design, most of which were in the interest of economy. These constraints included

- The use of commercially available equipment (seismic energy sources, geophones, amplifiers, and recorders), if at all possible.
- The use of a reasonably sized holographic aperture in the vicinity of the surface over the tunnels where the topography of the area is not extreme.

- The array geophones should be located at the surface instead of being buried in drill holes below the weathered layer (approximately 100 feet deep).
- Vibrator types of energy sources should be operated at the surface rather than below the weathered layer.

Calculations based on the model described in Section 1.3 were made to predict the signal amplitude at the holographic aperture due to reflections from the target tunnels when ensonified by a monofrequency hydraulic vibrator seismic source at the surface. These calculations were done for excitation frequencies of 100, 200, and 500 Hz. Calculations were also made to predict the amplitude of interfering reflecting and refracting waves, and an estimate of the Rayleigh wave signal was made. The amplitude of these interfering waves, compared to the desired signal, determines the dynamic range requirements of the recording equipment. For an excitation frequency of 200 Hz and below, the dynamic range requirements were found to be consistent with the available digital recorders. Frequencies above 200 Hz may also be used, especially to detect and image the shallow (780 feet) tunnel, but a decision on this should be postponed until preliminary experiments at the test site are made.

The spatial frequency due to signal reflections from the two tunnels were calculated. With 200 Hz excitation, reflections from the deep tunnel result in a spatial frequency giving slightly more than four fringes across a 1500-foot square aperture. (See Figure 4-1 for position of aperture with respect to target locations.) This will result in a rather poor resolution of the reconstructed image, but the fact that the tunnel is long should make the image recognizable. At 200 Hz, a spatial frequency giving approximately seven fringes will result from reflections from the shallow tunnel (760 feet). Here the resolution should improve and a reasonable reconstructed image is expected. The use of 300 Hz will give approximately 10 fringes due to reflections from the shallow tunnel, and resolution will be further increased. It appears that 300 Hz is the maximum frequency that can be used with vibratory-type energy sources, even for the shallow tunnel.

The ability to predict the amount of energy reflected from and scattered by the chimney (crushed zone) above the nuclear explosion is somewhat more difficult. Although the rock in the chimney area was crushed during the explosion, and is expected to be less consolidated, the velocity contrast, and hence the effective reflection coefficients, between it and the host rock is not known. Therefore, rather than an analytical prediction of signal strengths at the surface due to reflection and scattering from the chimney, an experimental determination during the proposed holographic field experiment is recommended. Since this target, being primarily a crushed zone of rock, is likely to be more of a scatterer than a reflector, and since it extends to within 500 feet of the surface, ensonification with higher frequencies than that used for detecting the tunnels might be feasible. Ensonification with an explosive source, and using the highest useful quasi-monofrequency component of this radiation, is suggested.

Although it appears that reasonable resolution of the shallow target can be obtained when the target is irradiated with a vibratory source, the use of explosives as a source of seismic energy was also considered. A relatively small charge of explosives (a few pounds) will induce many times the seismic energy into the earth than can be obtained with vibrator sources. Although this type of source is an impulsive source, that is, it radiates over a broad frequency spectrum, the energy contained in a very narrow (quasi-monofrequency) band can be greater than that obtained from a monofrequency vibrator. Proper design of the cavity into which the explosive is detonated can also enhance a particular frequency band. In this manner, the intensity of energy in the high frequency end of the spectrum can be optimized. For this reason, the use of explosives, as well as the use of a vibrator energy source, is recommended in acquisition of the seismic hologram. Rather than being detonated at the surface, however, the explosives would be set off in a drill hole below the weathered layer (100 feet deep). Detonating at this depth has the advantage that reflected signals from the weathered - altered layer interface are virtually eliminated. The use of explosives as an energy source does require filtering of the received signal to obtain a quasi-monofrequency signal, but this can be accomplished during the data processing in a digital computer.

To summarize, it is recommended that a vibratory seismic source be used at the surface to generate monofrequency continuous and pulsed signals of 200 Hz or greater for ensonification of various targets at the site, and that impulsive sources (explosives) also be used for target ensonification. Further, it is recommended that frequency modulated (chirp) excitation be used to compare the merits of these types of excitation as related to seismic holography.

1.5 EVALUATION OF SEISMIC ENERGY SOURCES AND DETECTORS

1.5.1 Seismic Energy Sources

Hydraulically driven vibratory sources have been used in the seismic exploration field for several years. Since they are primarily used for the petroleum industry and the need is to define the earth's layering structure at great depths, these sources are generally designed to operate at frequencies from about 5 to less than 100 Hz.

Two approaches can be taken to obtaining higher frequency sources capable of generating a monofrequency signal: a new type of source might be designed, or presently available vibrators might be modified for higher frequency operation. Since the first approach would be expected to be more costly, an effort was made to see if the second approach was feasible.

It was determined that presently available vibrators could be modified to operate as high as 500 Hz. The modifications required for a Wabco Vibrator Model 600 B-D, presently used by United Geophysical Corporation, a subsidiary of the Bendix Corporation, include

- Installation of a manifold and high frequency servovalve in lieu of existing valve
- Increase in the ram area to 9 square inches
- Installation of an electronic amplifier to drive the new servovalve
- Implementing a second feedback loop based on slave valve position
- Modification of ground contact pad to enhance coupling of higher frequencies into the ground
- Reinforcement of vibrator structure

With these modifications, the displacement of the reactionary mass (maximum displacement coupled to ground) will be 5×10^{-5} inches at 500 Hz, 2.5×10^{-3} inches at 200 Hz, and 10^{-2} inches at 100 Hz.

1.5.2 Seismic Detectors - Geophones

Commercially available geophones used in the seismic exploration field were found to be adequate for the holographic system requirements. The minimum useful output of geophones is related to the noise level of seismic amplifiers (typical amplifier noise is 0.1 μV); hence geophones capable of detecting ground displacements resulting in an 0.1 μV output are sufficient.

One such geophone is the Geo-Space Type GSC-110 detector. Its output of 0.6 V/in./sec. is constant over the frequency range from 100 to 500 Hz. This geophone will give an output of 0.1 μV at 200 Hz with a ground displacement 1.35×10^{-10} inch. Ground displacements greater than this are expected due to reflections from the deep tunnel at the selected test site.

1.6 HOLOGRAPHIC WEAK SIGNAL ENHANCEMENT STUDIES

The development of a holographic weak signal enhancement technique was initiated at Bendix Research Laboratories prior to the award of this contract. Further studies of this technique as it pertains to seismic holography were made during this program. This technique, which lends itself to computer simulation, has shown promise in defining images of targets that have signal strengths too weak to be seen by conventional holographic imaging (reconstruction) techniques, as is often the case when a scattering target is located above or below a strong signal-reflecting layer.

Two computer models describing a two-layer representation of the earth were investigated. The first model contained a weak scattering target below the reflecting interface of the two layers; the second model had the weak target located above the reflecting layer. In the computer

simulations, all mode conversions (for example, P-waves to S-waves) are allowed at both the reflecting and scattering surfaces.

Results using the first model (weak target below the reflecting surface) show that good image resolution can be obtained using the enhancement technique even when the ratio of strong to weak signals is 1000 to 1. Using conventional reconstruction techniques, the weak target cannot be resolved. Examples of these results are included in Section 6.

Results with the second model (weak target in the zone above the reflecting layer) indicate that unattenuated shear waves scattered from the target tend to interfere with the compressional waves, thereby reducing the resolution of the reconstructed image. If the shear waves are allowed to attenuate more rapidly than the compressional waves (by a factor of two or greater), image resolution is improved. Again, examples of these results are given in Section 6.

When the results from the two computer simulation models are compared, the image enhancement technique appears to give better results when the weak target is located below a reflecting plane. For the proposed holographic field test, the targets are located below the reflecting layer. This will probably be the case in most field problems.

SECTION 2

SELECTION OF FIELD TEST SITE

The original contract program plan specified that Bendix scientists and the Contracting Agent jointly identify the types of targets (for example, tunnels, mines, bunkers) of greatest interest to the government which could be detected and imaged using seismic holography. The type of earth in which these targets might be located was specified as "hard" or crystalline rock. At the first meeting with the Contracting Agent's Project Engineer on 18 June 1971, it became apparent that a far better approach would be to identify a specific field test site at which known and well defined targets existed and where the geologic conditions of the area were known and well documented. With this modification of the program plan, a search for a potential site was begun.

2.1 CRITERIA USED FOR SITE SELECTION

Before the search for a specific field test site was initiated, certain criteria were established to be used as guidelines for initial site evaluation. These guidelines are listed below.

- The area should have little or no soil overburden or weathering. This restraint will permit a higher operating frequency to be used for a field test without the need of planting seismic detectors and sources below the surface.
- The earth material at the site should be of a suitable rock type (i.e., igneous rock or crystalline limestone) to conform with the contrast requirement that the principal geologic medium of interest is hard or crystalline rock.
- The geology in the area of the site should be known and reasonably well documented.
- A suitable subsurface target must be present at the site.
- The area should preferably have a reasonably flat topography so that excessive phase compensations to correct for surface elevation differences are not required in an initial field experiment.
- Access to the site should be reasonable and there should be no restrictions to the use of explosives as a seismic energy source.

2.2 POTENTIAL SITES EVALUATED

Two Bendix consultants, Harry C. Kent, Head of the Department of Geology at the Colorado School of Mines in Golden, Colorado, and

Milton B. Dobrin, Geophysics Professor of the University of Houston, Houston, Texas, assisted Bendix personnel in the identification and evaluation of potential field test sites.

Preliminary evaluation of potential sites was primarily accomplished by accumulating and analyzing published geologic data. When possible, persons familiar with each site were contacted for additional information.

The area that was finally selected from the candidate sites was the "Piledriver" site in the Climax Stock on the U.S.A.E.C. test range in Nye County, Nevada. The selection was made in a joint meeting with Bendix personnel and consultants and the Contracting Agent's Project Engineer on 13 September 1971. The site was visited and inspected by Bendix personnel and consultants the following day, 14 September 1971.

A brief description of the potential sites that were considered was included in the Semiannual Technical Report, Bendix Report No. 6050, but are also included here for completeness.

2.2.1 Climax Stock, U.S.A.E.C. Nevada Test Range, Nye County, Nevada

The Climax Stock is an intrusive igneous body located in the north-central portion of the Oak Spring Quadrangle, Nye County, Nevada. This is in the northeastern portion of the Nevada Test Site and is immediately north of Yucca Flat.

The area of exposure of the stock is approximately 4 square kilometers and the rock types are granodiorite and quartz monzonite. The two rock types have been differentiated in field mapping, but there is a good possibility that the two rocks will have essentially similar physical and acoustic properties.

The general geology of the Nevada Test Site is treated in a publication of Eckel, et. al.,[1] The engineering and fracture properties of the rock of the Climax Stock has been studied by Ege.[2]

According to Ege, and on the map by Houser and Poole,[3] a vertical shaft of 385 feet, 450 feet of drifts, and a 70-foot-diameter unsupported hemispherical chamber were to be excavated in the rock of the Climax stock. The vertical entry shaft was sunk in the proximity of the contact between the granodiorite and the quartz monzonite, and the horizontal drift extended in the quartz monzonite toward the contact. Houser and Poole show the vertical shaft as labeled Station 1500 and the horizontal drift on their cross section F-F'. A number of drill holes are shown on the maps, and a more extensive system of underground openings may exist. (More details are given in Section 3).

There is approximately 1000 feet of topographic relief at the surface over the Climax stock. Slopes are steeper in the northern portion and more gentle to the south and southeast. Access to the area

should be good because of the numerous roads and trails put in by the Atomic Energy Commission.

2.2.2 Batholith of Southern California

Portions of Orange, Riverside, and San Diego Counties, California, are underlaid by a complex of igneous rocks, mostly of Cretaceous age, which are known collectively as the Southern California batholith. The northwestern portion of the batholith has been described by Larsen,[4] and other areas have been reported upon by a number of different authors. Two areas within the batholith seem to be of prime interest: the Cajalco area and the Cuyamaca Peak area.

Cajalco Area

This potential site is located in Sections 1 and 2, T. 4 S., R. 6 W., Riverside County, California. In addition to the publication by Larsen, a U.S. Geological Survey open-file report by Page and Thayer[5] should be available for examination at the Menlo Park, California office of the Geological Survey. A considerable amount of geologic mapping related to water projects has also been done for the Metropolitan Water District of Southern California, and it should be possible to obtain access to these maps.

The principal rock of the Cajalco area is the Woodson Mountain Granodiorite. The rock is typically white to pale brownish gray with scattered black grains and is rather coarse grained. It averages 33 percent quartz, 60 percent feldspar, 5 percent biotite, and small amounts of other minerals.

Potential targets in the area included the old workings of the Cajalco tin mine (this is also referred to as the Temescal mine or Temescal district in some reports) and the Cajalco water tunnel. Larsen (1948) quotes older reports (esp. Fairbanks, 1938) to the effect that the mine in the 1890's had two 180-foot vertical shafts and 300 feet of horizontal workings. The present state of these workings. From the topographic map the Cajalco tunnel appears to reach depths of 100 feet or so below the surface.

Topographic relief in the area is 200 feet or less, and access appears to be good. Proximity to the Lake Mathews reservoir and to facilities of the water district might restrict the use of dynamite in testing. Orchards now occupy an area adjacent to the tin mine property, and this might imply unfavorable soil conditions.

Cuyamaca Peak Area

The Cuyamaca Peak area has been described by Everhart.[6] This potential site is a rather large area which includes several more restricted locations of interest within the 15-minute Cuyamaca Peak quadrangle. The more important localities are the Boulder Creek district, the Stonewall Mine, the Oriflamme Mine, and the Descanso Mine.

The Boulder Creek district and the Stonewall Mine are located in areas where the country rock is a "mixed" rock of Stonewall Granodiorite and Julian Schist. The Julian Schist is an older, metamorphic rock, possibly of Triassic age, which has been invaded by the granitic igneous rocks of the Stonewall Granodiorite which is possibly of Jurassic age. This "mixed" rock might create problems because of lack of homogeneity, but if the invasion and assimilation of the metamorphic rock by the igneous rock is thorough, the resultant might be a fairly homogeneous rock. This would need further investigation. Many of the mines in the Boulder Creek district were being worked at the time of Everhart's paper or during earlier field work in the 1940's. Several of the mines have workings which extended through a vertical distance of some 200 feet and a lateral distance of several hundred feet. The workings of the Stonewall Mine extended through 600 feet vertically and 400 to 500 feet laterally. The Stonewall property has been largely inactive since 1895. There is about 1000 feet of topographic relief in the Boulder Creek district, but rather large areas of moderate relief are present in the district. The Stonewall Mine is in an area of low relief. The Boulder Creek district would apparently be accessible for work and for the use of dynamite. The Stonewall Mine might not be feasible because it lies within a state park, is along the shore of Cuyamaca Reservoir, and is near developed recreational facilities.

The Oriflamme Mine is located in Julian Schist. There may be sufficient inhomogenities within this rock to preclude its use. There were originally 1000 feet of underground workings, but the mine is long abandoned, and may be largely caved in. Access to the mine area would also be difficult due to lack of developed roads.

The Descanso Mine is located in the Bonsall Tonalite. This rock is light gray, medium- to coarse-grained, and consists of predominant feldspar, up to 25 percent quartz, biotite and hornblende. This is probably the most favorable rock type in the Cuyamaca Peak area for the proposed experiment. The mine originally had a 230-foot inclined shaft and three levels with about 80 feet of workings on each level. Access to the mine area should not be difficult, but the workings may be caved.

2.2.3 Pikes Peak Area, Colorado

Some sites in the Pikes Peak region of south-central Colorado should possibly be considered. These are the NORAD site in Cheyenne Mountain near Colorado Springs and the Cripple Creek area of Teller County, Colorado.

Both sites are located in granitic-type rocks of the Pikes Peak batholithic complex, but the Cripple Creek area has been further subjected to volcanic activity and mineralization related to the formation of the volcanic Cripple Creek caldera. The rocks of the NORAD site thus tend to be rather homogeneous while those at Cripple Creek are complex.

A number of geologic reports dealing with portions of the Pikes Peak area have been published, and Dr. R. M. Hutchinson of the Colorado School of Mines geology faculty is completing an extensive study of the entire Pikes Peak batholith. Dr. Hutchinson's maps are available in manuscript form and will soon be published.

The principal disadvantage to utilization of the NORAD site would be the steep surface topography. Topography would not be a significant factor in the Cripple Creek area. Extensive study of the records of the mines in the Cripple Creek district would be necessary to determine the best site for experimentation. Most of the mines are currently shut down; many of them are also deep and probably out of the desired depth range.

Should the NORAD site be considered for further investigation, a large volume of geologic, engineering and mining data was obtained during the planning and excavation of the underground facilities. It would be desirable to obtain access to this information.

2.2.4 Guadalupe Mountains Area, New Mexico and Texas

The area at the southern end of the Guadalupe Mountains in New Mexico and adjacent Texas is a classic region for reef limestone development and the formation of cave systems, such as Carlsbad Caverns. Topographic maps of the Carlsbad Caverns East, Carlsbad Caverns West, and El Paso Gap quadrangles, and geologic maps for two of the quadrangles, Carlsbad Caverns East and Carlsbad Caverns West have been obtained.

A considerable thickness of massive, reef limestone is developed in the general area indicated between the dashed purple lines on the topographic sheets. The limestones are of Permian age and include the Capitan Limestone and associated beds and the Goat Seep Limestone and associated beds. Extensive cave systems are developed in the limestones, and some of these caves have been well studied and surveyed.

Access to the area for the experiment may be hampered by the fact that a large portion of the area is included within Carlsbad Caverns National Park. Because of the high volume of visitors and the delicate nature of the cave formations, the National Park Service may be very reluctant to permit the use of explosives. However, there are locations away from high visitor use and outside the Park where experimentation might take place.

The topography of the reef front is very rugged, and access to the front itself would be virtually impossible for vehicles. The reef-top area is accessible through some of the canyons, and once the top area is reached the topography is not too rugged. A number of roads from the north permit access also.

2.2.5 Victorio Peak Area, Texas

The Victorio Peak area is located in westernmost Texas in Hudspeth and Culberson Counties and south of the Guadalupe Mountains. The larger region around Victorio Peak is known as Sierra Diablo and is described by King.[7]

In the vicinity of Victorio Peak there is as much as 1500 to 2000 feet of Permian limestone of the Bone Spring and Victorio Peak formations. Cave systems in these limestones are not well documented, but there are vague indications on the maps of the presence of some caves. Some mining has also been done in the vicinity of small igneous intrusions which cut the limestones.

The principal drawback to the Victorio Peak area is the topography. Along the east-facing slope of the Sierra Diablo there is a steep escarpment. The limestones also form cliffs. The topographic and geologic maps do show areas of relatively moderate relief along the crest of the Sierra Diablo escarpment, and if one of these areas could be located in conjunction with a cave, the site might be suitable. There may also be some difficulty with vehicular access because the road system is not well developed.

2.2.6 Big Bend Area, Texas and Mexico

Within Big Bend National Park in west Texas and in adjacent portions of Mexico, thick limestone of Early Cretaceous age are developed. The geology of the region is well described by Maxwell, et. al.[8] The best areas of exposure are in the Sierra del Carmen and its extensions on the eastern side of the Park (Boquillas Canyon area) and the Mesa de Anguila along the western side of the Park (Santa Elena Canyon area). Similar rocks are also exposed in the Mariscal Mountains in the south-central Park.

Cave systems do exist within the limestones and there have been mining activities in the Mariscal Mountains. Information on the cave systems is probably available in speleological references.

The topography of the region is rugged, but the tops of the limestone mesas are relatively flat. Vehicular access may be difficult, but there are some primitive roads in the area. Access to localities on the Mexican side may well be impossible except in the vicinity of Boquillas, Mexico which does have a road connection to the United States.

Since the areas are within a National Park for the most part, it might be difficult to obtain permission for the proposed experiments. However, the desirable areas are remote where the visitor use is low, so permission might be granted with less difficulty than in other National Parks. There is a slight possibility that a suitable site might be located outside the Park boundary, but the best locations appear to be within the Park.

2.2.7 Winnfield Salt Dome, Winn Parish, Louisiana

Although salt is not a hard rock material, its acoustic properties (high velocity) are similar. For this reason, salt-bearing areas were not excluded from the survey.

The Winnfield salt dome is located in Winn Parish, Louisiana, approximately midway between Shreveport and Alexandria. The salt, which extends within 300 feet of the surface, has been mined at a single level at a depth of about 800 feet. Maps are available of the mine workings. The cap rock on the salt has been quarried, leaving a layer of gypsum and anhydrite (which have physical properties similar to rock salt) between the surface and the salt.

Unfortunately, the tunnels and mine workings have been flooded with water in the past few years and the mine is no longer accessible. In addition, the area quarried over the salt is probably smaller than would be desired for a field test.

SECTION 3

ANALYSIS OF VIEWING SYSTEM REQUIREMENTS BASED ON GEOLOGY OF FIELD TEST SITE

In this section, the geology of the selected field test site is described in more detail and a model of the site is formulated. The seismic velocities (for compressional, shear, and surface waves) as well as Poisson's ratio are established for all zones in the model. The attenuation of seismic waves in the different layers are calculated. Calculations giving the response of the tunnels to seismic wave irradiation are also made.

3.1 TOPOGRAPHIC AND GEOLOGIC FEATURES OF THE CLIMAX STOCK, AREA 15, NEVADA TEST SITE, NEVADA

The primary geologic feature of Area 15, the Climax Stock, is shown on the enclosed geologic map, I-328, published by the U.S. Geological Survey. An index map locating the Nevada Test Site is also given.

Figure 3-1 details existing tunnels. All tunnels, entrance shafts and nuclear detonation areas from Hardhat and Piledriver experiments lie within the Climax Stock. This Stock is composed of two distinct petrological types in the immediate area of the target tunnels. The lithologic contact strikes irregularly west to northwest, with the granodiorite member to the north and quartz monzonite to the south. The granodiorite is oldest with the younger porphyritic quartz monzonite aged 230 $\pm$ 25 million years. Map I-328, sheet 2 of 2, contains sections through the Climax Stock. The Stock is thought to extend beyond 13000 feet in depth with the granodiorite, quartz monzonite contact dipping steeply to the south.

Drill holes and coring in the area indicate considerable jointing. No core recovery from depths above 20 feet is reported from any of the core holes. During the inspection of this site on 14 September 1971, core samples from a drill hole were viewed which indicated competent rock within 10 feet of the surface. Apparently, the combination of fracturing and weathering of rocks near the surface and drilling considerations have combined to inhibit core recovery at these shallow depths.

Some faulting or fracture zones exist as can be seen from the E-E' and F-F' sections which contain the U-15a exploratory drill hole.

Several joint sets have been mapped from drill cores. Detailed information can be obtained in the Geological Survey, TEM Report 836.[9] Some jointing and fracture zones are extensive and can be correlated between drill holes (See Figure 3-2 which is a section through the drill holes mapped in Figure 3-1.)

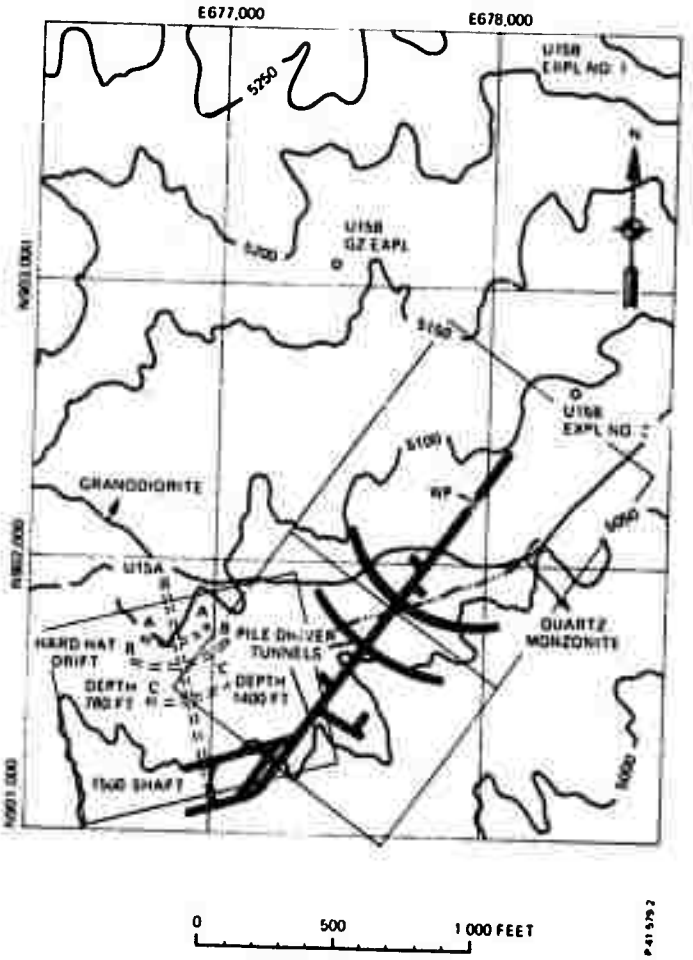

Figure 3-1 - Map Showing Location of Piledriver Tunnels Area 15, Nevada Test Site, Nevada

There are three prominent sets of joints in the area of the U-15a and Granite drill sites:

(1) Strike N30 to 40 degrees W, dip 15 to 35 degrees NE

(2) Strike generally NW, steep dip

(3) Strike generally NE, steep dip

The joints with low dip angle all seem to be firmly healed with secondary minerals (quartz, pyrite, and feldspar). The joints with nearly vertical dip are less well healed, but are generally filled with clay and calcite. Velocity surveys run from shot points 1000 feet away from the U-15a drill hole show that average horizontal velocities are slightly higher than average vertical velocities, indicating that open or loosely filled vertical joints are probably not an important factor. The number of

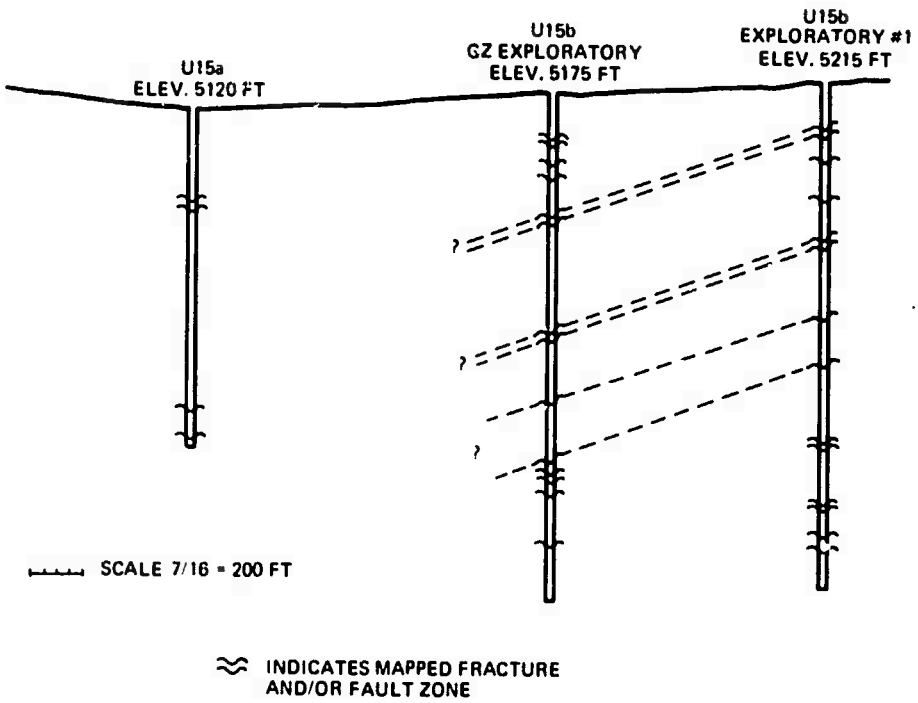

Figure 3-2 - Fault Zone Plunge Section

joints decreases with depth, especially below about 400 feet in the U-15a area, and the dip of the joints generally increases with depth. In fact, the extent of *in situ* jointing and fracture zones decreases with depth to a sufficient degree that detection of destressed fractured zones surrounding the tunnels has been reported.[10,11]

Additional geologic information consisting primarily of density and porosity data and the results of geophysical logs is given in a Geological Survey report by Roach, Izett, and Roller, June 1959,[12] Interpretation of Geophysical Logs of the Granite U-15a, Dolomite Hill No. 1 and Marble No. Me-2 Drill Holes, Nevada Test Site, Nye County, Nevada. The summary of the report indicates negligible variation in density or porosity between the two rock types. Unfortunately, data on the seismically important porosity are insufficient closer than 144 feet from the surface; however, the percent porosity of weathered surface samples of both the quartz monzonite and the granodiorite is higher than that of the unweathered rock. The grain density of both weathered and unweathered material is essentially the same, and the dry bulk density of both is nearly the same, although weathered values of dry bulk density appear to average less than those for unweathered material.

Weathering effects can extend to as much as 360 feet in the drill holes studied. In the upper portions of the drill holes, there is both

oxidation and alteration of the minerals. Oxidation and iron staining along fractures extends to a depth of 27.5 feet in the "Granite" hole. Alteration of the feldspar minerals to clay may be effective in the "Granite" hole to 360 feet.

The complex of tunnels in the Climax Stock lies almost completely in the quartz monzonite portion. The Hardhat drift lies at a depth of 780 feet and the Piledriver tunnel system at 1400 feet. The entrance shaft (1500 shaft) will serve as a vertically oriented target, as will the fracture zone surrounding the Piledriver detonation area.

3.2 COMPILATION OF GEOPHYSICAL INFORMATION CLIMAX STOCK, AREA 15

The earliest seismic investigations which have been carried out at Area 15 are reported as part of project Vela Uniform, Operation Blanca-Logan-Lollipop, Project 7.4, October 1961.[13]

Of the surveys carried out in 1961, the most significant were the near-surface velocity profiles (refraction survey), the near-surface wave attenuation measurements, and some uphole velocity plots.

Figure 3-3 indicates the area covered by these surveys. They lie generally to the north of the Hardhat and Piledriver tunnels. The Lollipop refraction line No. 1 (Figure 3-4) traverses the site of the Piledriver detonation.

The Vela Uniform reports have provided a substantial amount of information about the seismic properties of the Climax Stock; however, the location of the Lollipop survey lines and drill hole data requires an extrapolation southward to the proposed site for the seismic holography experiments. A search for more information has not been successful; in particular, missing data from the 1500 entrance shaft are desirable since it is a focal point of the proposed site. Also, there are almost no velocity data within 150 feet of the surface.

The results of the Lollipop No. 1 refraction survey indicate the existence of a near-surface layer composed of highly weathered granite and some alluvium in the range 15 to 25 feet in thickness. Below this layer, velocities average approximately 12500 ft/sec, although observed values range between approximately 11200 and 13500 ft/sec. These differences are undoubtedly due to weathering, alteration, and subsequent changes in porosity. Correlation between velocity and composition is usually valid only when porosity is reduced, i.e., at high pressure. Other factors which affect velocities in rock are mineral composition, fluid content, temperature, pressure, grain size, cementation direction with respect to bedding or foliation, and alteration. However, scatter in velocity at small depths and low pressure can usually be ascribed to porosity. The intrinsic velocity of rock is only achieved at pressures of approximately 1 kbar where porosity is reduced to a point that solid contract between grains is restored.

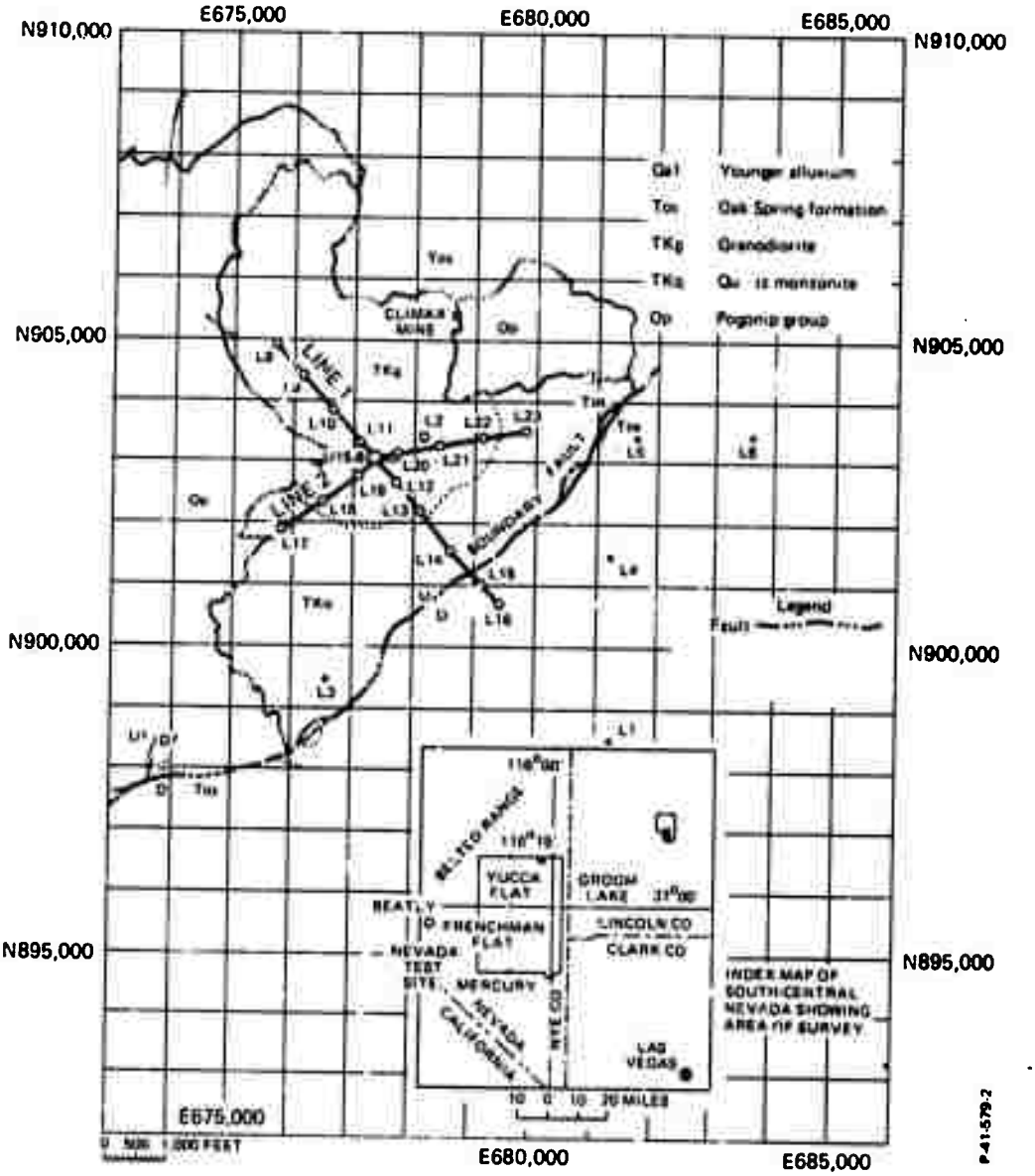

Figure 3-3 - Map of Climax Stock Area

Additional data are obtained from uphole surveys in the area such as Figure 3-5 which is an uphole velocity plot for the L-2 drill hole, the nearest to the proposed experiments. The entire hole lies within the granodiorite, and the values can only suggest the characteristics of the quartz monzonite. The velocity profile suggests a finer weathering structure than noted in the refraction survey. The two zones will be termed the near-surface layer (NSL) with a thickness of approximately 20 feet and the weathered layer (WL) with a thickness of approximately

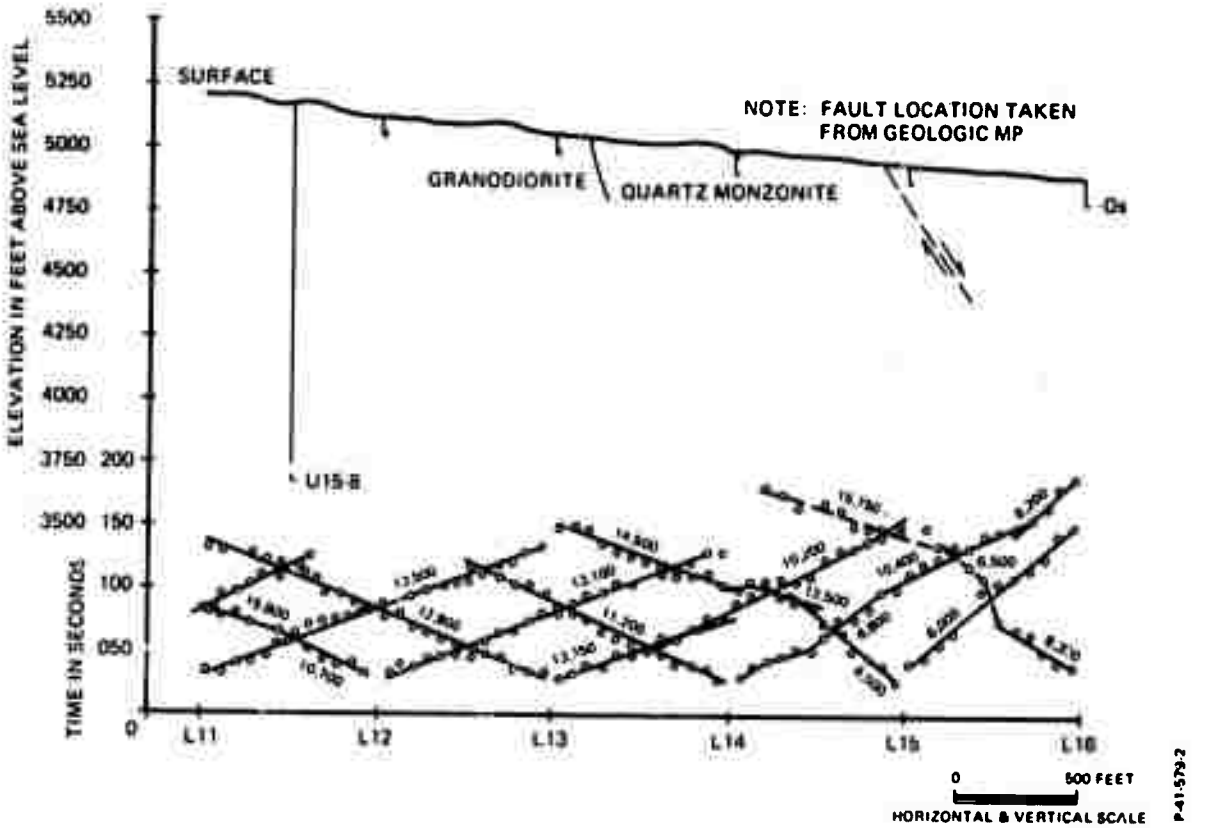

Figure 3-4 - Lollipop NSVP Line No. 1

80 feet. The high speed refraction 12900 ft/sec would correspond to a refraction in the layer below (WL), i.e., an altered layer (AL) in which some lithologic change has taken place but weathering is not predominant.

The geologic report, TEM Report 836,[9] gives detailed petrologic information on the U-15a Exploration Hole. This hole penetrates both rock types. Generally, quartz monzonite extends to 325 feet and granodiorite was occasionally encountered in the 0 to 325 feet zone. The geologic report yields evidence of hydrothermal alteration of the quartz monzonite and granodiorite. The alteration products include clay minerals, chlorite, secondary feldspar, sericite, quartz, epidote and sulfide minerals, mainly iron sulfide. The clay minerals and chlorite occur in zones throughout the rock and are concentrated with other alteration products along prominant northeast dipping joints. The clay minerals, predominantly montmorillonite, constitute only a fraction of the total rock and appear to be more common in zones 1 to 15 feet thick associated with steeply dipping fractures. The minerals formed by hydrothermal alteration were abundantly distributed from the surface to a depth of about 360 feet. In this zone, both the granodiorite and quartz monzonite contain portions in which the alteration is extensive.

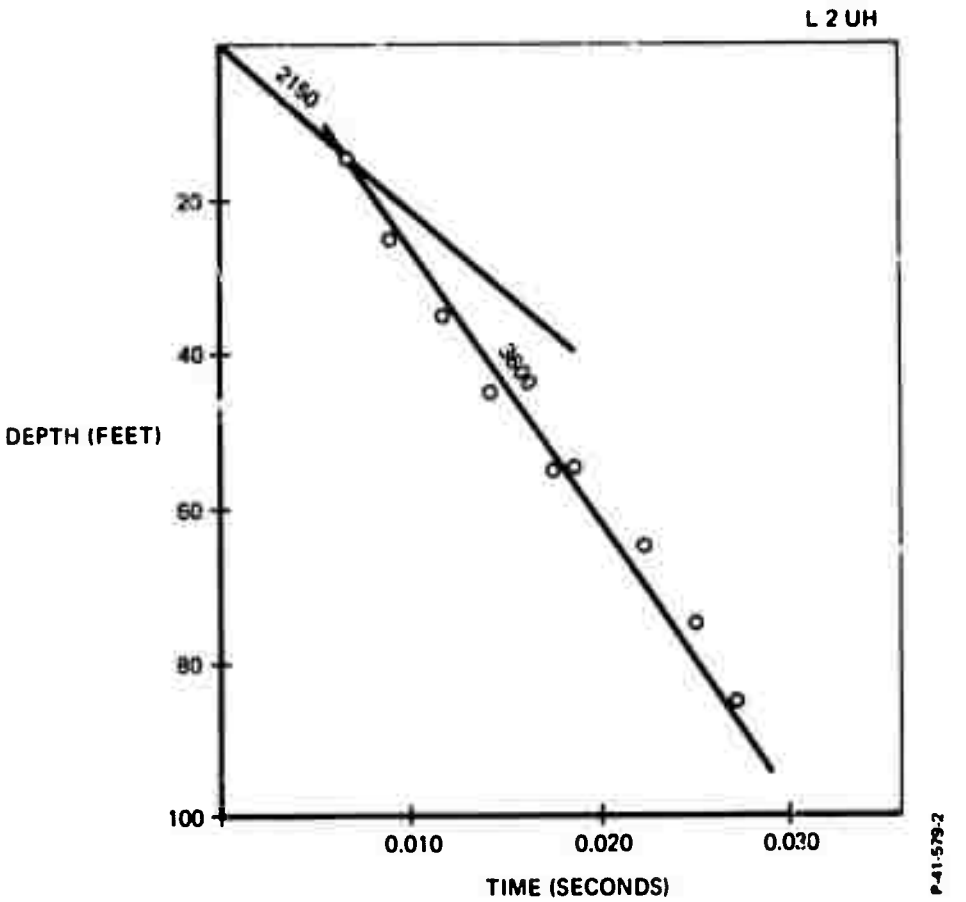

Figure 3-5 - Uphole Time Depth Curves

A summary of the above information suggests the following model of the seismic characteristics for the Climax Stock.

Layer 1. Near-Surface Layer

Thickness 20 feet ± 10 feet. Composition highly weathered quartz monzonite and alluvium. The alluvium referred to here is the result of several low southeast-trending ridges which have 40 to 60 feet of relief. The intervening valleys contain intermittent streams and are partly filled with rock debris derived by weathering of the Climax intrusive mass. Velocity of compressional waves is 2150 ft/sec and density is 5.15 slug/ft^3. The porosity is undetermined but certainly greater than 3 percent.

Layer 2. Weathered Layer

Thickness 80 feet ± 20 feet. Composition, weathered and hydrothermally altered quartz monzonite. In this layer, the weathering effect upon elastic wave propagation is predominant. The quartz monzonite is medium gray to light gray and contains phenocrysts in a fine-to-medium grained ground mass. Occasional penetrations of granodiorite may occur in this zone, particularly over the northernmost end of the tunnels. The granodiorite is mostly light gray to greenish gray, equigranular, and medium grained. However, this difference is not expected to change velocity significantly in the two rock types, particularly when they are highly weathered. Compressional wave velocity is 3600 ft/sec.

Layer 3. Altered Layer

Thickness 200 feet ± 50 feet. This layer is characterized by a significant compressional wave velocity change when compared with the weathered layer. Average velocity is 12900 ft/sec. A significant velocity scatter is observed from the refraction data, which probably indicates variation in the thickness and extent of alteration zones. This layer will act as a strong reflector when surface sources are used.

Layer 4. Unaltered Layer

This layer is sufficiently thick so that it may be considered a half-space. Data obtained from seismic studies in the Piledriver tunnels yield an average velocity of 19400 ft/sec. Density is 5.15 slug/ft^3. This implies no substantial difference in density for the entire test site. A destressed zone consisting of fractured and jointed rock has been observed surrounding the Piledriver tunnels. From uphole surveys and refraction shooting, a range of values of velocity and depth of the zone has been reported. Velocity ranges from 4300 to 15200 ft/sec and the thickness of destressed zone from 0.3 to 19.8 feet.

3.3 EVALUATION OF SHEAR WAVE VELOCITIES AND POSSION'S RATIO FOR ALL ZONES AT NEVADA TEST SITE

A tabulation of measured shear wave velocities for igneous rocks can be found in Clark, Handbook of Physical Constants.[14] The range of values for quartz monzonite and granodiorite are 9500 to 10500 ft/sec. When pressure and temperature are low, corresponding compressional wave velocities are 15100 to 17250 ft/sec which suggests rather competent rock, comparable to the altered or unaltered layers found at the Nevada Test Site. The Poisson's ratio calculated from the above velocities lies in the range 0.17 to 0.21. In general, the value of Poisson's ratio will increase for less competent rock, but data from rock with a greater burial depth indicate that Poisson's ratio will rarely decrease below a value of 0.17. If value of 0.2 is assumed for both altered and unaltered layers, then the respective shear velocities will be 7900 and 11900 ft/sec.

Some shear wave data were collected during the investigation of destressed zones in the Piledriver tunnel. The value range for the competent zone behind the destressed zone is 9400 to 12400 ft/sec. Calculated Poisson's ratios range from 0.21 to 0.29. Using average reported shear velocity for the data of 10100 ft/sec, the calculated average Poisson's ratio is 0.26. This value is higher than expected. If the reported data are interpreted as surface wave velocity, the two velocities are related by a factor of 0.92.

$$(\text{Velocity, Rayleigh}) = 0.92\ (\text{Velocity, Shear})$$

Applying this equation to the data and calculating the shear velocity yields 11000 ft/sec. The related Poisson's ratio is 0.2, in agreement with published values.

Near-surface values of Poisson's ratio obtained from seismic refraction experiments usually lie between 0.35 and 0.45. A value of 0.4 will be tentatively postulated for the Nevada Test Site. The weathered layer must have a Poisson's ratio between 0.4 and 0.2. The value 0.3 is chosen to represent this zone. Shear velocity for NSL is then calculated to be 860 ft/sec; for WL, 1930 ft/sec.

3.4 ATTENUATION

During the refraction experiments[13] at the Nevada Test Site, an effort was made to obtain information on compressional wave attenuation, using fixed gain recording of the 24 amplifiers in the geophone spread. The amplifiers were also tapered so that amplifier sensitivity was increased at greater distances from the source. From a paper record, the half-wave amplitudes were measured for the first or second excursion on the record. The resulting amplitude responses were plotted in db versus the log of horizontal distance from shot point. The slope of these plots provides a measure of an inverse power relationship between seismogram trace amplitude and distance from the shot point origin. The statistical variation in the data is very large and the derived attenuation values can only provide an estimate of the exact conditions. Particularly unfortunate was the lack of frequency information since attenuation is frequency dependent. Normal refraction surveys are low frequency, in the range 20 to 60 Hz. It is assumed in this case that the data were plotted at about 40 Hz. The total length of each refraction spread was 1400 feet. Figure 3-6 includes applicable plots of attenuation from Lollipop Refraction Line No. 1. Average values of slope are given in Table 3-1.

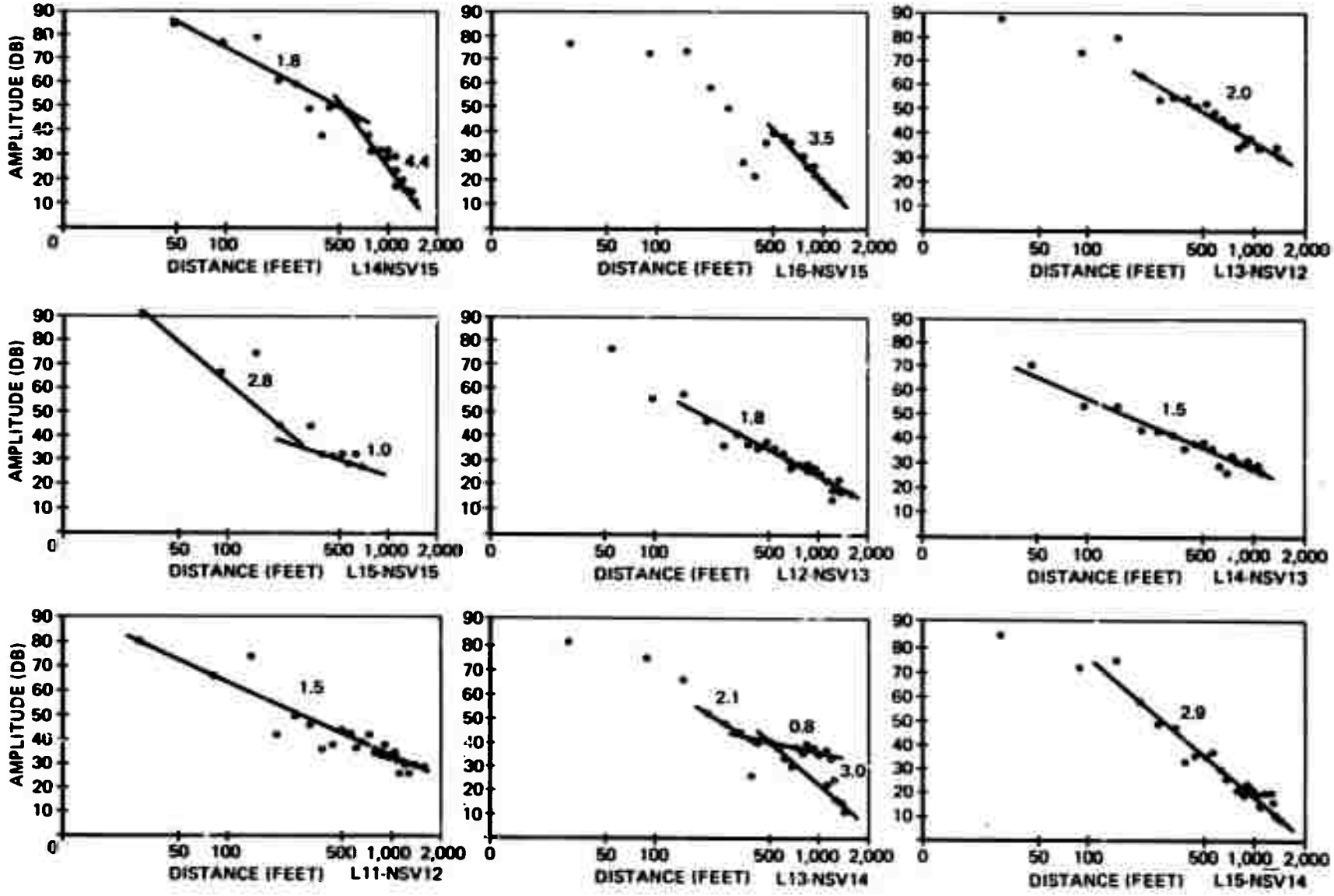

Figure 3-6 - Attenuation Plots for Lollipop Refraction Line No. 1

Table 3-1 - Average Slope Values

Spread	Slope	Velocity	Rock Type
L12-NSV13†	1.8	13100 ft/sec	Granodiorite
L11-NSV12	1.5	13500	Granodiorite
L13-NSV12	2.0	12800	Granodiorite
L13-NSV14	2.1	13750	Granodiorite
	? *	10200	Quartz monzonite
L14-NSV13	1.5	11200	Granodiorite and Quartz monzonite
L15-NSV14	2.9	14500	Quartz monzonite

†L12-NSV13 means shot point at L12, spread extends toward L13 along Lollipop Line No. 1. Shot point separation is 740 feet.

*The break in attenuation on L13-NSV14 is probably due to the change in lithology from granodiorite to quartz monzonite. There is also a change to a lower velocity along the refraction line.

From this table, the average attenuation slope is 1.8 for granodiorite and the average compressional wave speed is 12900 ft/sec. For quartz monzonite, the slope is 2.2 and the average velocity 12000 ft/sec. This suggests a generally higher attenuation and lower velocity in quartz monzonite, which is to be expected when the differences in petrology of the two rock types are taken into consideration. However, statistically the error inherent in the quartz monzonite data precludes a definite statement. Therefore, the average values obtained from the granodiorite will be used as representatives of the altered layer for the entire Nevada Test Site.

Attenuation of elastic wave energy in rock is known to be distance dependent of the form $\exp(-\alpha y)$, where α is frequency dependent. Attewell and Ramana,[15] "Wave Attenuation and Internal Friction as Functions of Frequency in Rocks" have compiled values of α, and White[16] lists specific experimental values in Seismic Waves, Radiation, Transmission and Attenuation. Figure 3-6 contains a series of semilogarithmic plots of attenuation. A straight line plot is described by the linear form equation

$$Y = Bx$$

where

Y = log y

y is horizontal distance in feet

x is decibels (dB)

B is slope

Changing decibel to nepers yields

$$\log y = B\ (8.686)\ n$$

where n is nepers. Slope is -1.8 and

$$\log y = 15.65\ (-n)$$

Values for n are

y	n	dB	α = dB/y
500 ft.	0.1725	1.5	0.003
1000 ft.	0.192	1.67	0.00167
1500 ft.	0.203	1.765	0.00118

Average value of $\alpha = 2 \times 10^{-3}$ dB/ft.

Following the assumption that first arrivals on the record have a frequency of approximately 40 Hz, then $\alpha = \alpha^{*}f$ is

$$\alpha = 5 \times 10^{-5}\ f\ \frac{dB}{ft}$$

where f is frequency in Hertz.

This value of attenuation is of the correct order of magnitude when compared with published values.[15,16] and corresponds to the attenuation for the altered layer.

Once this value for the altered layer has been obtained, rough estimates for the attenuation in the other layers can be made by scaling the data based upon the assumption that equal wavelengths have equal attenuation. Such an assumption indirectly takes into account the

important weathering, alteration, and porosity changes which occur in the rock. These factors determine the wave speed and therefore also the wavelength.

First the values of α for 100 Hz, 200 Hz and 500 Hz in the altered layer are calculated

$$\alpha_{100\ Hz} = 5 \times 10^{-3}\ dB/ft$$

$$\alpha_{200\ Hz} = 1 \times 10^{-?}\ dB/ft$$

$$\alpha_{500\ Hz} = 2.5 \times 10^{-2}\ dB/ft$$

For the unaltered half space, the scaled values are

$$\alpha_{100\ Hz} = 3.3 \times 10^{-3}\ dB/ft$$

$$\alpha_{200\ Hz} = 6.6 \times 10^{-3}\ dB/ft$$

$$\alpha_{500\ Hz} = 1.65 \times 10^{-2}\ dB/ft$$

For the near surface layer

$$\alpha_{100\ Hz} = 3.1 \times 10^{-2}\ dB/ft$$

$$\alpha_{200\ Hz} = 6.1 \times 10^{-2}\ dB/ft$$

$$\alpha_{500\ Hz} = 1.525 \times 10^{-1}\ dB/ft$$

For the weathered layer

$$\alpha_{100\ Hz} = 1.8 \times 10^{-2}\ dB/ft$$

$$\alpha_{200\ Hz} = 3.6 \times 10^{-2}\ dB/ft$$

$$\alpha_{500\ Hz} = 9.0 \times 10^{-2}\ dB/ft$$

Since estimates are now available for compressional velocity, shear velocity, and attenuation, it is possible to calculate reflection and transmission coefficients for all layers at the Nevada Test Site.

3.5 REFLECTION AND TRANSMISSION COEFFICIENTS FOR LAYERING AT THE NEVADA TEST SITE

At the surface, the source of wave energy will be a hydraulic vibrator. The forces acting on the surface of the ground will be oriented vertically. Wave propagation is characterized by a displacement which attenuates with distance from the source. In the near-surface layer, the wavelength of the 500 Hz compressional wave is 4.03 feet, and for the 500 Hz shear waves is 1.72 feet. These wavelengths are of the order of the dimensions of the vibrator ground contact pad. For a contact pad with dimensions small compared to the wavelength, the relationship between input force and output wave displacement is well known.[16]

For the compressional wave displacement u_r

$$u_r = \frac{G_o \cos\delta \left[1 - 2\,(V_s/V_p)^2 \sin^2\delta\right] e^{-i\omega r/v_p}\, e^{i\omega t}}{2\pi\rho V_p{}^2 r \left\{ \left[1 - 2\,(V_s/V_p)^2 \sin^2\delta\right]^2 + 4\,(V_s/V_p)^3 \sin^2\delta \cos\delta \left[1 - (V_s/V_p)^2 \sin^2\delta\right]^{1/2} \right\}}$$

For the shear wave displacement u_ϕ

$$u_\phi = \frac{-G_o \sin\delta \cos\delta \left[(V_s/V_p)^2 - \sin^2\delta\right]^{1/2} e^{-i\omega r/V_s}\, e^{i\omega t}}{\pi\rho V_s{}^2 r \left\{(1 - 2\sin^2\delta)^2 + 4\sin^2\delta\cos\delta \left[(V_s/V_p)^2 - \sin^2\delta\right]^{1/2}\right\}}$$

where $G_o e^{i\omega t}$ is the input point force

r is radius

δ is angle from vertical

ω is radians (source)

V_p is compressional wave speed

V_s is shear wave speed

For reflection and holographic experiments, the wave energy entering at almost vertical angles of incidence is of greatest importance. Plotting the curves for u_r and u_ϕ shows immediately that u_r is the predominant wave mode in this range. In addition, reducing the pad-to-wavelength ratio results in increasing the directional characteristic so that even more compressional wave energy is concentrated into a narrow cone about the vertical. If then the u_ϕ component is neglected, only the u_r component will arrive at the first boundary between NSL and WL. The u_r displacement can be divided into horizontal and vertical components. Indeed for angles of incidence close to vertical, u_r approximates u_x, the plane wave displacement.

Transmission and reflection coefficients can be obtained for the various layers, based upon an analysis by Muskat and Meres.[17] The coefficients are based upon the propagation of plane waves in an elastic medium. Therefore, this theory only approximates the wave front obtained from the vibrator source. The approximation is improved however, as the passes through successive layers, an effect discussed by Cagniard,[18] Reflection and Refraction of Progressive Seismic Waves.

Whenever waves are incident upon an interface, mode conversion will occur. This splitting of wave energy at every interface yields a proliferation of waves which are a major complication in record interpretation. At steep entrance angles, the compressional wave dominates whereas at angles away from the vertical, downgoing shear waves from the surface source become important and at some angles are dominant. The calculations of reflection and refraction coefficients as presented by Muskat and Meres separate the problem into two parts by considering the incoming compressional and shear waves individually. The resulting expressions for reflection and transmission coefficients are of sufficient complexity to require computer calculation. Such calculations have been carried out that were necessary to evaluate the Nevada Test Site. They show that only one boundary, that between WL and AL, has a significant mode conversion. In terms of energy, 31 percent goes into the reflected compressional wave, 64 percent is transmitted through as a compressional wave, and 5 percent is a transmitted shear wave yielding a total of 100 percent from the incident compressional wave.

3.6 MODEL OF TUNNEL RESPONSE

An estimate of the amplitudes of reflected waves returning to the surface from the tunnel is required. Two feasible methods of obtaining the estimate are a diffraction model which considers the tunnel as a wave scatterer, and a conical wave model in which boundary conditions at the tunnel walls are considered and the amplitude of emitted conical waves are calculated.

Investigation of these two approaches indicated that the conical wave model was more useful. This model yields values of displacement for any point in a geophone array.

Discussion of conical wave models can be found in Seismic Waves, Radiation Transmission, and Attenuation by White.[16] These models, developed primarily to investigate the wave propagation along cylindrical bore holes, are based on the assumption that incident waves on the bore hold have a wavelength long compared with bore hole diameter. The cylindrical symmetry of the bore hole then determines the wave modes which it can emit when the walls are displaced. Both compressional and shear-type waves are possible. Axial symmetry permits describing the wave field with two potentials.

The potential equations are

$$\frac{\partial^2\phi}{\partial r^2} + \frac{1}{r}\frac{\partial\phi}{\partial r} + \frac{\partial^2\phi}{\partial z^2} = \frac{1}{\alpha^2}\frac{\partial^2\phi}{\partial t^2}$$

$$\frac{\partial^2\psi}{\partial r^2} + \frac{1}{r}\frac{\partial\psi}{\partial r} - \frac{\psi}{r^2} + \frac{\partial^2\psi}{\partial z^2} = \frac{1}{\beta^2}\frac{\partial^2\psi}{\partial t^2}$$

Where α is compressional conical wave speed

β is shear conical wave speed

r is radial distance from center of tunnel

z is distance along tunnel axis.

NOTE: It is assumed throughout that the conical wave speed does not differ significantly from plane wave speed. Similarily, spherical wave speed is the same as for plane waves.

The displacements can be obtained from the potentials as follows:

$$u_r = \frac{\partial\phi}{\partial r} - \frac{\partial\psi}{\partial z}$$

$$u_z = \frac{\partial\phi}{\partial z} + \frac{\partial\psi}{\partial r} + \frac{\psi}{r}$$

The potentials obtained by solving the above equations for the case $\beta < \alpha < |c|$ where c is phase velocity are

$$\phi_c = \left[A_1 H_0^1 (mr) + A_2 H_0^2 (mr)\right] e^{-i\ell z} e^{i\omega t}$$

$$\psi_c = \left[B_1 H_1^1 (kr) + B_2 H_1^2 (kr)\right] e^{-i\ell z} e^{i\omega t}$$

$$\ell = \omega/c;\ m = \omega (1/\alpha^2 - 1/c^2)^{1/2};\ k = \omega (1/\beta^2 - 1/c^2)^{1/2}$$

where $\omega = 2\pi$ (frequency)

c is phase velocity

H indicates a Hankel function

Before applying these equations, it is necessary to evaluate their validity for the Nevada Test Site. In addition, it is useful to simplify the relationships as much as possible. The compressional wave speed in the rock surrounding the tunnel is 19200 ft/sec and the wavelength is 38.4 feet at 500 Hz. At 200 Hz, the wavelength is 96 feet. Tunnel diameter can vary from 20 feet to 30 feet so that at maximum frequency, the wavelength approaches tunnel dimensions; however, with the vibrator source, the frequency can be adjusted to increase the ratio between wavelength and the tunnel diameter to any desired value.

Of particular interest are ratios of

$$\omega a/\alpha < 1.0$$

where a is tunnel radius. For a 30 foot tunnel a = 15 feet, and with α = 19200 ft/sec this implies a frequency of 200 Hz or less. Under these conditions, the reflected wave energy is concentrated in the compressional wave for decreasing values of the phase velocity. At the Nevada Test Site, the layering is such that angles

$$\gamma_p = \arcsin (\alpha/c)$$

will not be less than 60 degrees and the reflected compressional wave will never contain less than 75 percent of the incident wave energy.

For this reason, it is possible to omit the mode conversion and consider only the compressional wave contribution to the displacements. This simplification is not mandatory, but only a convenience for calculation. If conditions at the Nevada Test Site warrant, a more detailed consideration of conical shear waves can be conducted.

The displacements reduce to

$$u_r = \frac{\partial \phi}{\partial r}$$

$$u_z = \frac{\partial \phi}{\partial z}$$

The calculational procedure is as follows for determination of tunnel response.

In general, it is only necessary to consider a source located at the interface between AL and UAL, for example, a small explosive charge. Let this charge be the source of a spherical compressional wave with potential ϕ_s.

$$\phi_s = \frac{A_s}{r'} e^{i(kr'-\omega t)}$$

where k is the wave number (ω/α)

r' is radial distance from source.

Theddisplacement $u_{r'}$ is obtained in the usual way

$$u_{r'} = \frac{\partial \phi s}{\partial r'} = \frac{A_s}{r'} \frac{\omega_o}{\alpha}$$

In this case, $u_{r'}$ is the known input value and corresponds to a fixed value of r'.

Hence, A_s is determined

$$A_s = \frac{u_{r'}}{(\omega_o/\alpha)}$$

Now $u_{r'}$ can be determined for any r', and then multiplication by the attenuation factor exp(-αr') yields the final value at the tunnel boundary.

For a local region in the vicinity of the tunnel, it is possible to approximate the displacement of the spherical wave by a plane wave. The potential for the plane wave can be written.

$$\phi_p = A_p e^{-\alpha x} e^{-i\ell z} e^{i\omega t}$$

The displacements are defined by

$$u_x = \frac{\partial \phi p}{\partial x} \; ; \; u_z = \frac{\partial \phi p}{\partial z}$$

The relationships between $u_{r'}$ and the plane wave displacements are

$$u_x = u_{r'} \cos\theta$$

$$u_z = u_{r'} \sin\theta$$

where θ is angle to the vertical.

The value of A_p is determined as in the spherical wave case and the approximate plane wave is completely defined.

The incident plane wave upon arrival at the tunnel displaces the tunnel walls. This displacement will cause the formation of conical waves and surface waves at the tunnel walls. At angles of incidence near to vertical, coupling to conical waves will be predominant. This is similar to the reflection at a plane boundary where coupling to surface wave decreases with increasing angle of incidence. The establishment of completely symmetrical conical waves is, of course, impossible with an incident plane wave; however, an approximation is possible in the illuminated zone and at large wavelength-to-tunnel-diameter ratios.

The two potentials ϕ_p and ϕ_c can, of course, only be matched at a single point because the plane wave amplitude decreases with increased

depth and the conical wave diminishes with increasing radius from the axis of the tunnel.

$$\phi_p = A_p\, e^{imx}\, e^{-i\ell z}\, e^{i\omega t} = A_1 H_0^{1}(mr)\, e^{-i\ell z}\, e^{i\omega t} = \phi_c$$

Equating real and imaginary parts

$$A_p \cos mx = A_1 J_0(mr)$$

$$A_p \sin mx = A_1 N_0(mr)$$

where r is tunnel radius and at the tunnel wall r = a.

The reflection coefficient A_2/A_1 can be obtained as

$$\frac{A_2}{A_1} = -\frac{Q\ ma\ H_1^{1}(ma) + H_0^{1}(ma)}{Q\ ma\ H_1^{2}(ma) + H_0^{2}(ma)}$$

where

$$Q = -\frac{2(k^2 - \ell^2)}{a^2 (k^2 - \ell^2)^2}\left[1 - \frac{2\ell^2\, ka\, H_0^{2}(ka)}{(k^2 + \ell^2)\, H_1^{2}(ka)}\right]$$

Once A_2 has been determined, the outgoing compressional conical wave is defined

$$\phi_{(\text{conical outgoing})} = A_2\, H_0^{2}(mr)\, e^{-i\ell z}\, e^{i\omega t}$$

For large r (i.e., large radial distance from the tunnel), the Hankel function can be approximated as an exponential.

$$\phi_{(\text{conical outgoing})} = A_2 \, (2/\pi mr)^{1/2} \, e^{-i(mr-\pi/4)} \, e^{-i\ell z} \, e^{i\omega t}$$

The partial derivative of this potential with respect to r yields the displacement due to the outgoing conical wave.

$$u_r = \left(\frac{2}{\pi}\right)^{1/2} A_2 \, m^{1/2} \, e^{i\pi/4} \, \frac{e^{-imr}}{r^{1/2}} \, e^{-i\ell z} \, e^{i\omega t}$$

To evaluate u_r at the boundary between AL and UAL, it must be multiplied by the attenuation exp(-ar).

Calculations of the type described above have been carried out to estimate tunnel response. It is apparent from the model that optimum response will be obtained when the seismic source is as close as possible to the tunnel. At the Nevada Test Site, this means directly over the tunnel. For the holographic array, an offset must exist between source and geophones. The minimal offset distance is optimal from the signal strength viewpoint, since shallow incident angles increase mode conversion to shear waves for a geophone spread parallel to the tunnel

3.7 SURFACE RAYLEIGH WAVES

Surface Rayleigh waves are expected to be generated whenever a vibrator is operated at the surface. These waves are usually of greater amplitude than any other on a seismic record.

For normal reflection records, the source-geophone spread is arranged so that arrivals from reflecting interfaces are not coincident with the passage of the surface Rayleigh wave from a transient input pulse. With holographic viewing, longer input signals are desirable to obtain increased monochromaticity of input. It is therefore useful to consider the characteristics of Rayleigh waves due to continuous sources. When layering occurs in the propagation medium such as at the Climax Stock area, the Rayleigh wave may be dispersive. Plots of characteristic Rayleigh dispersion may be found in Elastic Waves in Layered Media by Ewing, Jardetsky, and Press.[19]

Generally, if the wavelength of the Rayleigh wave is short compared to the layer thickness, the layer appears as a half-space. The Rayleigh wave will not be dispersive and the Rayleigh velocity approaches 0.92 of the shear velocity. For the high frequencies (200 Hz to 500 Hz) to be used in holography experiments, the shear wavelength will be very short due to the very low shear velocity of the near surface layer (860 ft/sec). The equivalent wavelength at 200 Hz is 4.3 feet. The

thickness of the near-surface layer is 20 feet so that the wavelength is only a fraction of the thickness. Hence, it is expected that the Rayleigh wave will be nondispersive and have a wavelength of approximately 4 feet. Layering variations along the geophone spread can modify this analysis and suitable corrections can be made according to information gained from the refraction survey. No difficulty is anticipated in calculating the variations in Rayleigh wave mode since the theory is well known.

Attenuation of [illegible] a continuous source can often be accomplished by summation of [illegible] components from a multi-geophone emplacement [illegible] will be used at the Nevada Test Site if required.

3.8 TUNNEL DESTRESS[illegible] TRANSMISSION

A destressed zone has been reported to exist surrounding the Pile-drive tunnel complex. This destressed zone is a low velocity zone of rock which has variable thickness ranging from 2 feet to 20 feet. An average depth for the zone is 8 feet. The low velocity is the result of fracturing of the rock [illegible] during the excavation process.

The primary interest in the destressed zone is its effect upon the incident wave [illegible]. First, the tunnel can appear larger to the [illegible], mode conversion can occur. Data presented [illegible] show correlation between degree of fracturing [illegible] the destressed zone range from [illegible] ft/sec. An overall average is about 11000 ft/sec. [illegible] zone on wave propagation can be calculated. An example [illegible] into different modes from an incident compressional wave is tabulated below.

CASE: Incident compressional wave at an angle of 30 degrees with vertical.

Reflected [illegible]	0%
Reflected [illegible]	29%
Transmitted [illegible]	71%
Transmitted shear	9%
Total Incident [illegible]	100%

Therefore, mode conversion [illegible] distribution of energy will vary according to incident angle. In this case, no reflection of compressional energy is expected [illegible] due to the destressed zone. The incident wave will be attenuated [illegible] subsequently reflected by the tunnel wall.

The Piledriver data indicate thatffracturing is a major factor inrreducing wave velocity. There is therefore some concern as to the effects of the nuclear detonations which have occurred near the tunnel complex. Figure 3-7 is a cross section of the Hard Hat detonation site and Figure 3-8 shows the extent of crushed and collapsed zones. Based upon geologic observation, no explosion-produced fractures are reported from the 1500 entrance shaft and extending 280 feet toward the U15a shot point. The actual effect upon elastic wave propagation can only be inferred, since no post-shot geophysical investigations have been carried out.

At the Piledriver site, the tunnels were resurveyed after the detonation and permanent displacements were noted at all points.

Displacement at 1000 feet is 0.86 foot

Displacement at 1500 feet is 0.38 foot

These measurements were, of course, made on the destressed zone and the validity when extended into the higher velocity rock surrounding the tunnel is uncertain. Of greater importance and significance are bore hole data from the U-15.01 PS 1V drill hole Survey of Piledriver Results, by I. Y. Borg.[20] This drill hole penetrated into the cavity formed by the Piledriver event. Permeability data, which are related to degree of rock fracturing, indicate a zone of increased permeability with a maximum vertical extent of 1032 $\pm$ 36 feet above shot level or approximately 500 feet from the surface. The Climax Stock has many fracture planes and these have mostly been healed with secondary minerals. The Piledriver detonation has most certainly opened large numbers of these fractures at least to a distance of 1050 feet from the shot point. The effect beyond 1050 feet is uncertain, but it must in any case be assumed that some velocity and attenuation changes have taken place. It is also quite likely that these opened fractures are now filled with perched water. For this reason and for layering corrections, the preliminary refraction and reflection tests are recommended.

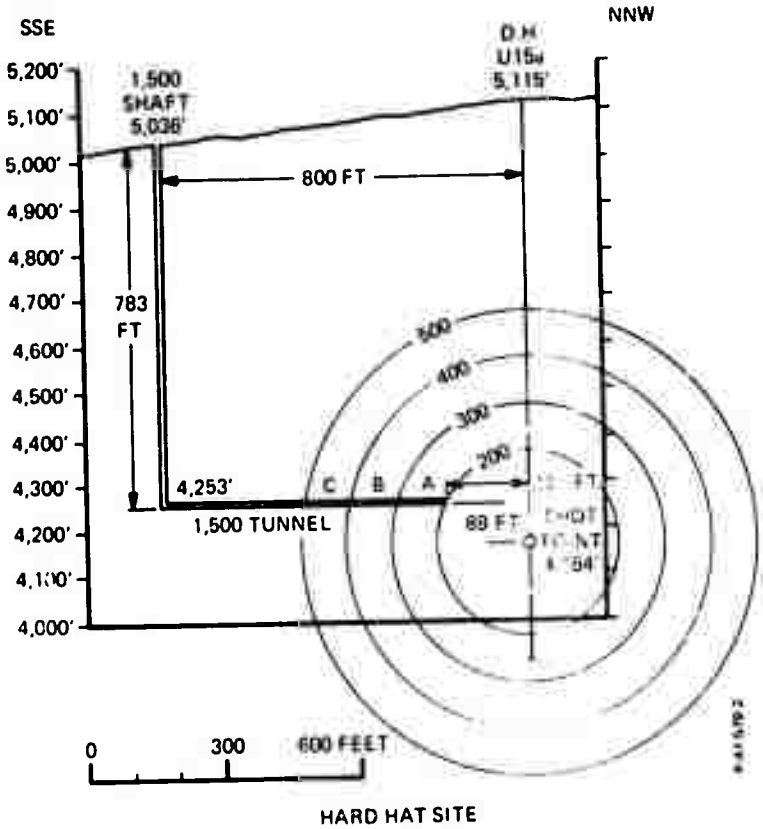

Figure 3-7 - Generalized Cross Section of 1500 Tunnel Showing Relation of Tunnel to Shot Point

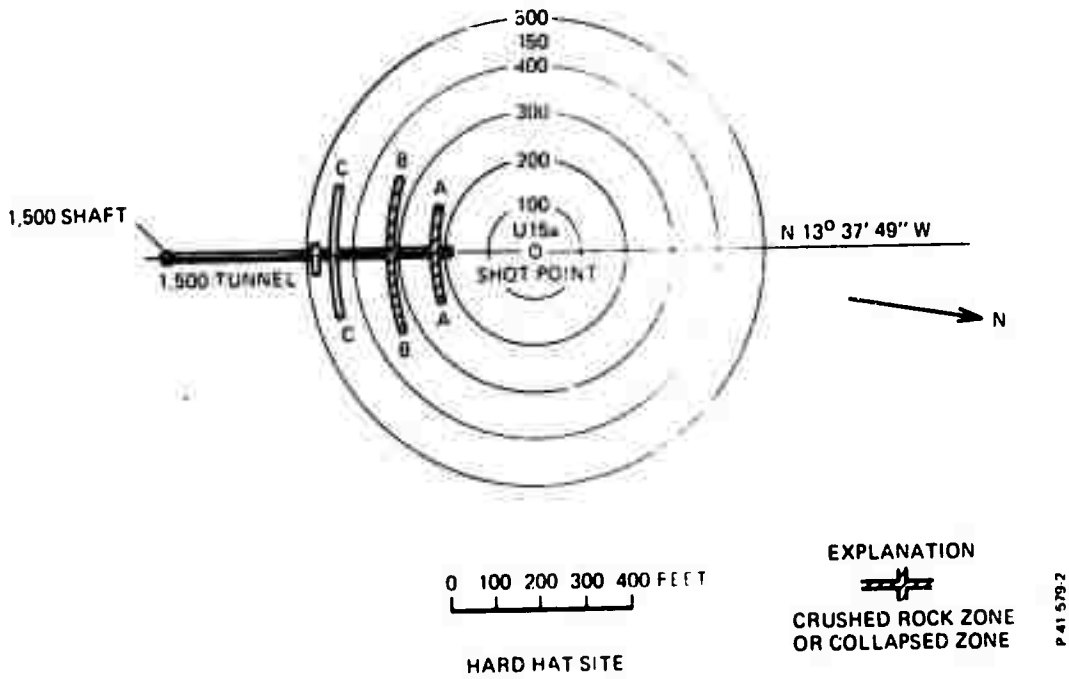

Figure 3-8 - Generalized Map of 1500 Tunnel Showing Crushed and Collapsed Zones Due to the U 15a Explosion

SECTION 4

DESIGN OF UNDERGROUND VIEWING SYSTEM - SEISMIC HOLOGRAPHY EXPERIMENT

In this section the design of the underground viewing system - or more accurately - the design of the seismic holography experiment is discussed. Based on the analysis of the selected field test site geology described in Section 3, calculations are made to predict signal strengths present at the surface. These signals include those from the targets, as well as reflections and refractions from reflecting interfaces. Once the signal strengths are known, the following information can be obtained: the maximum frequency (from a vibrator energy source) that can be used to ensonify the targets, the maximum spatial frequency (minimum fringe spacing) across the aperture, the number of sampling points required in the holographic aperture, and the size and position of the aperture. The latter can be determined by considering the target signal strengths and the topographical features of the site. Data acquisition with different types of seismic excitations (CW and pulsed CW using a vibrator, and impulses using explosives) are considered. Finally the equipment and instrumentation requirements are given.

4.1 CALCULATED AMPLITUDES OF RECEIVED SIGNALS BASED UPON THE COMPOSITE MODEL OF THE NEVADA TEST SITE

The vibrator source is described and the expected ground displacements are given in Section 5. With these values of displacement as inputs, expected amplitudes from important wave paths have been calculated. The values obtained consider the tunnel response, geometrical spreading, attenuation, energy loss through mode conversion at layer boundaries, the destressed zone surrounding the tunnels, and coupling of the incident wave into an outgoing conical wave.

A complete calculation is carried out as follows: At 500 Hz the surface displacement at the source is 5×10^{-5} in. The wave enters the ground almost vertically downward at an angle of incidence from normal of 30 degrees for the Piledriver case (see Figure 4-1). The wave propagates downward as a spherical wave and attenuates due to geometrical spreading as 1/R. In addition, the wave is attenuated at a rate which is determined by its frequency. The attenuation factor is $\exp(-\alpha R)$, where α corresponds to attenuation factors previously calculated. These factors combine to determine the wave amplitude in the near-surface layer just before crossing into the weathered layer.

$$U_{R(final)} = \frac{U_{r(incident)}}{R} e^{-\alpha R}$$

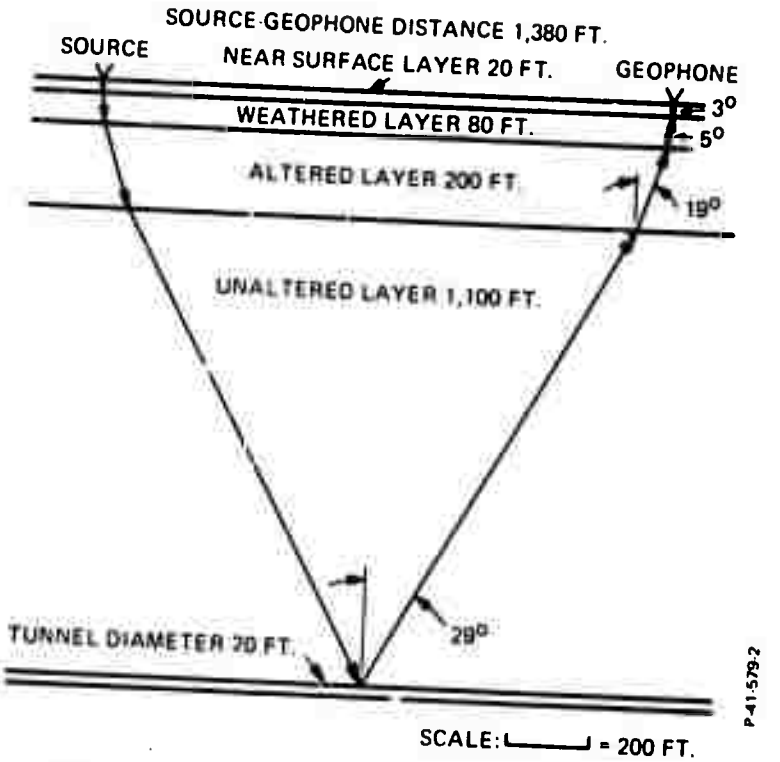

Figure 4-1 - Hard Hat Site, Ray Paths for Sample Calculation.

$U_{r(incident)} = 5 \times 10^{-5}$ inch

R (thickness of layer) = 20 feet

α (for NSL at 500 Hz) = 1.5×10^{-1} dB/ft or 1.76×10^{-2} neper/ft

$e^{-\alpha R} = 0.705$

$U_{r(final)} = 1.76 \times 10^{-6}$ inch

Of particular interest is the vertical component of displacement (U_x), since this is the component measured by vertical geophones. For the NSL the incident angle is 3 degrees and $U_x = U_r$.

To determine the effect of a boundary, the reflection and transmission coefficients are calculated using the analysis of Muskat and Meres. These coefficients relate the potentials on either side of the boundary. Let I_1 represent the potential amplitude on the incident side and I_2 the potential amplitude on the opposite side. For the NSL-WL boundary, $I_2/I_1 = 1.25$. I_1 is determined from U_x as $I_1 = U_x U_p/\omega$ where ω is 2π (frequency of wave) and V_p is compressional wave speed.

In this case, $\omega = 2\pi f = 3140$ and $V_p = 2150$ ft/sec.

$$I_1 = 1.21 \times 10^{-6}$$

$$I_2 = \frac{I_2}{I}\,(I_1) = 1.51 \times 10^{-6}$$

Vertical displacement in the weathered layer becomes

$$U_x = I_2 \frac{\omega}{V_p} = 1.32 \times 10^{-6} \text{ inch}$$

The angle of incidence for the weathered layer is 5 degrees, so that U_x is approximately equal to U_r.

The wave amplitude is again corrected for geometrical spreading and attenuation factor α corresponding to the weathered layer.

$$U_{r(final)} = 1.16 \times 10^{-7} \text{ inch}$$

A new value of the incident potential amplitude is calculated

$$I_1 = \frac{U_x\, V_p}{\omega} = 1.33 \times 10^{-7}$$

where V_p corresponds to compressional wave speed in the weathered layer.

The potential amplitude ratio for the altered layer is $I_2/I_1 = 1.56$. Thus,

$$I_2 = 2.07 \times 10^{-7}$$

$$U_x = 4.58 \times 10^{-8}$$

Correcting U_x for geometrical spreading and attenuation yields

$$U_{x(final)} = 8.62 \times 10^{-8}$$

The new potential is

$$I_1 = 3.53 \times 10^{-8}$$

For the boundary between altered layer and unaltered half-space

$$\frac{I_2}{I_1} = 1.24$$

$$I_2 = 4.37 \times 10^{-8}$$

$$U_x = 7.08 \times 10^{-9}$$

Correcting for geometrical spreading and attenuation

$$U_{x(final)} = 1.26 \times 10^{-10}$$

Therefore, the potential wave amplitude is

$$I_1 = 7.78 \times 10^{-10}$$

In order to calculate the tunnel response it is necessary to determine the potential of the outgoing conical wave. First, the compressional plane wave potential is matched to the potential of a conical wave at the boundary of the tunnel. This matching can only occur on the ensonified side of the tunnel and along the center line of the tunnel. The contribution of U_x to a radial displacement of the tunnel wall drops off rapidly along either side of the center line. The emitted conical wave will therefore not be symmetrical.

Matching is carried out for real and imaginary parts

Real part: $I_1 \cos(mx) = A_1 J_o(ma)$

$$m = \frac{1}{V_p} = 1.62 \times 10^{-1}$$

$$A_1 = -1.05 \times 10^{-9}$$

Imaginary part: $I_1 \sin mx = A_1 N_o(ma)$

$$A_1 = 1.46 \times 10^{-9}$$

Using the previously developed expressions for A and A_2/A_1,

$$Q = -0.318 - i\,(0.337)$$

$$A_2/A_1 = -0.033 + i\ (1.65)$$

The real or imaginary part of A_1 must be chosen so that U_r of the conical wave is positive and real. The following are chosen to satisfy this condition.

$$e^{i\omega t} \rightarrow i \sin \omega t$$

$$e^{i\ell z} \rightarrow \cos \ell z$$

$$e^{imr} \rightarrow \cos mr$$

$$e^{i\pi/4} \rightarrow \cos \pi/4$$

The amplitude is determined when $\sin \omega t = 1$.

$$\cos \ell z = 0.809$$

$$\cos mr = -0.309$$

Hence $A_1 = 1.46 \times 10^{-9}$ is chosen to yield U_r positive.

$$U_r = 4.08 \times 10^{-12} \text{ inch}$$

Including attenuation

$$U_{r(final)} = 5.07 \times 10^{-13} \text{ inch}$$

Next, the potential is calculated as if the emergent conical wave were an approximation to a plane wave.

$$I_1 = \frac{U_x V_p}{\omega} = 3.13 \times 10^{-12}$$

For the boundary of unaltered layer into the altered layer, $I_2/I_1 = 0.748$

$$I_2 = 2.34 \times 10^{-12}$$

$$U_x = 5.72 \times 10^{-13}$$

Including conical wave spreading and attenuation.

$$U_{x(final)} = 2.96 \times 10^{-13}$$

The potential becomes

$$I_1 = 1.21 \times 10^{-12}$$

For the boundary of altered layer and weathered layer $I_2/I_1 = 0.337$. Repeating the calculation as above including wave spreading and attenuation yields

$$U_{x(final)} = 1.51 \times 10^{-13}$$

$$I_1 = 1.73 \times 10^{-13}$$

I_2/I_1 for the weathered layer, near-surface layer boundary is 0.742

$$I_2 = 1.28 \times 10^{-13}$$

Wave spreading and attenuation yield a surface value of

$$U_{x(final)} = 1.3 \times 10^{-13} \text{ inch}$$

No consideration has so far been given to the destressed zone surrounding the tunnel. The zone will cause mode conversion and calculation of these indicate that only 71.3 percent of the incident wave energy will reach the tunnel through the destressed zone. Upon re-emerging, the wave will lose 12.3 percent of wave energy to a trapped mode surrounding the tunnel. Correcting for this energy loss yields a resultant surface displacement of 9.7×10^{-14} inch.

A compilation of expected signal returns is shown in Table 4-1. These include the response of Hard Hat (Figure 4-2) as well as Piledriver tunnels to various frequency inputs.

It is seen that these responses are quite low and consideration must be given to the possibility that other signals may interfere with detection of th tunnel signal.

Coherent signal returns from layering and surface wave interference will tend to use up the dynamic range of the recording system, particularly when the input is a continuous wave (CW). An investigation of possible strong reflections and refractions has been undertaken. The

Table 4-1 - Wave Amplitudes for Piledriver and Hard Hat Test Sites

	500 Hz	200 Hz	100 Hz
Input displacement from vibrator	5×10^{-5}	2.5×10^{-3}	1×10^{-2}
Tunnel Response, Hard Hat Source-geophone distance 695 feet	5.3×10^{-12}	4.7×10^{-9}	5.4×10^{-8}
Tunnel Response, Piledriver Source-geophone distance 1380 feet	9.7×10^{-14}	8.2×10^{-10}	1.6×10^{-8}
P refraction at 695 feet	7.7×10^{-11}	1.2×10^{-8}	1.1×10^{-7}
P refraction of 1380 feet	7.7×10^{-12}	4.4×10^{-9}	8.6×10^{-8}
Rayleigh Wave at 695 feet	7.1×10^{-8}	3.6×10^{-6}	1.4×10^{-5}
Rayleigh Wave at 1380 feet	3.6×10^{-8}	1.8×10^{-6}	7×10^{-6}
P reflection (15 degrees from vertical)	1.6×10^{-8}	8.1×10^{-7}	3.2×10^{-6}

strongest reflections from the reflecting layer will occur near the source. P-waves entering the ground at 15 degrees from the vertical and reflected from the WL-AL interface will give a ground displacement amplitude as tabulated below.

Reflection (15 degrees from vertical, 45 feet from source)

500 Hz = 1.6×10^{-8} inch

200 Hz = 8.1×10^{-7} inch

100 Hz = 3.2×10^{-6} inch

P-waves entering the ground at an angle greater than 15 degrees (the critical angle) will be refracted rather than reflected. The strongest returning body wave due to this refraction is the $P_1P_2P_3P_2P_1$ refraction. This wave enters as a compressional wave, is refracted by the WL-AL

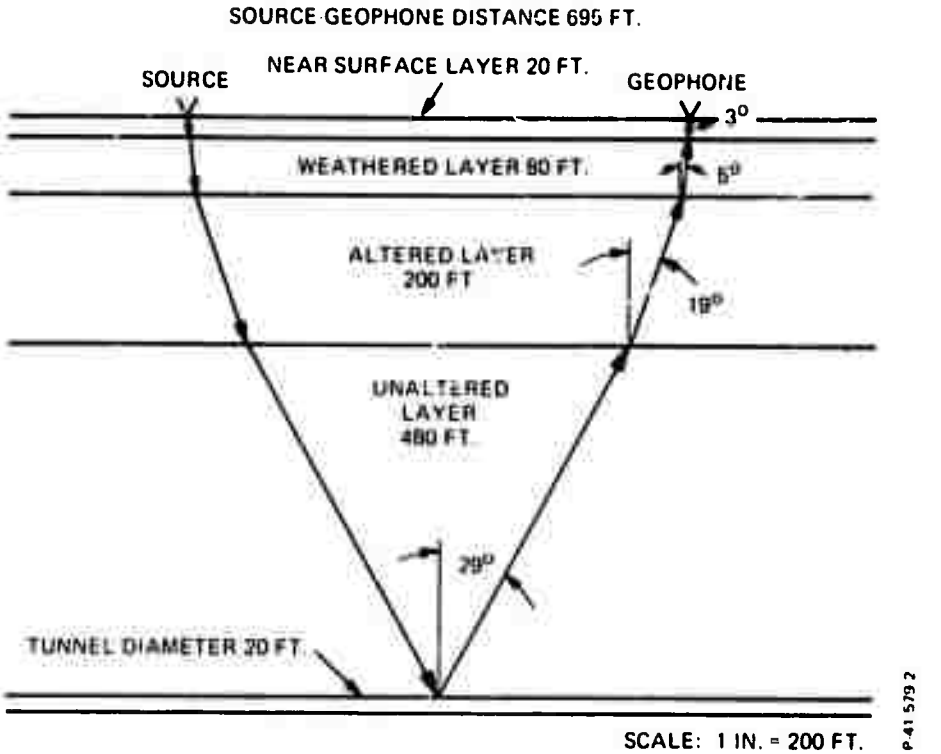

Figure 4-2 - Piledriver Site, Ray Paths for Sample Calculation

boundary, travels with compressional wave speed in AL, and then returns to the surface as a compressional wave. The discovery that this is the strongest body wave return is not surprising, since it is the prominent wave mode reported in the Vela Uniform reports.[13] Amplitudes for this refraction are tabulated below.

Refraction at 695 feet

500 Hz ≡ 7.7×10^{-11} inch

200 Hz ≡ 1.2×10^{-8} inch

100 Hz ≡ 1.1×10^{-7} inch

Refraction at 1380 feet

500 Hz ≡ 7.7×10^{-12} inch

200 Hz ≡ 4.4×10^{-9} inch

100 Hz ≡ 8.6×10^{-8} inch

These amplitudes are not sufficiently great to exceed the dynamic range of the recording system and therefore will not mask the tunnel response.

The surface wave at the higher frequencies, greater than 100 Hz, is essentially not dispersive and can be attenuated by a geophone group. Methods for estimating the effective attenuation can be found in A Graphical Method for Computing Geophone Group Response, by Verma and Roy.[21] For a continuous sinusoidal input, the normalized response R_n of n single geophones of equal sensitivity in a linear, equally spaced array is

$$R_n = \frac{\sin (n \pi D/\lambda)}{n \sin (\pi D/\lambda)}$$

where λ is the wavelength and D is the distance between consecutive geophones.

For geophones of equal sensitivity, the effective attenuation is strongly dependent upon the exact placement of the geophones. This criticality can be reduced by adjusting the relative sensitivity of the geophones in the group. As an example, a six-element array with spacing varying from $\lambda/1.5$ to $\lambda/4$ will give a normalized response of 0.06 or less to a wave with wavelength λ.

Determination of an optimal spacing and sensitivity can be established by summing terms of the form F_n. Estimation of Rayleigh wave amplitudes is difficult for near-surface materials. However, for low frequencies, Jolly and Mifsud[22] have reported that amplitude varies roughly as the reciprocal of shot detector distance for the vertical component. This decay in amplitude is the combined result of wave spreading and attenuation. At frequencies above 100 Hz, the amplitude is expected to decrease more rapidly due to higher attentuation. A suitable attenuation factor has not been determined for surface waves; therefore, amplitude will be calculated using the inverse distance relationship only. It is recognized that this is only an upper limit to the expected amplitude.

Rayleigh wave amplitudes at 700 feet

500 Hz; 7.1×10^{-8} inch

200 Hz; 3.6×10^{-6} inch

100 Hz; 1.4×10^{-5} inch

Rayleigh wave amplitudes at 1400 feet

500 Hz; 3.6×10^{-8} inch

200 Hz; 1.8×10^{-6} inch

100 Hz; 7.0×10^{-6} inch

As pointed out previously, the use of multiple geophones can reduce the effective amplitude of Rayleigh waves by a factor of 0.06.

Effective Rayleigh wave amplitudes at 700 feet

500 Hz; 4.3×10^{-9} inch

200 Hz; 2.2×10^{-7} inch

100 Hz; 8.4×10^{-7} inch

Effective Rayleigh wave amplitudes at 1400 feet

500 Hz; 2.2×10^{-8} inch

200 Hz; 1.1×10^{-7} inch

100 Hz; 4.2×10^{-7} inch

The Rayleigh wave amplitudes will be greater than those listed above nearer the source. The maximum value, occurring a few wavelengths (for example 35 feet) from the source, will be approximately 20 times greater than the amplitudes listed above. This indicates that the dynamic range requirements may be exceeded at geophones near the source, but this should not be a serious problem since the a "hole" in the aperture will not drastically affect the reconstruction.

Table 4-1 summarizes the displacement amplitudes of the various reflections, refractions, and Rayleigh waves calculated in this section. According to this table, the strongest signal will be due to the Rayleigh wave. At 200 Hz, the ratio of the Rayleigh wave signal to the signal from the deep Piledriver tunnel will be within the dynamic range of the recording equipment at geophones greater than 200 feet from the source. If the Rayleigh wave is attenuated by using multiple geophones, the ratio is reduced by greater than a factor of 10.

4.2 HOLOGRAPHIC APERTURE DESIGN

The signal strength calculations of Section 4.1 indicate that the maximum excitation frequency that can be used to ensonify the deep (1400 feet) tunnel is 200 Hz. Further, extrapolating between the signal strength from the shallow (780 feet) tunnel, frequencies as high as 300 Hz might be used. For the purpose of the report, however, a vibrator excitation frequency of 200 Hz will be assumed. If initial field reflection results indicate that either higher or lower frequencies can or must be used, the layout of the holographic aperture (geophone spacing) can be adjusted accordingly.

The use of explosives as a seismic energy source is also recommended. Since explosives are capable of radiating much more seismic energy than a vibrator source, even in a narrow frequency band, quasi-monofrequencies of

greater than 200 Hz may be obtained. Whether frequencies with high intensities greater than 200 Hz can be realized will be determined by the frequency analysis of records in the field.

The maximum holographic aperture that can be used is estimated to be 1500 feet square. This estimate is based primarily on the long path signal strengths from targets as calculated in the previous section. Figure 4-3 illustrates the outline of the aperture recommended for the experiment. The size of the aperture, and its position, was also influenced by the topography of the area. Roads run parallel to the west and south sides of the aperture and the topography becomes more rugged outside the aperture outline shown.

The seismic energy source (vibrator or explosives) is shown in the southeast corner of the aperture in Figure 4-3. This position, near the intersection of the two tunnels, was selected so that both tunnels could

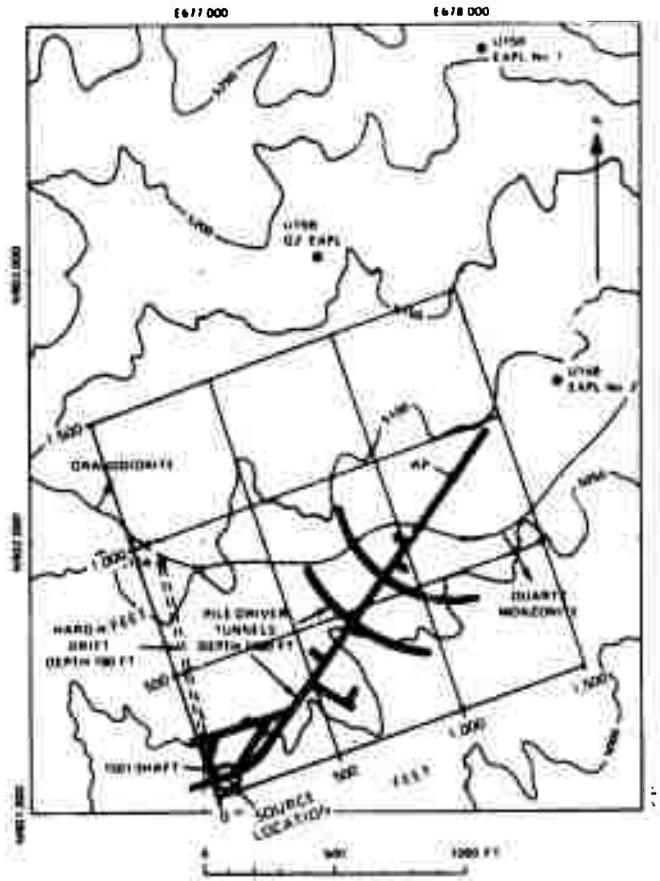

Figure 4-3 - Map Showing Location of Holographic Aperture with Respect to Nevada Test Site

be ensonified together more effectively to provide a maximum number of fringes across the aperture, and because it is further removed from the chimneys above the two nuclear shot points.

The number of fringes obtainable across the aperture due to reflections from the targets was determined by calculating the maximum difference in path lengths from a point on the tunnel vertically to the surface and to the edge of the array (see Figure 4-4). Velocity changes in the near-surface layers were accounted for. From these calculations, at a frequency of 200 Hz, the number of fringes across the aperture due to reflections from the deep tunnel is slightly more than four. The shallow tunnel will give seven fringes. The use of higher or lower frequencies will increase or decrease, respectively, the number of fringes.

The minimum fringe spacing across the aperture will determine the sampling interval (geophone spacing) required. In this case the minimum fringe spacing will be determined by reflections from the shallow tunnel. From Figure 4-4, the minimum spacing is 60 feet for an excitation frequency of 200 Hz. Since a function is adequately sampled if at least two samples per cycle (fringe) are taken,[23] a maximum geophone spacing of 30 feet is required. To ensure adequate sampling, however, a geophone spacing of 25 feet is specified.

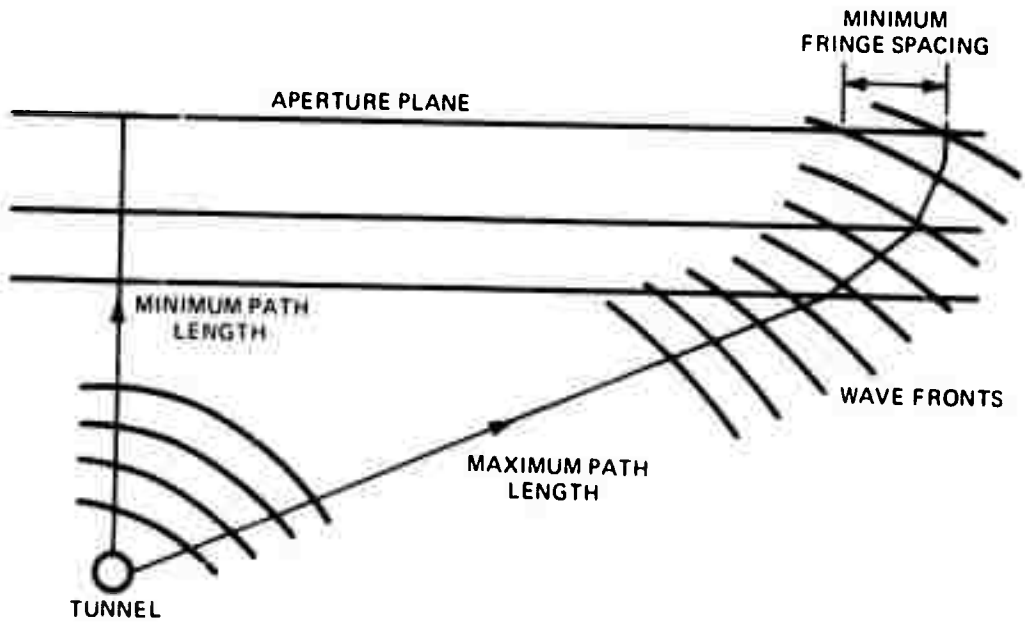

Figure 4-4 - Determination of Number of Fringes

The angular resolution α of a square aperture A with an illuminating wavelength λ is[24]

$$\alpha = \sin^{-1} (\lambda/A)$$

For this case, with f = 200 Hz,

$$\alpha = \sin^{-1} (100/1500) = 0.067 \text{ radians}$$

Since the two target tunnels are 780 and 1400 feet deep, the minimum distance Δ resolved will be

$$\Delta_{1400 \text{ Tunnel}} = 1400\ \alpha \tilde{=} 94 \text{ feet}$$

$$\Delta_{700 \text{ Tunnel}} = 760\ \alpha \tilde{=} 50 \text{ feet}$$

The resolvable distances are larger than the tunnel diameters (20 feet), hence images of the tunnels in the reconstructions will appear wider than they actually are.

4.3 HOLOGRAPHIC DATA ACQUISITION

Holographic data can be gathered using four different types of excitation: monofrequency CW, pulsed monofrequency CW, and frequency modulated or "chirp" pulses with a vibrator source, and with impulsive sources using explosives.

4.3.1 Monofrequency CW

Ensonification of a target area with a continuous monofrequency wave long enough to establish steady state conditions is the method that usually comes to mind when holography is considered. Using this method, every sampling point in the aperture simultaneously receives signals from every reflecting and scattering point and from every noise source in the earth within its range after steady state conditions are established. Theoretically, one could instantaneously sample each point in the array and obtain a hologram.

The disadvantage of this method in the seismic case is that strong reflections and refractions and signals from various noise sources (wind, traffic noise, etc.) are present along with weak signals from the desired targets. Random noise can be virtually eliminated from the received signal using phase detection and integration schemes, but the relative amplitudes of coherent reflecting, refraction, and scattering noises to the desired target signal remain high. The ratio of these strong undesired signals to desired target signals approaches 80 dB near the source (see Table 4-1), and in the present case is barely within the dynamic range of digital recording equipment.

The large amplitude ratios of undesired strong-to-weak target signals indicate that weak signal enhancement techniques (described in Section 6) might be used in order to image the target tunnels when a continuous monofrequency wave is used for seismic excitation.

An alternate method of defining the weak target signals in the presence of large interfering signals is to subtract the large signals from the total signal. The amplitude and phase of the Rayleigh wave at each geophone can be determined from a pulsed CW experiment (see Section 4.3.2). With this information, the Rayleigh wave can be effectively removed from the total signal during computer processing. Strong signals from the WL-AL reflecting interface may also be removed from the total signal in a like manner. The phase and amplitude of the interfering signals must be measured accurately to accomplish this, however.

Figure 4-5 shows the method in which data acquisition is accomplished. The geophone signal is amplified by a seismic amplifier, mixed with a reference signal and phase detected, integrated to eliminate random noise, and recorded on a digital recorder after analog-to-digital conversion. The "raw" received signal would also be recorded.

4.3.2 Pulsed Monofrequency CW

Ensonification with pulsed monofrequency waves differs from the CW case in that the pulse length is not long enough to establish steady state conditions. Hence, signals received at the sampling points in the aperture vary with time, and individual signals originating from various reflectors and scatterers and the Rayleigh wave signal can be separated on a travel-time basis. Random noise can be reduced from the received signals by recording and "stacking" (averaging) the received signal of several pulses. The stacking process increases the signal-to-random-noise ratio by a factor of $\sqrt{N}$, where N is the number of records averaged.

The advantage of this technique is that, although the relative amplitudes of strong and weak signals are not changed from the CW case, many of the undesired strong signals can be discriminated against in the time domain.

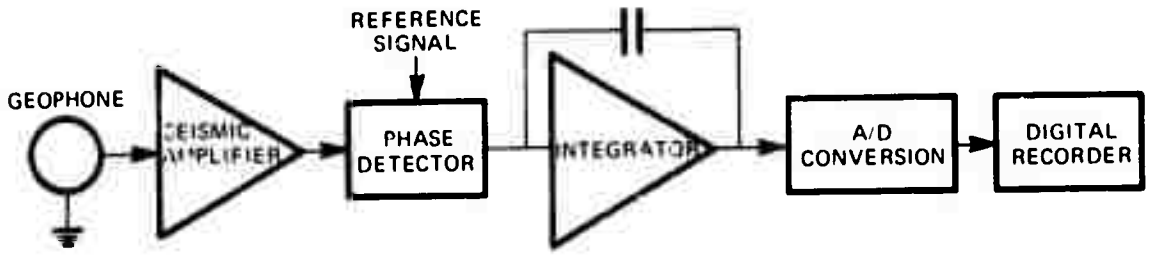

Figure 4-5 - Holographic Data Acquisition of Continuous Monofrequency Waves

The method of data acquisition for this case is shown in Figure 4-6. The geophone signal is amplified, converted from an analog to a digital signal, stacked (time averaged), and recorded on a digital recorder.

4.3.3 Impulsive (Explosive) Sources

The use of an explosive to generate seismic waves has two advantages. First, explosives are capable of radiating much more energy than that achieved with vibrator sources, even in a narrow band of frequencies. Second, if the explosive charge is detonated below the major reflecting layer (100 feet deep), the reflected and refracted waves no longer exist in the aperture plane. A large direct wave from the source is present. However, since this wave arrives at the geophones prior to reflections from the targets, it can be discriminated against by time gating or time discrimination.

Because explosives radiate a wide band of frequencies, the received signal must be filtered to obtain a quasi-monofrequency signal. This is most conveniently done in a digital computer. The minimum useful bandwidth Δf that can be analytically filtered depends on the duration T of the signal and is[25]

$$\Delta f = \frac{1}{4\pi T}$$

In this case the minimum signal length is expected to be 0.2 seconds resulting in $\Delta f = 0.4$ Hz. For a center frequency of 200 Hz, the bandwidth-to-frequency ratio is then 1 to 500.

The temporal coherence L of this monofrequency wave is[26]

$$L = \frac{1}{4} \frac{c^2/f^2}{\frac{c\Delta f}{f^2}} = \frac{c}{4\Delta f}$$

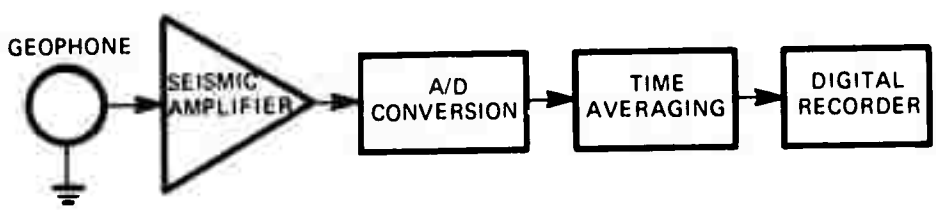

Figure 4-6 - Holographic Data Acquisition of Pulsed Monofrequency Waves

For a wave velocity of 20,000 feet/sec in granite, this gives a coherence length of 12,500 feet. This length is much greater than any target to be illuminated and greater than any signal path length; thus coherent illumination is assured.

The holographic data acquisition for this case is the same as used for pulsed CW (Figure 4-6) except that the time averaging of several records is not used.

4.3.4 Frequency Modulated (Chirp Pulses)

The application of holographic methods to the seismic problem is still fairly novel. We therefore feel that it is appropriate to incorporate a more conventional type of measurement into the test program in order to allow the holographic approach to be related to existing methods.

One relatively common seismic approach is to use a "chirp" input signal (i.e., an FM pulse) and employ correlation techniques to determine the elapsed time of a given reflected or scattered component quite accurately. At least three receivers are required to localize the point of scattering and, in practice, an array of geophones is used (either a true array or an array synthesized by moving one or more receivers). Under these conditions, there is quite a strong similarity between holography and the "chirp" technique. The main difference lies in the fact that use of the spatial bandwidth is emphasized in holography, whereas, the temporal bandwidth is most important in the "chirp" method.

Since a source which can be driven in a "chirp" manner is available, we propose that "chirp" experiments be carried out at the same time as the CW, pulse-modulated CW, and explosive measurements are made and with the same array.

4.3.5 Detection of Chimney Formed by Nuclear Explosion

The holographic experiments described in the previous subsections have been designed primarily to detect the tunnel targets. To ensonify the chimney area formed by the Piledriver nuclear explosion, the seismic source should be moved to a point in the aperture over the chimney. It is recommended that an explosive charge be used as the energy source. This recommendation is made primarily in the interest of economy.

During the holographic data acquisition described earlier, one line of geophones (24 detectors) will be used at a time to sample the aperture. With this line in place, data will be obtained with the different methods of seismic excitation. The line of geophones will then be moved to sample other points in the aperture for the same excitations. This process will be repeated until all the sampling points in the aperture have been interrogated. During this whole operation, it is desirable that the vibrator source be left in the same position to ensure that the coupling remains as constant as possible. Since the vibrator position

will be fixed, the use of the vibrator to ensonify the chimney would require "sweeping" out the entire array another time. If an explosive source is used to ensonify the tunnel, however, the data can be acquired during the original aperture sampling operations.

The frequency component of the explosive source used to ensonify the chimney area will be the highest useful quasi-monofrequency determined from preliminary experiments performed during the field test (see Section 4.4).

4.4 AUXILIARY EXPERIMENTS

The calculations previously carried out to determine the important parameters of the Nevada Test Site will be supplemented by a series of preliminary tests. These tests will be separated into two operations as described below. The purpose of each test is listed and interpretation of the records will be done in the field. In this way, an optimum holographic recording array will be specified. Preliminary tests will be run with the geophone spread parallel to tunnel and directly over it. Both Hard Hat and Piledriver tunnels will be investigated.

4.4.1 Refraction Survey

The reflection survey using the vibrator source will be made at 200 Hz and 500 Hz. The vibrator will be moved to both ends of the geophone line. Paper records will be interpreted on site to obtain local wave velocities, evaluate local variations in layering, and determine surface wave characteristics. In addition, changes which have occurred due to the nuclear detonations will be evaluated.

4.4.2 Reflection Experiments

Using information obtained in the refraction survey, geophones will be spaced as they will be in the holography array. A reflection survey will be run using explosives emplaced in the altered layer. Shooting will be done from both ends of the line and paper records obtained. The purpose is to determine the highest frequency which can be obtained from explosives and provide a strong signal to ensonify the tunnel. The explosive charge weight will be adjusted to enhance higher frequencies. In addition, good control will be obtained on vertical velocities by observing the travel times of body waves which emerged directly from the detonation. Following this, a reflection survey will be made with the vibrator source at the surface and geophones placed in drill holes which extend down to the altered layer. The vibrator will be run from both ends of this geophone spread. A survey of this type will be especially useful as a check on validity of the tunnel response model since surface waves and the strong P refraction arrival will be attenuated.

The geophones will then be removed from the holes and placed on the surface. The spacing of a cluster of geophones at the

surface will be optimized to attenuate Rayleigh waves. The vibrator will again be run from both ends of the line. Paper and magnetic tape records will be obtained from these tests. Evaluation of this reflection survey to optimize the holography experiment will include travel time corrections, attenuation, time gating criteria for pulse mode experiments, and stacking requirements.

4.5 EQUIPMENT REQUIREMENTS FOR HOLOGRAPHIC FIELD EXPERIMENT

Essentially all the equipment and instrumentation required to perform a seismic holography field experiment is presently available at United Geophysical Corporation, a subsidiary of The Bendix Corporation. Modifications of an existing vibrator source (described in Section 5.1) is required. The design and fabrication of phase detection and integration instruments for the recording of CW holographic data is also required. Similar instrumentation has been designed and used by the Bendix Research Laboratories in the past, however, so a minimum of design effort is required here.

A brief description of some of the key equipment available for this experiment is given below.

4.5.1 Vibrator Source for Holographic Surveys

The vibrator system which will be used for all holographic surveys is a modified version of an existing unit operated by United Geophysical Corporation. The unmodified and modified vibrator characteristics are given in Section 5.1.

The modified vibrator system will provide an actuator output of full rated force (10,000 pound vector) at 500 Hz. The displacement amplitude of the reaction mass will be 5×10^{-5} inch. At 200 Hz the expected amplitude is 2.5×10^{-3} inch and at 100 Hz, 1×10^{-2} inch.

The vibrator can give a continuous wave (CW) output, pulse modulated (PM) or sweep frequency (chirp) output depending upon survey needs.

4.5.2 Geophones for Holographic Surveys

Geophones of the required capability (i.e., high voltage output, and sensitive to high frequencies) are readily available. The Geo Space Corporation Type GSC-11D is an example as is the Electro-Technical Labs. Division EVS-2 detector. For placement in drill holes, special cases are available to protect the geophone mechanism from water intrusion. For placement at the surface, a normal Spike base will be used. The United Geophysical Corporation uses such geophones in its daily operations.

- Characteristics of the GSC-11D

  Natural undamped frequency, 10 Hz

  Frequency response essentially flat from 30 Hz to 500 Hz

  Sensitivity, 0.6 V/in/sec

- Characteristics of Electro-Tech EVS-2

  Natural undamped frequency, 20 Hz

  Frequency response essentially flat from 100 Hz to 300 Hz

  Sensitivity, 0.4 V/in/sec

4.5.3 Amplifier and Recording System for Holographic Surveys

Recording of seismic signals will be carried out using an amplifier system of the United Geophysical Corporation. The unit is a Geo Space Model 211 High Gain/Low Distortion Digital-Analog Seismic Amplifier System. This system combines 24 channels of seismic auxiliary channels, control circuitry including gain programming. Solid state components and circuit techniques are used. The amplifier fully meets the needs of digital recording and analog recording. The system can be operated with automatic gain control or in a programmed gain mode.

Some characteristics of the system are:

Frequency Response, 3 to above 500 Hz

Equivalent Input Noise, 0.1 microvolt

Dynamic Range, 120 dB

The recording system is a Leech Control Recorder System Model 3309. This system includes a Model 339 Pulse Code Modulation System, Model 3200 Magnetic Tape Recorder, Model 3330 Power Supply and a MTR-3200 Recorder-Reproducer Tape Deck.

Some characteristics are:

Sampling Rate, 1 millisecond

Dynamic Range, 78 dB

Recording Time, 3 sec to 10 sec
in increments of 1 sec or Manual

4.6 SUMMARY OF EXPERIMENTS

It is recommended that an experimental field test be performed to evaluate the capability of holographic techniques in detecting and imaging underground objects. The experiments to be performed are discussed in Section 4.3 and 4.4 and include preliminary refraction and reflection experiments to optimize the holographic data acquisition. Holographic data would be obtained using monofrequency continuous wave

excitation, pulsed monofrequency excitation, frequency modulated (chirp) excitation, and quasi-monofrequency excitation using impulsive (explosive) sources. A comparison of the results using these different excitations should give an insight into the merits of each.

It is estimated that a field experiment of this magnitude will require about one month to perform. The total time required to prepare for the experiment and to process and analyze the data would be aproximately one calendar year.

A possible daily schedule of activities during the field experiment is given below.

Day	Operations
1.	a. Move on site.
	b. Survey Hard Hat refraction line.
	c. Test vibrator and recording truck systems.
2.	a. Refraction survey of Hard Hat site.
	b. Initial geophone spread based upon previously established geologic model.
	c. Survey Piledriver refraction line.
3.	a. Drill Hard Hat reflection line. Spacing of drill holes and depth of drilling is determined from geologic model and interpretation of Hard Hat refraction survey.
	b. Refraction survey Piledriver line.
4.	a. Complete drilling of Hard Hat reflection line.
	b. Emplace geophones and load shot holes.
	c. Start survey of two-dimensional holographic array.
	d. Interpretation of Piledriver refraction survey data.
5.	a. Hard Hat reflection survey Part 1. Shot in altered layer and geophones at surface. Shoot both ends of the line.
	b. Drill Piledriver reflection line.
	c. Continue survey of holographic array.
6.	a. Continue reflection survey at Hard Hat site Part 2. Vibrator on surface and geophones in drill holes.

	b.	Complete drilling of Piledriver reflection line. Emplace geophones and load shot holes.
	c.	Continue survey of holographic array.
7.	a.	Continue reflection survey at Hard Hat site Part 3. Vibrator on surface and surface geophones. The number of geophones per amplifier and spacing of geophones will be determined by the geologic model and modifications to that model obtained from the reflection and refraction data.
	b.	Continue survey of holographic array.
8.	a.	Continue reflection survey at Hard Hat.
	b.	Continue survey of array.
9.	a.	Reflection survey at Piledriver. Part 1. Shot in altered layer and geophones at surface.
	b.	Continue survey to delineate nuclear detonation area
10.	a.	Reflection survey at Piledriver. Part 2. Vibrator at surface and geophones in altered layer.
	b.	Continue survey of holographic array.
11.	a.	Reflection survey at Piledriver. Part 3. Vibrator on surface and geophones on surface.
12. ↓ 20.	a.	Begin holographic data acquisition. For a square array containing 900 sampling points, by sampling 24 points at a time (one line of geophones), approximately 9 days will be required to sample the entire aperture. This allows about 4 moves of the geophone line per day.
21.	a.	Move out with equipment.

SECTION 5

EVALUATION OF SEISMIC ENERGY SOURCES AND DETECTORS

Presently available commercial seismic energy sources and detectors were evaluated to determine if their characteristics were consistent with system requirements. The characteristics of the useful available or modified components which were used in the design of the holographic experiment were discussed in Section 4.

5.1 SEISMIC ENERGY SOURCES

Hydraulically driven vibratory sources have been used in the seismic exploration field for several years. Since they are primarily used for the petroleum industry and the need is to define the earth's layering structure at great depths, these sources are generally designed to operate at frequencies from about 5 to less than 100 Hz.

Two approaches can be taken to obtaining higher frequency sources capable of generating a monofrequency signal: a new type of source might be designed, or presently available vibrators might be modified making them capable of higher frequency operation. Since the first approach would be expected to be more costly, an effort was made to see if the second approach was feasible.

It was determined that presently available vibrators could be modified to operate as high as 500 Hz. Shore Western Co., Monrovia, California, has had experience in modifying vibrator assemblies to operate at higher frequencies. Discussions with Shore Western resulted in their proposing the modification of a Wabco Vibrator Model 600 B-D (used by a subsidiary of the Bendix Corporation) capable of operating in the frequency range from 5 to 500 Hz.

The unmodified vibrator is described below.

Vibrator Model 600 B-D mounted on a special off-road vehicle.

Electronics: (Solid State)

Designed by Bendix Research Laboratories

Phase Compensator - Zero Crossover Principle

Wabco Vibrator Assembly:

Frequency range to 200 Hz

Servo Valve - Hydraulic Controls DS4-50G

Weight Assembly - Wabco Low Profile;
5 Square Inches Ram Area;
Vertical Displacement ±1.25 inch

Reactionary Mass - 4000 pounds

Base Plate - 83.5 inches x 36.75 inches
Air Bag Isolation

Base Plate Hold Down Weight - 2)000 pounds

Hydraulic Power Supply

GMC Diesel 6-21

Kline Pump Model 1265, 110 GPM

The modifications required to provide 5-500 Hz operating capabilities are listed below.

(1) Installation of a manifold and high frequency servovalve (Model SV-220) in lieu of the existing valve

(2) Increase Ram area to 9 square inches

(3) Install an additional electronic amplifier (200 Watt peak) to drive the new valve

(4) Implement a second feedback loop based on slave valve (second stage) position

(5) Perform major modifications to the ground contact pad to transmit the 500 Hz vibration into the ground

(6) Reinforce vibrator structure to assure that high frequency vibration will not cause failures when subjected to extended field use

(7) Establish the exact performance of the unit in terms of ground vibration versus frequency

These modifications to the system will provide an actuator output of full-rated force (10000 pounds vector) at 500 Hz. The displacement of the reaction mass will be 5×10^{-5} inch. At 200 Hz, the expected displacement amplitude is 2.5×10^{-3} inch and at 100 Hz 1×10^{-2} inch.

5.2 SEISMIC DETECTORS - GEOPHONES

Commercially available geophones used in the seismic exploration field were found to be adequate for the holographic system requirements. Since the minimum useful output of geophones is related to the noise level of seismic amplifiers (typical amplifier noise is 0.1 μV), geophones capable of detecting ground displacements resulting in an 0.1 μV output are sufficient.

One such geophone is the Geo-Space Type GSC-11D detector. It is a velocity-sensitive phone and has a flat response of 0.6 V/in/sec over the frequency range 20 to 500 Hz.

Since a minimum output of 0.1 μV is required, the minimum velocity must not be less than

$$v = \frac{10^{-7}\ V}{0.6\ V/in/sec} \approx 1.7 \times 10^{-7}\ in/sec$$

Since $v = 2\pi fd$, where d is ground displacement, the minimum displacement required to obtain 0.1 μV is

$$d(100\ Hz) = 2.7 \times 10^{-10}\ inch$$

$$d(200\ Hz) = 1.35 \times 10^{-10}\ inch$$

$$d(500\ Hz) = 5.4 \times 10^{-11}\ inch$$

These minimum displacements indicate that both tunnels at the field test site (see Table 4-1) are not detectable at 500 Hz, but both can be detected at lower frequencies.

SECTION 6

HOLOGRAPHIC WEAK SIGNAL ENHANCEMENT STUDIES

The development of a holographic weak signal enhancement technique was initiated at Bendix Research Laboratories prior to the award of this contract. Further studies of this technique as it pertains to seismic holography were made during this program. This technique, which lends itself to computer simulation, has shown promise in defining images of targets that have signal strengths too weak to be seen by conventional holographic imaging (reconstruction) techniques, as is often the case when a scattering target is located above or below a strong signal reflecting layer.

The theory used to develop this technique and its implementation were described in a paper by R. K. Mueller, R. R. Gupta, and P. N. Keating, "Holographic Weak-Signal Enhancement Technique," J. Appl. Phys., Vol. 43, February 1972.[7] Rather than duplicating much of this paper here, a copy is included in this report as Appendix A.

During this program, two different computer models representing a two-layer model of the earth were investigated. The first model (Figure 6-1) contained a weak scattering target below the reflecting interface of the two layers. This case closely corresponds to the earth model developed in Section 2 to represent the selected field test site. The second model contained a weak scattering target above the reflecting layer. In the computer simulations, all mode conversions (for example, P-waves to S-waves) are allowed at both the reflecting and scattering surfaces except when otherwise specified. Lossless media, however, are assumed for both models.

The scattered fields in the holographic plane are based upon the theoretical analysis of Knopoff[8] who has derived expressions for the scattering coefficients for a plane P-wave incident on a perfectly rigid spherical obstacle. The sphere is assumed small compared to the incident wavelength. Knopoff's analysis finds that the scattered P-wave spatial distribution is doubly circular, equal in the forward and back directions with nulls normal to the direction of the propagation. The scattered S-wave distribution is also doubly circular, with a maximum amplitude about three times greater than the scattered P-waves, but rotated in space through 90 degrees so the null lies in the direction of propagation.

Results using the first model are shown in Figures 6-2 through 6-4. Figure 6-2 shows a conventional reconstruction of the strong reflecting target (hereafter called S_1) and the weak scattering target (hereafter called S_2) in the image plane of S_1. Only the image of S_1 can be seen. Figure 6-3 is again a conventional reconstruction, this time in the image plane of S_2. Again only the out-of-focus image of S_1 is

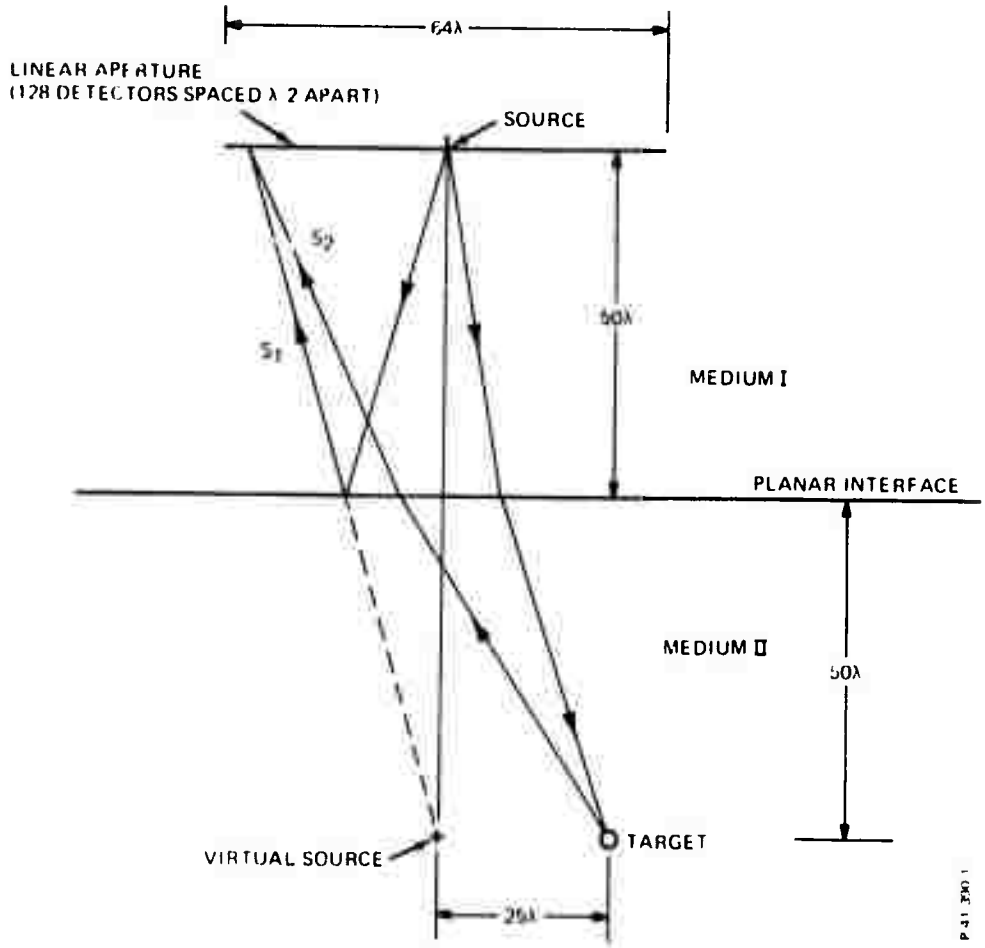

Figure 6-1 - Layout in the Computer Simulation Model

visible. Figure 6-4 shows the results when weak signal enhancement techniques (WSET) are applied. The image of S_2 is clearly visible, along with its conjugate image, and the image of S_1 is suppressed.

The results using the second model (Figure 6-5) are shown in Figures 6-6 through 6-15. Figure 6-7 shows a conventional reconstruction for the case of a single scattering target. The reconstruction is in the plane of the scatterer. Only the out-of-focus image due to the reflecting layer can be seen; S_2 cannot be resolved. Figure 6-7 shows the result for the same case when WSET is used and only scattered P-waves are allowed. The image S_2 is now well resolved. Figure 6-8 is the result for the same case as Figure 6-7 except that random scattering targets (noise) are now included in the model. Again, good image resolution is obtained. Figure 6-9 again gives the results for a single scatterer (S_2), but here both scattered P- and S-waves are allowed. In this case,

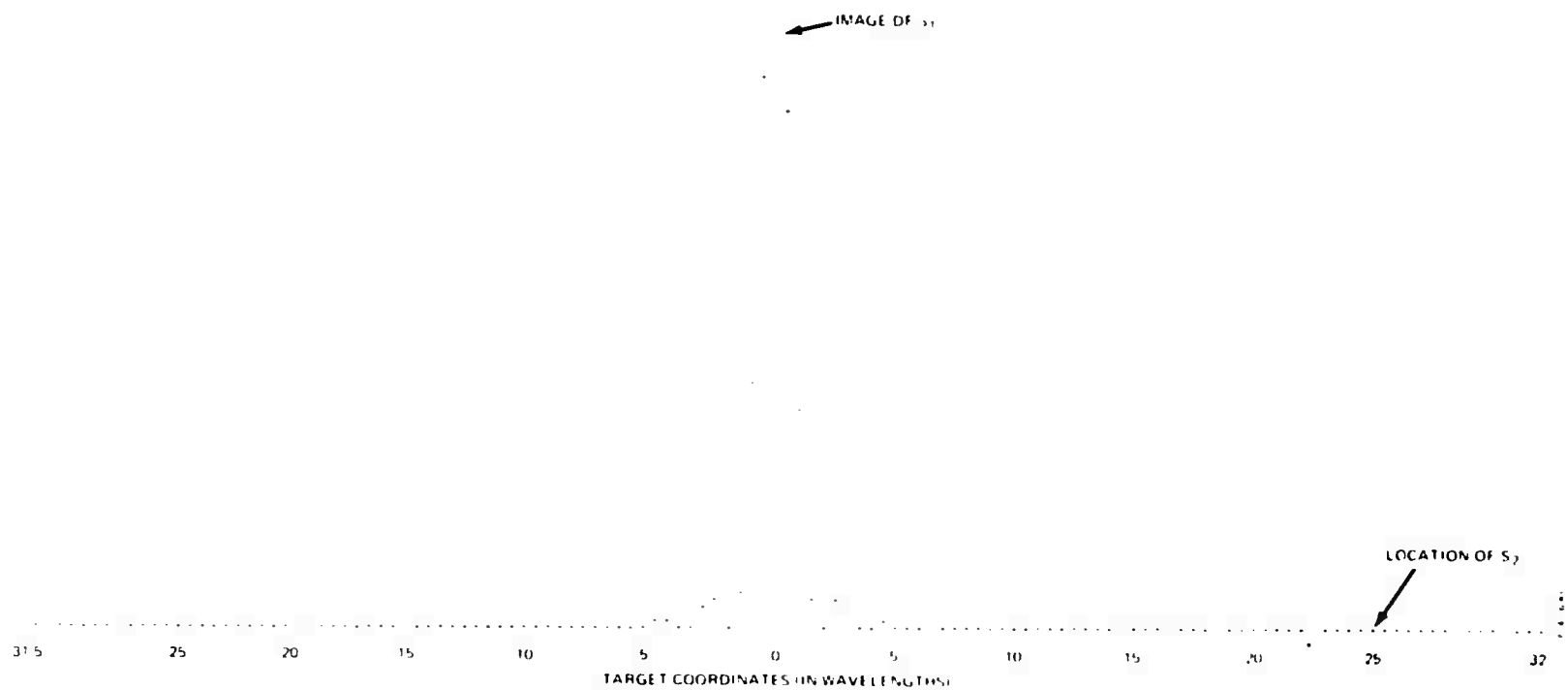

Figure 6-2 - Conventional Holographic Reconstruction of (S_1 + S_2) in Image Plane of S_2. S_2 is Not Visible.

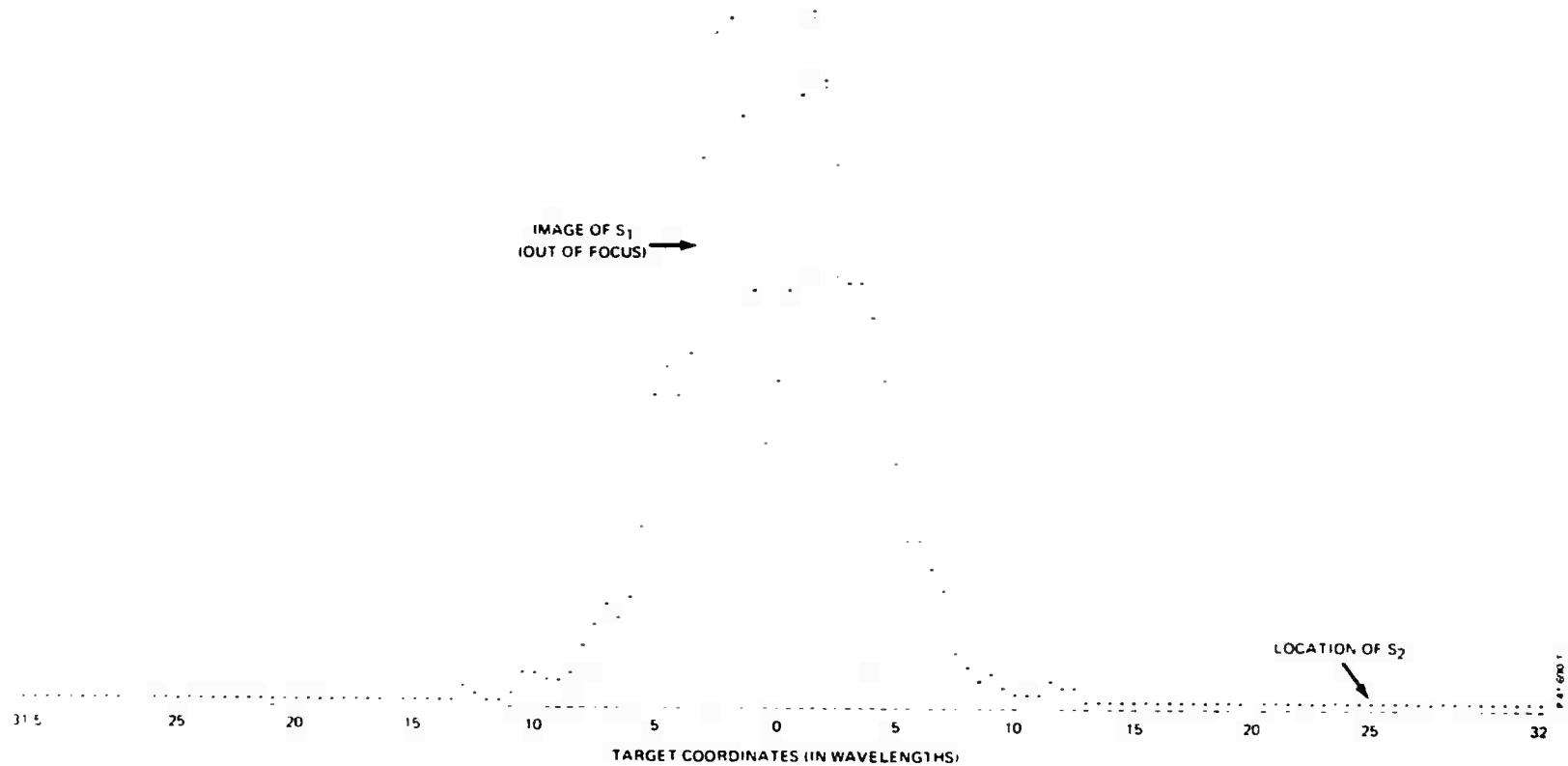

Figure 6-3 - Conventional Holographic Reconstruction of (S_1 + S_2) in Image Plane of S_1. S_2 is Not Observable.

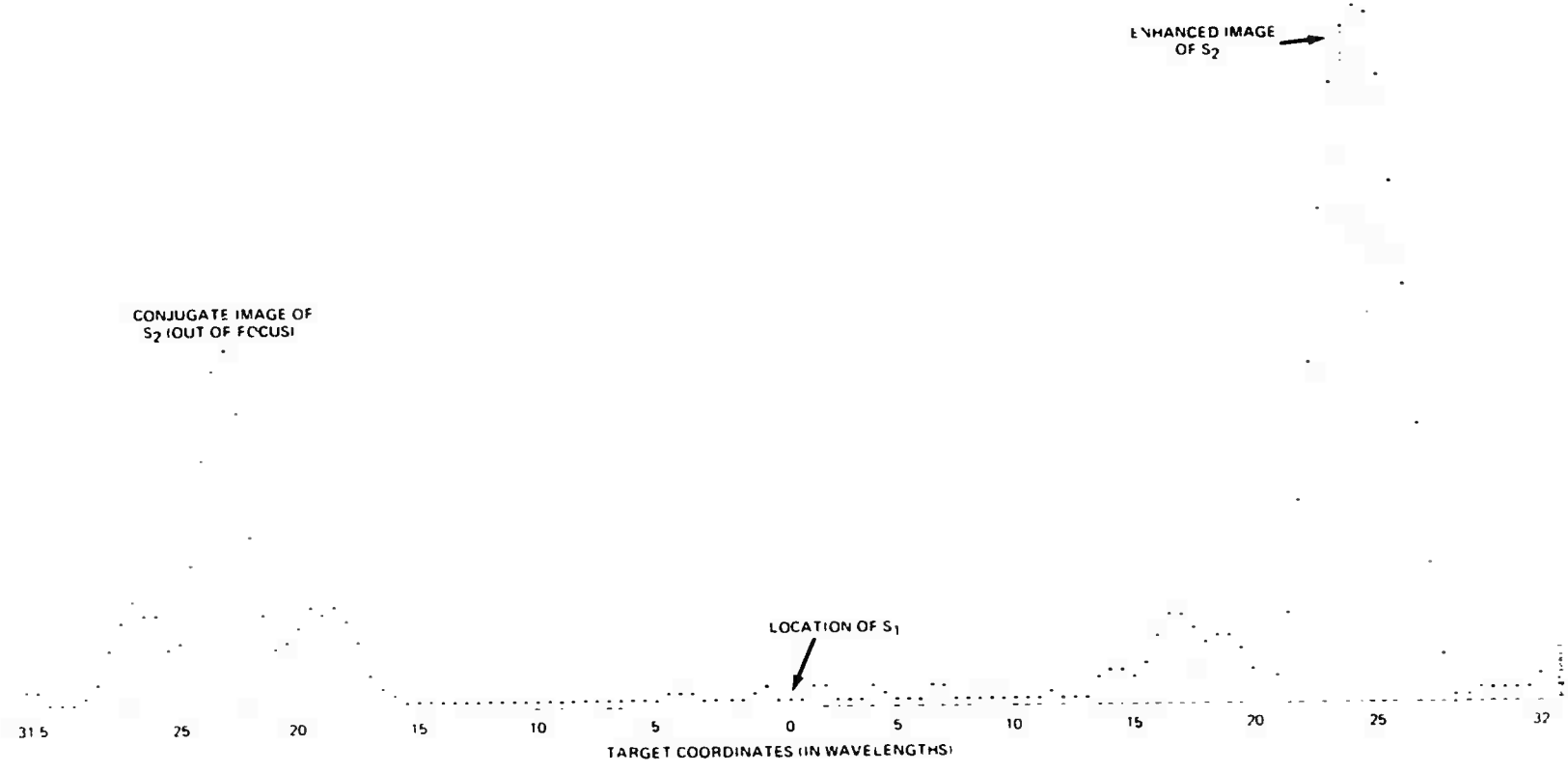

Figure 6-4 - Weak Signal Enhancement Reconstruction in the Image Plane of S_2. S_2 is Much Larger Than S_1 After Enhancement.

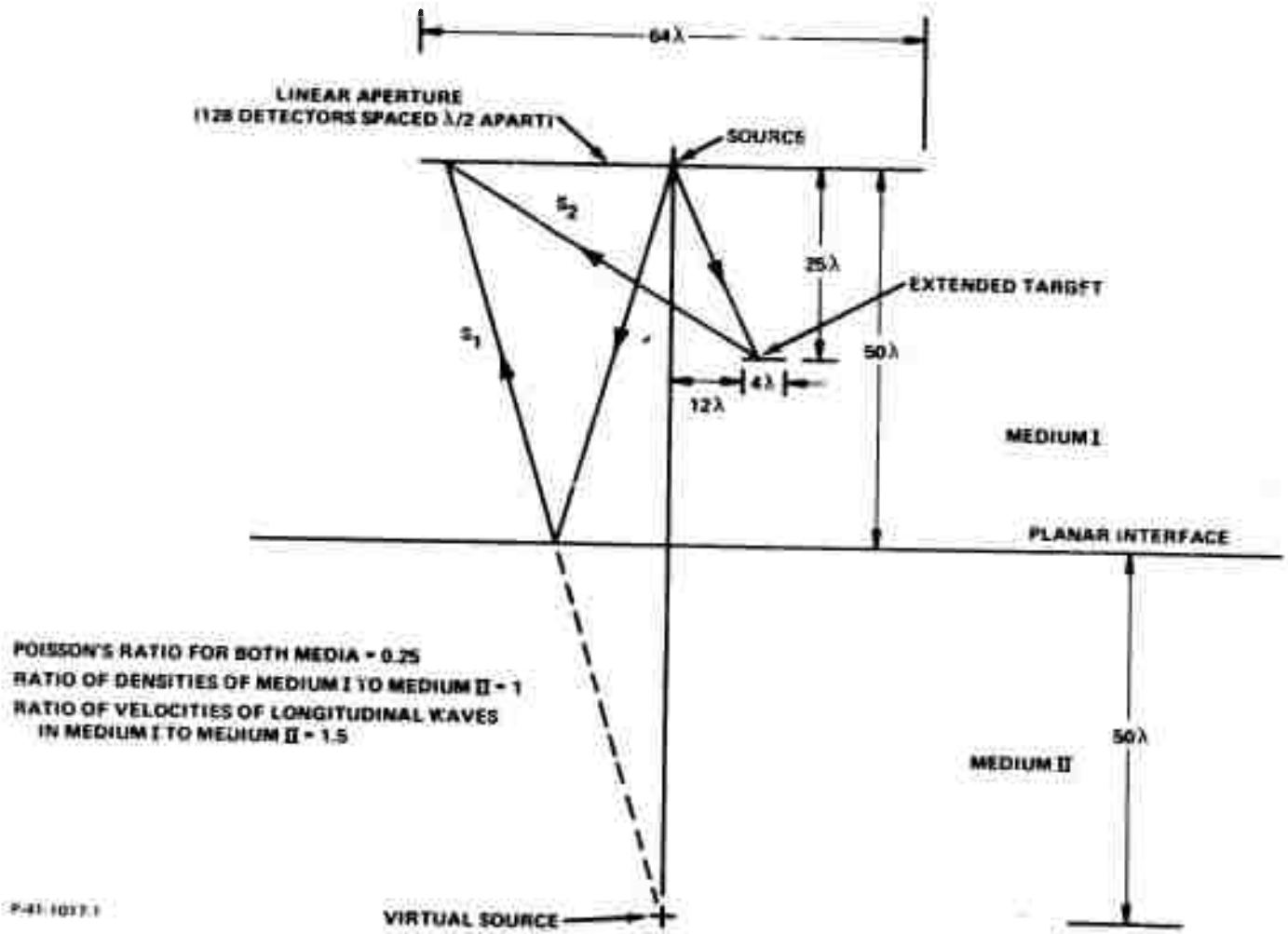

Figure 6-5 - Computer Simulation Model

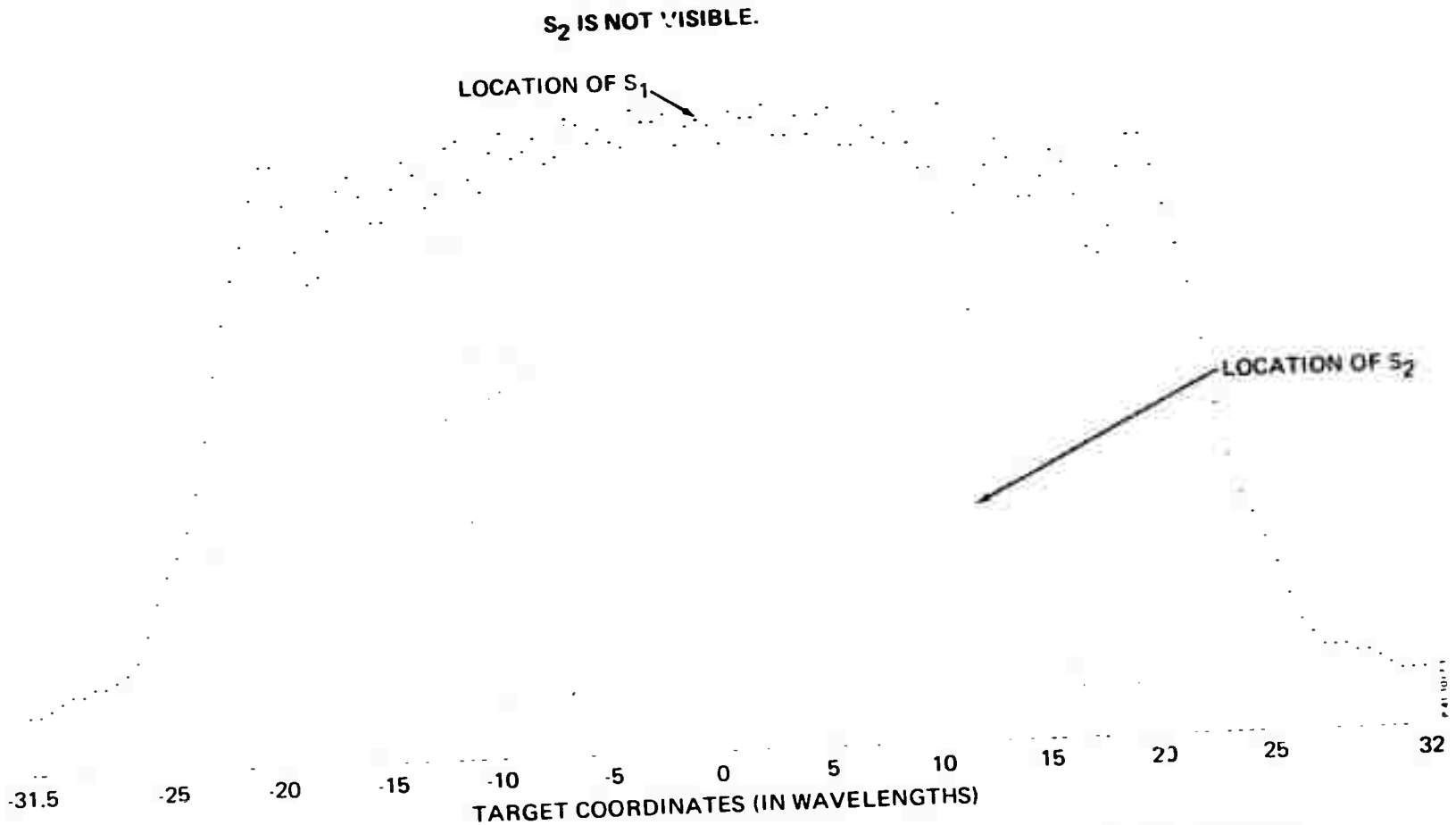

Figure 6-6 - Reconstruction of $(S_1 + S_2)$ in Image Plane of S_2. (S_2 is Not Visible)

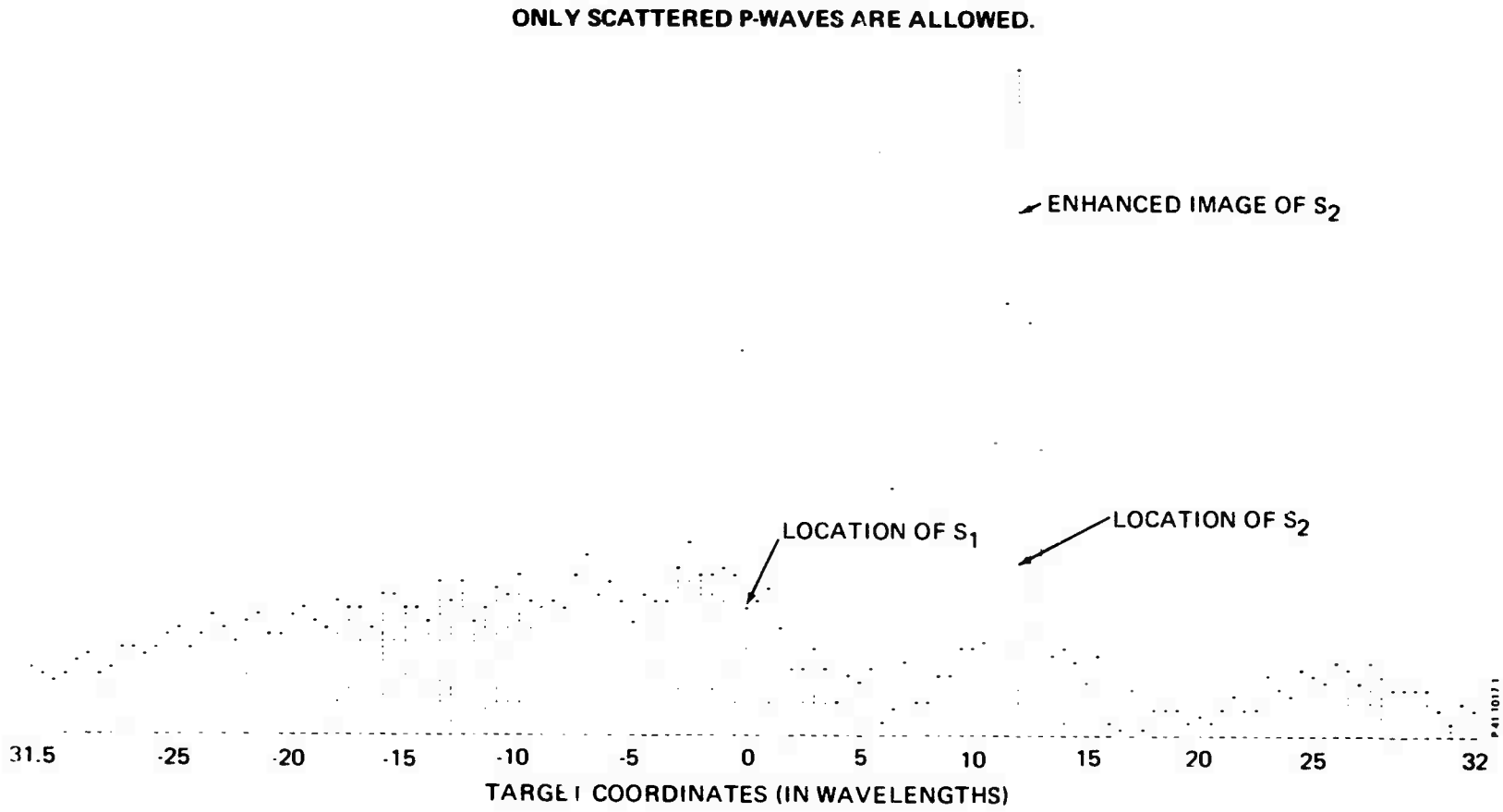

Figure 6-7 - Weak Signal Enhancement Reconstruction of a Single Scatterer in Image Plane of S_2. Only Scattered P-Waves are Allowed.

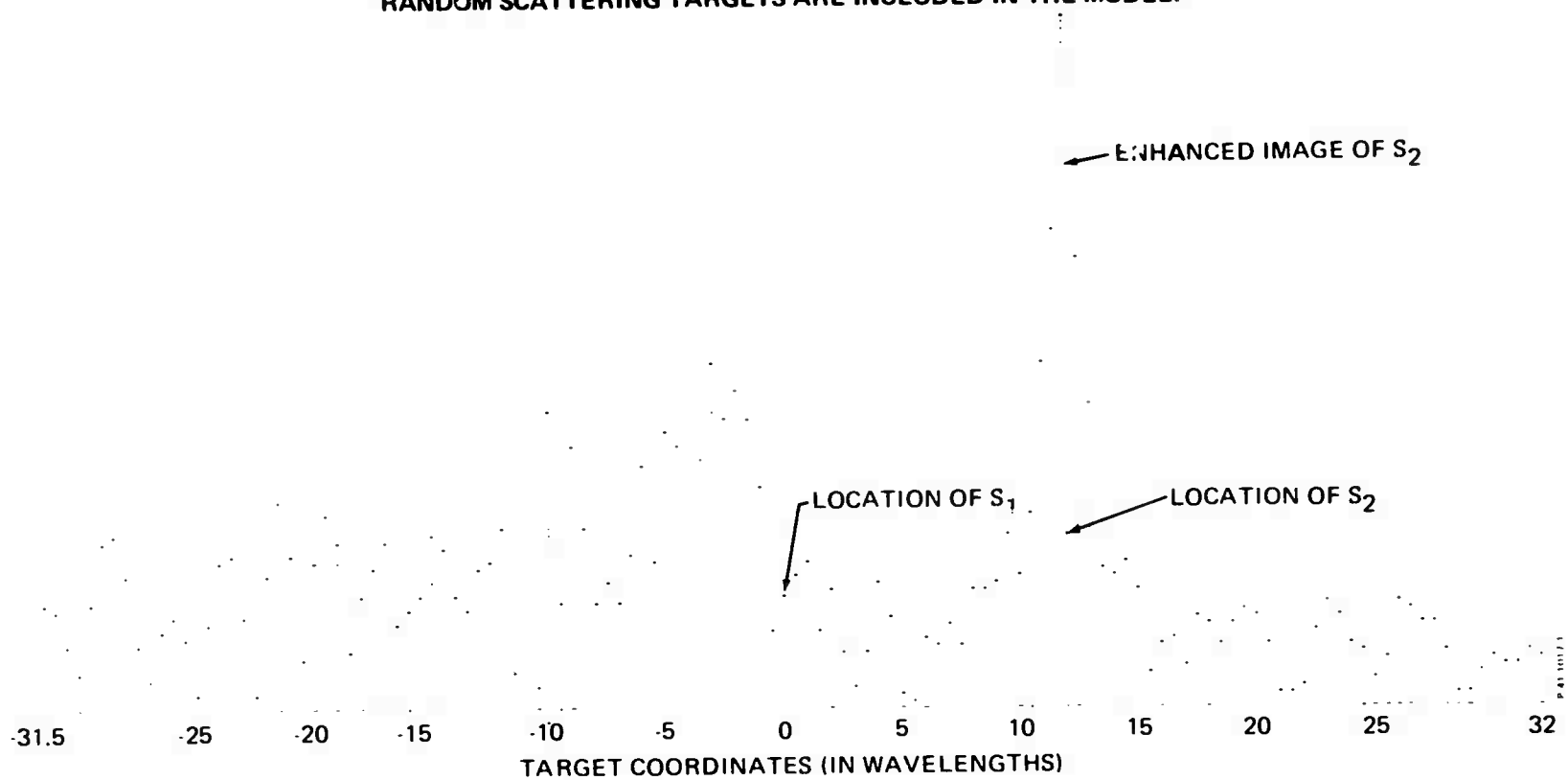

Figure 6-8 - Weak Signal Enhancement Reconstruction of a Single Scatterer in Image Plane of S_2. Random Scattering Targets are Included in the Model.

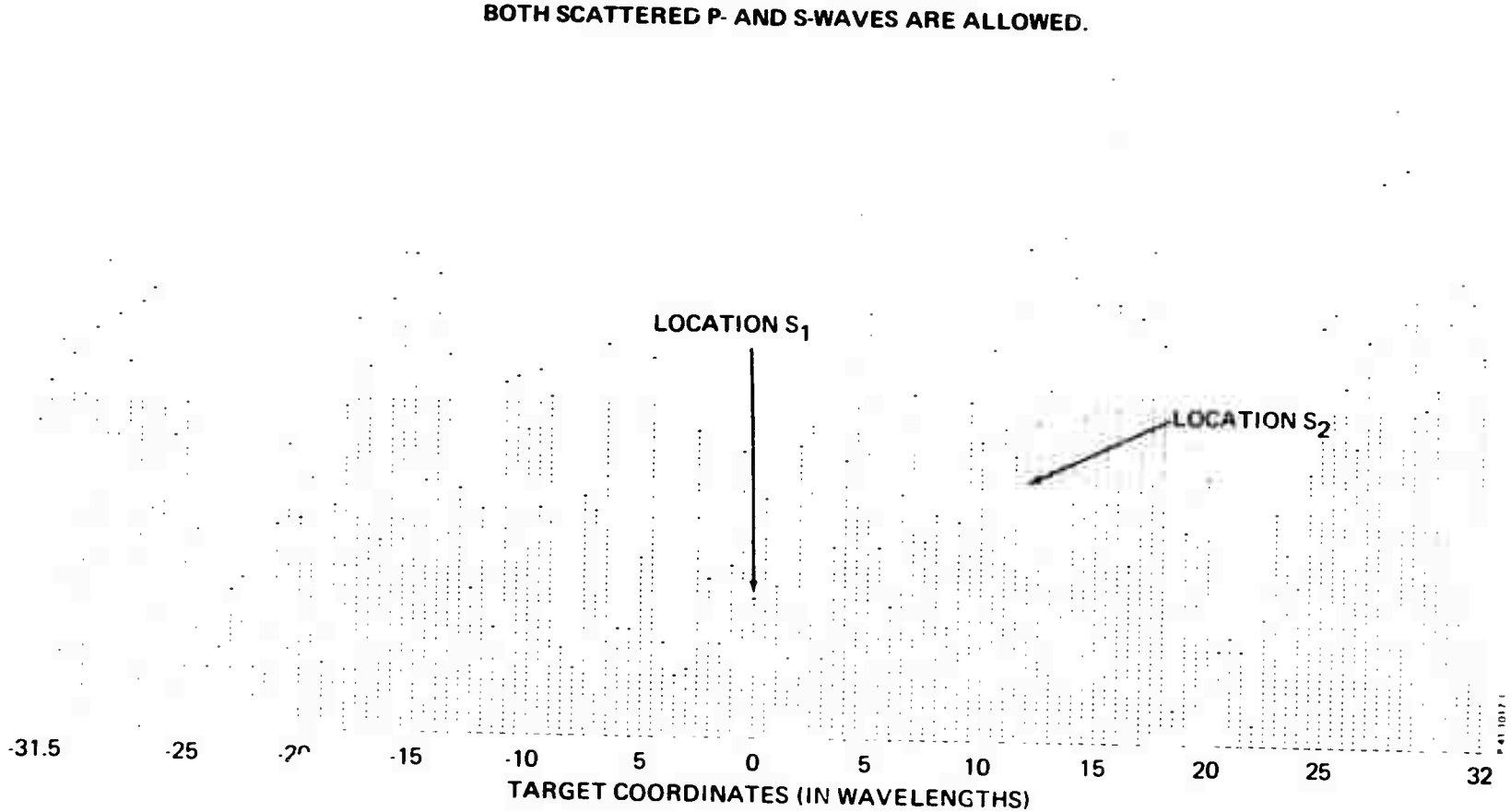

Figure 6-9 - Weak Signal Enhancement Reconstruction of a Single Scatterer in Image Plane of S2. Both Scattered P- and S-Waves are Allowed.

interference between S- and P-waves greatly reduce the resolution of the reconstructed image.

When an extended scatterer (S_2) is used instead of a single scatterer, the results are as follows. The conventional reconstruction is essentially the same as shown in Figure 6-7 for a single scatterer, i.e., S_2 cannot be resolved. Figure 6-10 shows the results when only scattered P-waves are allowed and with no random scatterers. Figure 6-11 is for the same case, except random scatterers are included in the model. In both cases, S_2 is again well resolved. Figure 6-12 gives the results when both scattered P- and S-waves are allowed. The S-wave interference is again apparent in that it greatly reduces the S_2 image resolution.

The results given above indicate that, at least for the model shown, interference due to scattered S-waves influence the resolution of the desired image to a greater extent than does the presence of random noise sources. The computer model used, in which a lossless medium is assumed, is actually a worse case condition with respect to S-wave interference. In a lossy medium, S-waves typically attenuate more than P-waves, which should result in less S-wave interference at the hologram plane. Examples of the increase of resolution obtained when shear waves are allowed to attenuate more than compressional waves are shown in Figures 6-13 through 6-15. In Figure 6-13 the shear waves are attenuated by a factor of 2, in Figure 6-14 by a factor of 4, and in Figure 6-15 by a factor of 8. As would be expected, the image resolution improves with shear wave suppression.

The results given in this section indicate that the weak signal enhancement technique can be a powerful tool in the reconstruction of seismic holograms.

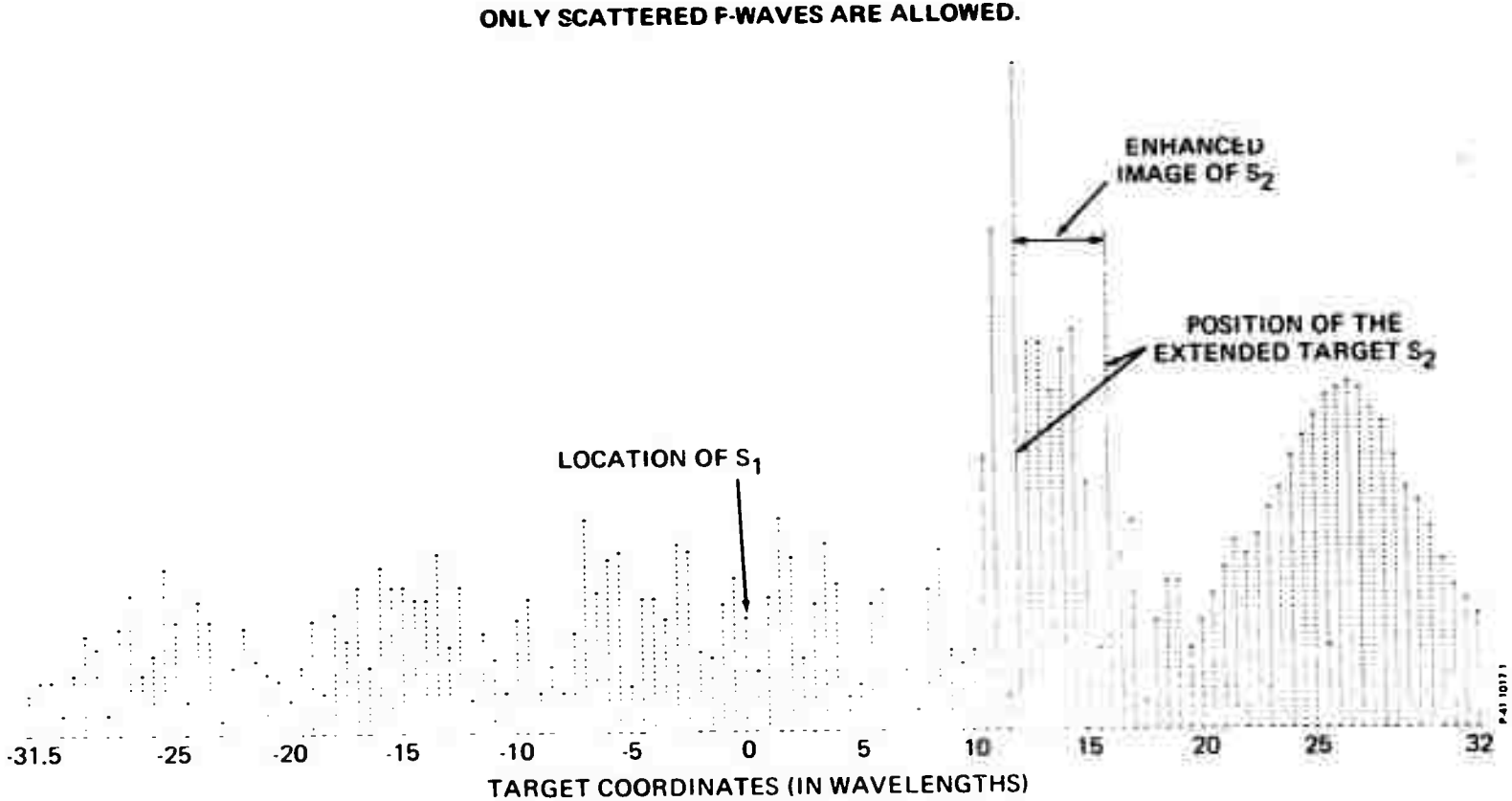

Figure 6-10 - Weak Signal Enhancement Reconstruction of Extended Scatterers in the Image Plane of S_2. Only Scattered P-Waves are Allowed.

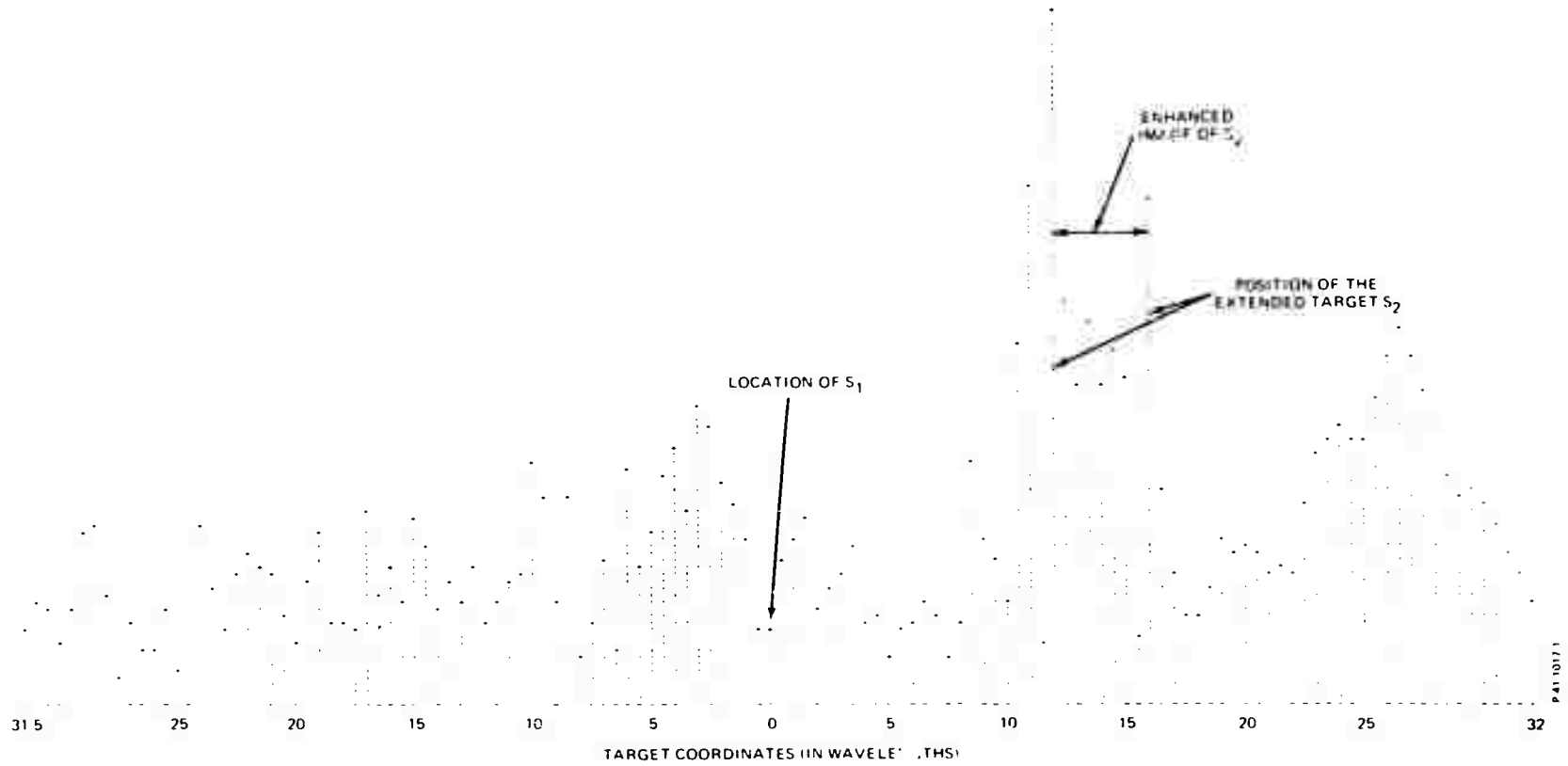

Figure 6-11 - Weak Signal Enhancement Reconstruction of Extended Scatterers in the Image Plane of S_2. Random Scattering.

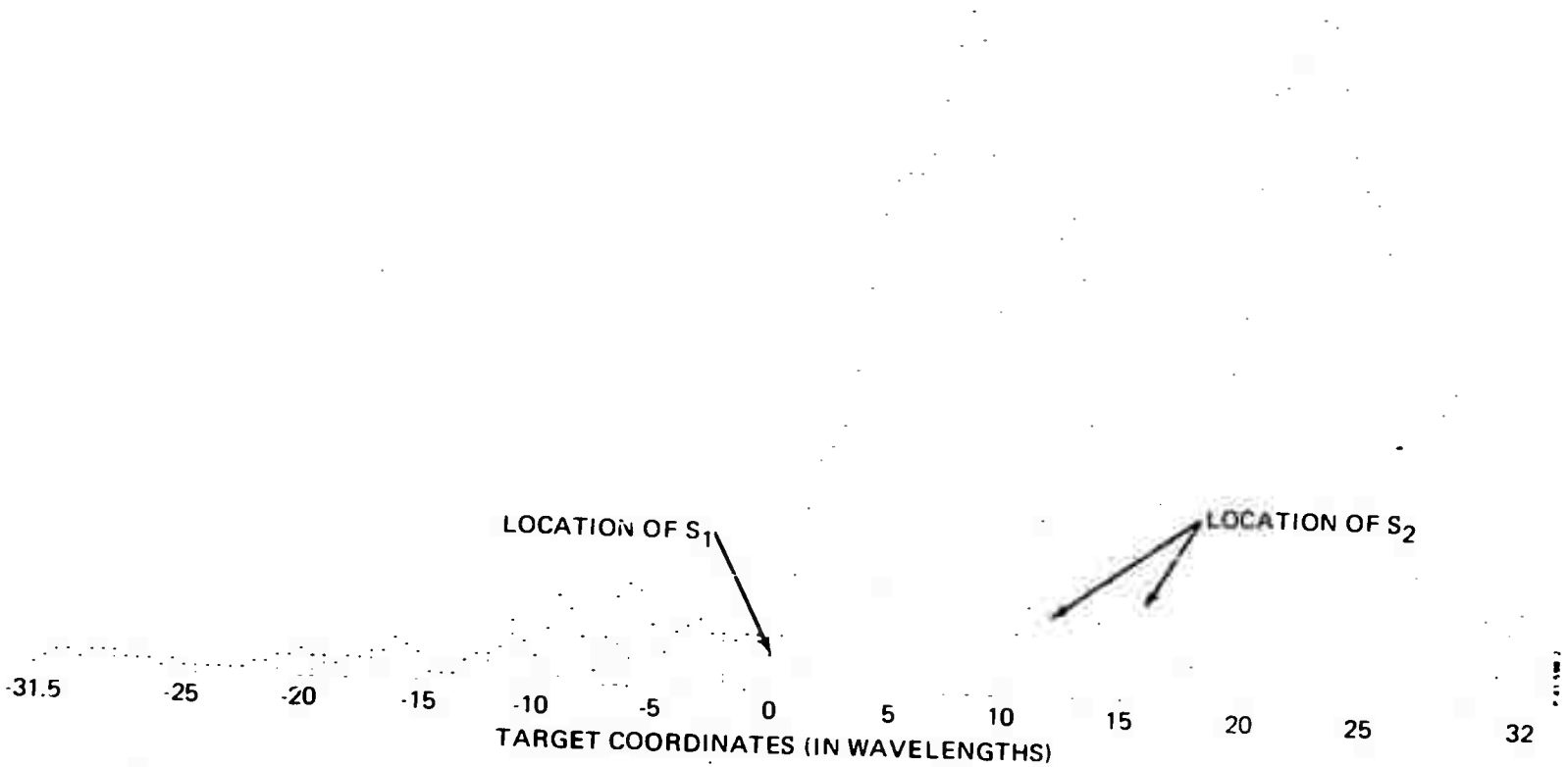

Figure 6-12 - Weak Signal Enhancement Reconstruction of an Extended Scatterer (4λ) in Image Plane of S_2. Both Scattered P- and S-Waves are Allowed.

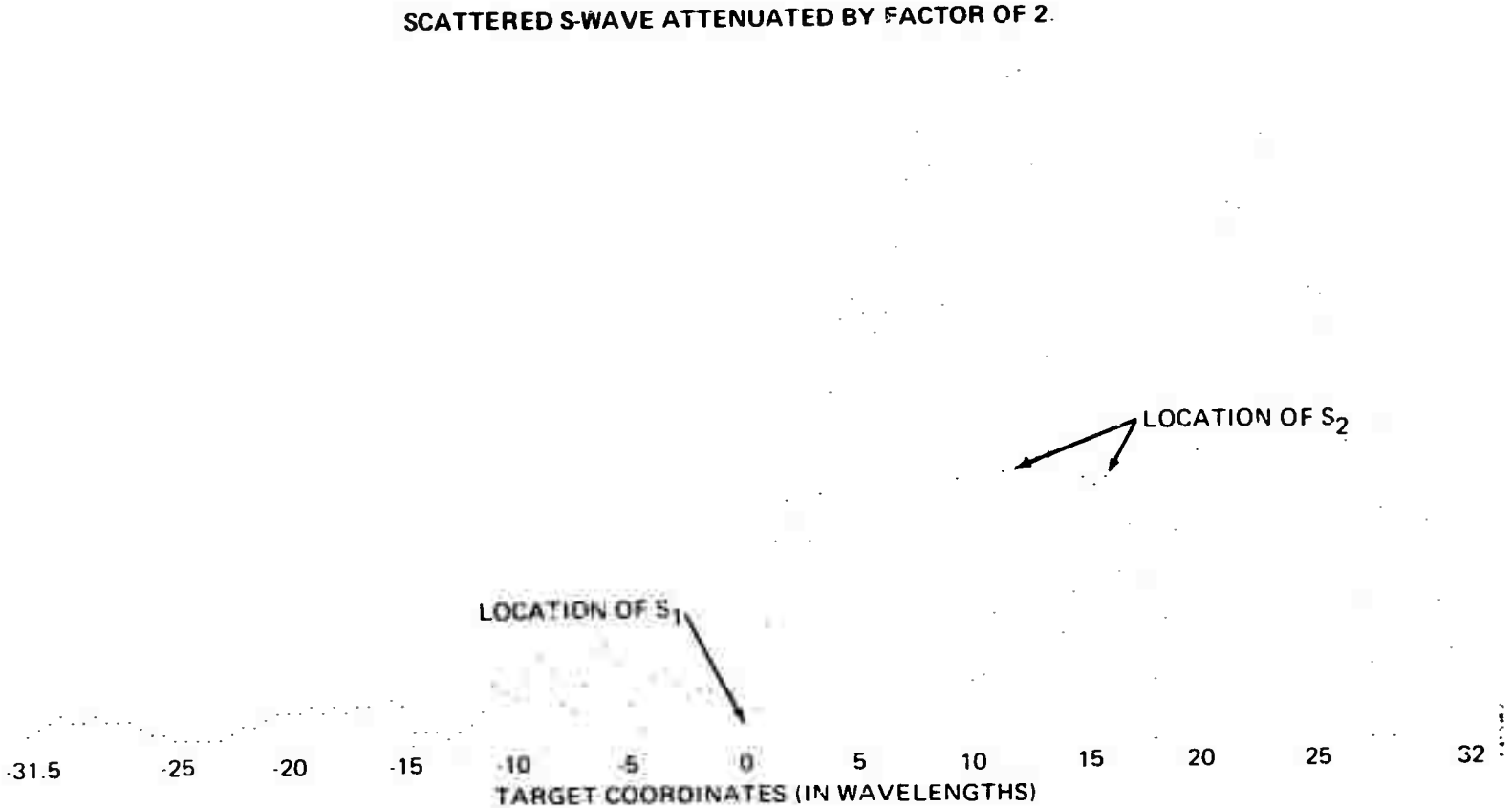

Figure 6-13 - Weak Signal Enhancement Reconstruction of an Extended Scatterer (4λ) in Image Plane of S_2. Scattered S-Wave Attenuated by a Factor of 2.

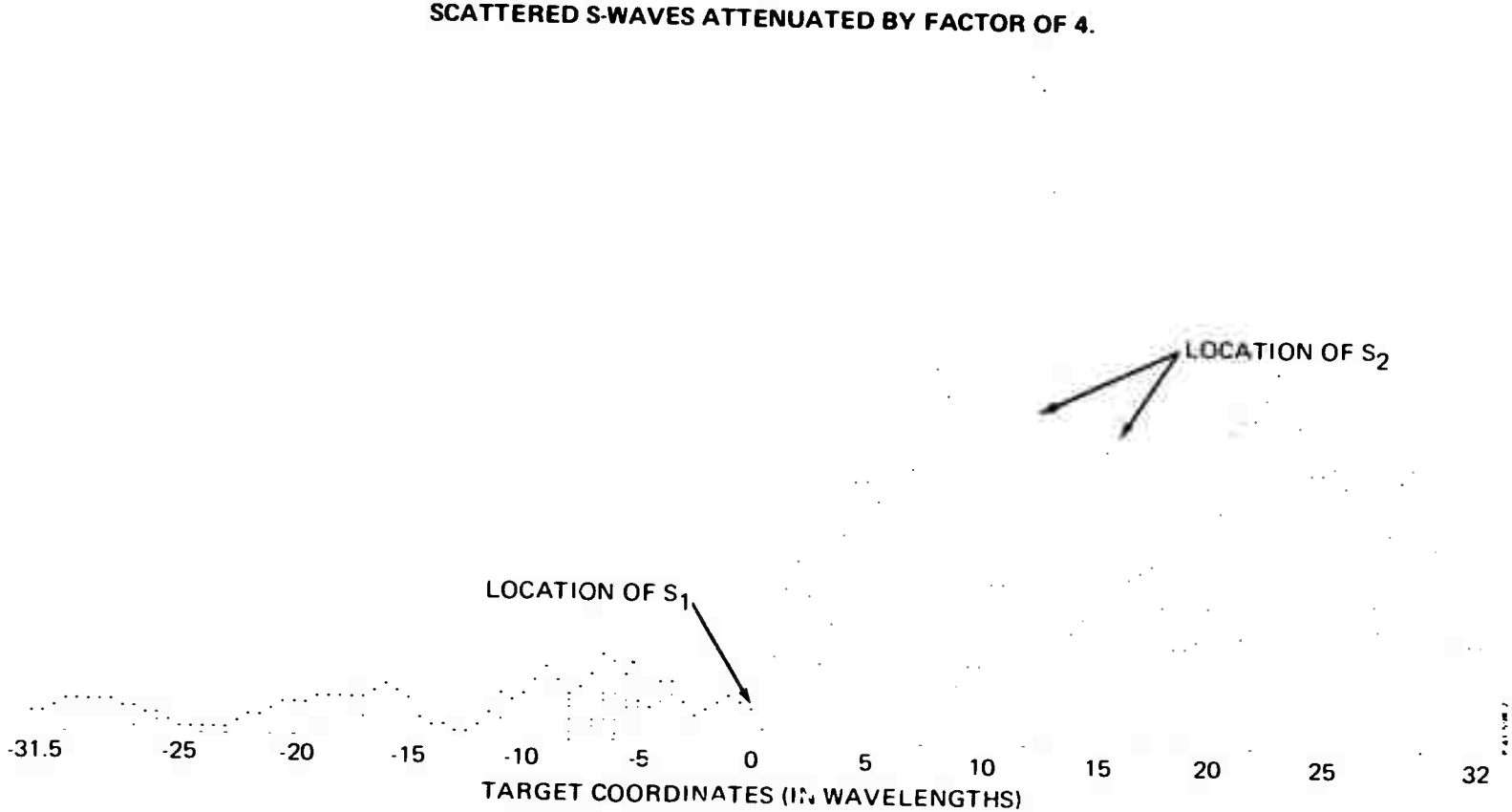

Figure 6-14 - Weak Signal Enhancement Reconstruction of an Extended Scatterer in Image Plane of S_2. Scattered S-Waves Attenuated by a Factor of 4.

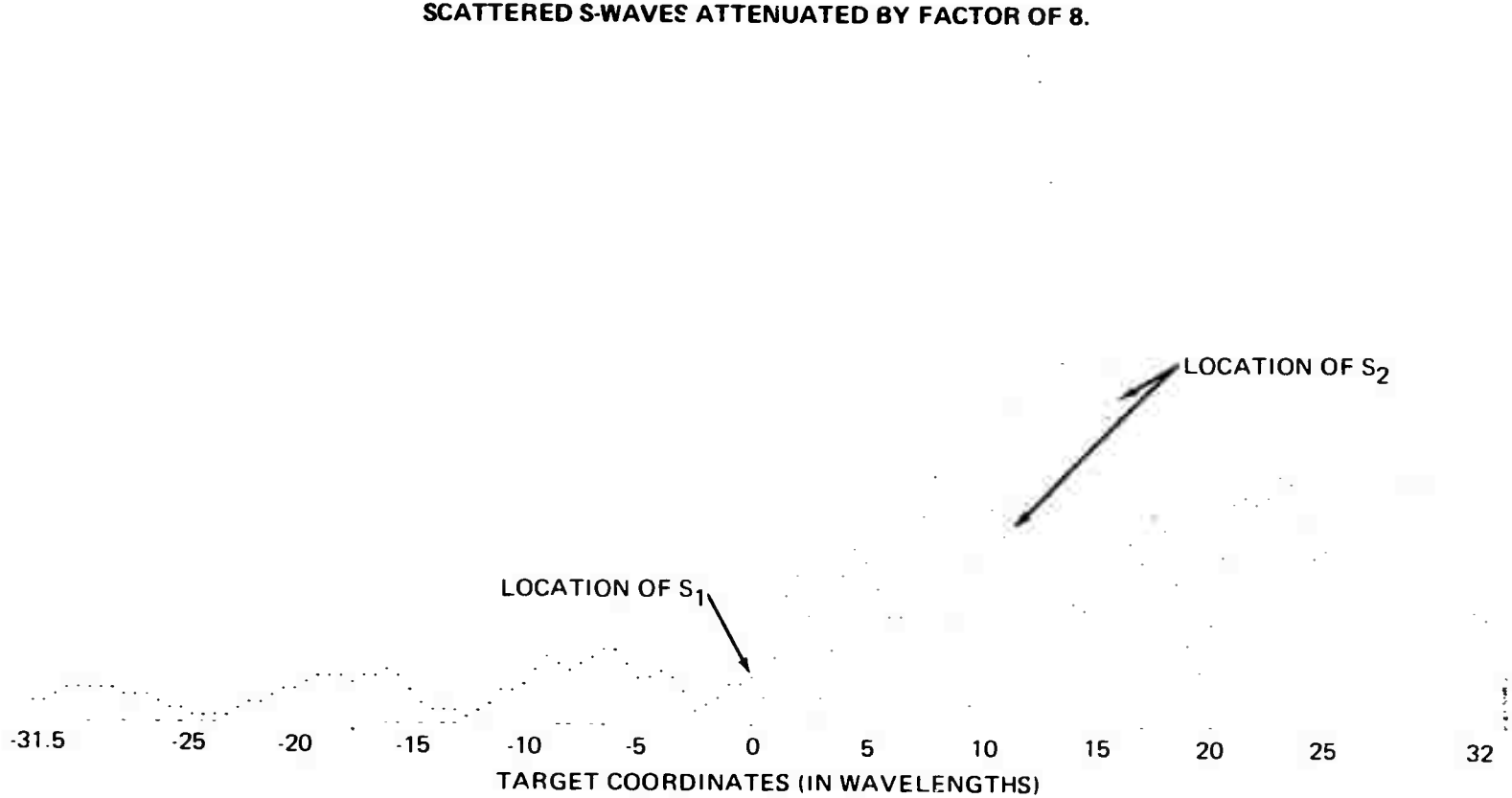

Figure 6-15 - Weak Signal Enhancement Reconstruction of an Extended Scatterer in Image Plane of S_2. Scattered S-Waves Attenuated by a Factor of 8.

SECTION 7

RELEVANT LITERATURE

7.1 REFERENCES

1. E. B. Eckel, "Nevada Test Site," Geological Society America Memoir, 110, 1968.

2. J. R. Ege, Stability Index for Underground Structures in Granitic Rock, pp. 185-197, 1968.

3. F. N. Houser and F. G. Poole, "Preliminary Geologic Map of the Climax Stock and Vicinity, Nye County, Nevada," U.S. Geological Survey Miscellaneous Investigation, Map I-328 (enclosure 3), 1960. Enclosed with this report.

4. E. S. Larsen, Jr., "Batholith and Associated Rocks of Corona, Elsinore, and San Luis Rey Quadrangles, Southern California," Geological Society America Memoir, 29, 1948.

5. L. R. Page and T. P. Thayer, "Thin Deposits of the Temescal District, Riverside County, California," U.S. Geological Survey open file report, 1945.

6. D. L. Everhart, "Geology of the Cuyamaca Peak Quadrangle, San Diego, County, California," in Crystalline Rocks of Southwestern California, California Division of Mines Bulletin, 1951,pp. 51-115.

7. P. B. King, "Geology of the Sierra Diablo Region, Texas," U.S. Geological Survey Prof. Paper 480, 1965.

8. R. A. Maxwell and others, "Geology of Big Bend National Park, Brewster County, Texas," University of Texas, Bureau of Economic Geology Publication No. 6711, 1967.

9. F. N. Houser and F. G. Poole, "Granite Exploration Hole, Area 15, Nevada Test Site," Interim Report, Part A, Structural, Petrographic and Chemical Data, TEM Report 836, U.S. Geological Survey, July 1959.

10. J. H. Scott, R. D. Carroll, and D. R. Cunningham, Technical Letter: Piledriver-1, "Seismic Studies in Piledriver Tunnels Area 15," Nevada Test Site, U.S. Department of the Interior, Geological Survey, June 1965.

11. J. E. Scott, "Corrected Values of Thickness of Rock in Low Velocity Layer Piledriver Tunnels, Area 15, Nevada Test Site," Technical Letter: Piledriver-1, Errata, U.S. Geological Survey, July 1966.

12. C. H. Roach, G. A. Izett, and J. C. Roller, "Interpretation of Geophysical Logs of the Granite U-15A Dolomite Hill No. 1 and Marble No. ME-2 Drill Holes," Nevada Test Site, U.S. Department of the Interior, Geological Survey, June 1959.

13. C. B. Forbes, R. A. Peterson, C. L. Heald, Vela Uniform T/179, "Operation Blanca-Logan-Lollipop Project 7.4," United Electrodynamics, Incorporated, Pasadena, California, October 1961.

14. S. P. Clark, Jr., Handbook of Physical Constants, Geological Society of America, New York, 1966.

15. P. B. Attewell and Y. V. Ramana, "Wave Attenuation and Internal Friction as Functions of Frequency in Rocks," Geophysics, 31, 1049 (December 1966).

16. J. E. White, Seismic Waves, Radiation, Transmission, and Attenuation, McGraw Hill Book Company, New York, 1965.

17. M. Muskat and M. W. Meres, "Reflection and Transmission Coefficients for Plane Waves in Elastic Media," Geophysics, 5, 115 (April 1940).

18. L. Cagniard, Reflection and Refraction of Progressive Seismic Waves, McGraw Hill Book Company, New York, 1962.

19. W. M. Ewing, W. S. Tardetzky and F. Press, Elastic Waves in Layered Media, McGraw Hill Book Company, 1957.

20. I. Y. Borg, "Survey of Piledriver Results and Preliminary Interpretation of Three Postshot Cores In and Near the Cavity," Lawrence Radiation Laboratory, University of California, Livermore, UCRL-50865, April 1970.

21. R. K. Verma and A. Roy, " A Graphical Method for Computing Geophone Group Response," Geophysics, 35, 704 (August 1970).

22. R. N. Jolly and J. F. Mifsud, "Experimental Studies of Source-Generated Seismic Noise," Geophysics, 36, 1138 (December 1971).

23. R. B. Blackman and J. W. Tukey, The Measurement of Power Spectra, Dover Publications, New York, 1959.

24. J. M. Stone, Radiation and Optics, McGraw-Hill Book Company, Incorporated, New York, 1963.

25. G. L. Fitzpatrick, J. R. Nicholls, and R. D. Munson, "An Experiment in Seismic Holography," Bureau of Mines RI No. 7607, 1972.

26. G. W. Stroke, An Introduction to Coherent Optics and Holography, Academic Press, 1966.

27. R. K. Mueller, R. R. Gupta, and P. N. Keating, "Holographic Weak-Signal Enhancement Technique," Journal of Applied Physics, 43, 457 (1972). Appendix A.

28. L. Knopoff, "Scattering of Compression Waves by Spherical Obstacles," Geophysics, 24, 30 (1969).

7.2 SUPPLEMENTARY BIBLIOGRAPHY

W. L. Emerick, R. P. Snyder, and W. E. Bowers, Technical Letter: Area 15-3, "Summary of Post-Shot Geologic Effects in the 1500 Tunnel, Area 15, Nevada Test Site," U.S. Department of the Interior, Geological Survey, July 1962.

A. W. Musgrave, "Seismic Refraction Prospecting," Society of Exploration Geophysicists, Tulsa, 1967.

J. C. Peck, "Plan-Strain Diffraction of Transient Elastic Waves by a Circular Cavity," California Institute of Technology Doctoral Thesis, 1965.

N. K. Yaconb, J. H. Scott and F. A. McKeown, "Computer Ray Training Through Complex Geological Models for Ground Motion Studies,' Geophysics, 35, 586 (August 1970).

H. Pursey, "The Power Radiated by An Electromechanical Wave Source," Physical Society (London) Proceedings, B69, 139 (1956).

K. E. Bullen, An Introduction to the Theory of Seismology, 3rd Edition, Cambridge University Press, 1965.

L. Knopoff, R. W. Fredricks, A. F. Gangi, and L. D. Porter, "Surface Amplitudes of Reflected Body Waves," Geophysics, 22, 842 (October 1957).

A. W. Trorey, "A Simple Theory for Seismic Diffractions," Geophysics, 35, 762 (October 1970).

J. Miklowitz, "Scattering of a Plane Elastic Compressional Pulse by a Cylindrical Cavity," International Congress of Applied Mechanics, Munich, 1964.

J. S. Watkins, R. H. Godson, and K. Watson, "Seismic Detection of Near-Surface Cavities," Geological Survey Professional Paper 599-A, 1967.

M. A. Biot, " Propagation of Elastic Waves in a Cylindrical Bore Containing a Fluid," Journal of Applied Physics, 23, 997 (September 1952)

W. E. Bowers and W. L. Emerick, "Technical Letter: Area 15-4, Supplementary Geologic Mapping in the 1500 Re-entry Tunnel, Area 15, Nevada Test Site," U.S. Geological Survey, January 1963.

C. E. Price, "Granite Exploration Hole, Area 15, Nevada Test Site," Interim Report, Part B Hydrologic Data, TEM Report 836-B, U.S. Geological Survey, November 1959.

F. N. Houser, "Lithologic Logs of Three Exploration Core Holes, U15b Area, Climax Stock, Nevada Test Site," TEI Report 792, U.S. Geological Survey, August 1961.

F. N. Houser, "Some Physical Property Data of Samples from U15a Site, Nevada Test Site," Technical Letter: Area 15-2, January 1962.

J. C. Cook, "Seismic Mapping of Underground Cavities Using Reflection Amplitudes," Geophysics, 30, 527 (August 1965).

L. Knopoff, "Scattering of Compressional Waves by Spherical Obstacles," Geophysics, 24, 30 (February 1959).

F. F. Evison, "Seismic Waves from a Transducer at the Surface of Stratified Ground," Geophysics, 21, 939 (October 1956)

G. F. Miller and H. Pursey, "The Field and Radiation Impedance of Mechanical Radiators on the Free Surface of a Semi-Infinite Isotropic Solid," Royal Society of London, Proc. (A), 232, 521 (1953).

F. F. Evison, "The Pulsed Vibrator as a Seismic Source," in Geophysical Prospecting, 1957, p. 381.

G. A. Izett, "Granite Exploration Hole, Area 15, Nevada Test Site, Nye County, Nevada," Interim Report, Part C, Physical Properties, Trace Elements Memorandum Report 836-C, U.S. Geological Survey, January 1960.

F. N. Houser and F. G. Poole, "Summary of Physical and Chemical of Granitic Rocks at the U15a Site, Climax Stock, Nevada Test Site," Technical Letter: Area 15-1, U.S. Geological Survey, December 1961

APPENDIX A

HOLOGRAPHIC WEAK SIGNAL ENHANCEMENT TECHNIQUE

Holographic Weak-Signal Enhancement Technique

R. K. Mueller, R. R. Gupta, and P. N. Keating
Bendix Research Laboratories, Southfield, Michigan 48076
(Received 16 June 1971)

A holographic weak-signal enhancement technique (WSET) is described which enhances the image of the source of a weak signal of interest in the presence of an unwanted strong signal with very little *a priori* knowledge of the latter. The technique is most suitable for imaging applications in fields such as seismic or oceanographic holography, where the desired weak-scattered signal is often overwhelmed by a strong reflected signal from interfaces between different media. The feasibility of the WSET has been shown by simulating a two-solid-layer acoustic problem on a digital computer. Well-defined enhanced images have been obtained for target scattering which is so much weaker than a strong reflected signal that the target images were lost in noise using conventional holographic reconstruction.

I. INTRODUCTION

Imaging systems, as all other information-carrying systems, are plagued with the problem of identifying weak signals in the presence of noise. For example, "noise" from the wings of a nearby strong signal often dominates and obliterates a weak signal, especially if the former is out of focus i.e. the desired image plane. This type of weak-signal identification problem frequently arises when conventional holographic imaging techniques are used to image underground or oceanographic weak-scattering targets. In these applications the weak desired signal scattered from the targets can be lost in the background of the strong signal due to the reflection of the propogating waves from, for example, the stratified layers of the earth, or from the ocean bottom. In addition, there may be noise due to other sources, such as propagating surface waves. In such applications it is very desirable to have a processing technique which could enhance the (desired) weak image in the presence of a strong (unwanted) signal of simple form. For convenience, the unwanted strong signal is referred to as a reflected signal unless otherwise stated, throughout the article.

In this paper we describe a new weak-signal enhancement technique (WSET) which enhances the image of weak targets when accompanied by a strong reflection, with virtually no *a priori* knowledge of the scene. The WSET would be applicable to problems where the following two conditions are met: (i) The unwanted signal is coherent with the target signal and its intensity at the holographic plane is relatively slowly varying (ii) Some spatial separation of the weak target and the strong-signal virtual source is obtainable. The first condition is likely to be met in a wide class of cases; for example, for the strong reflection from an interface. In the case of such a strong signal, the second requirement can be met by placing the receive aperture so that the virtual source associated with this reflection is suitably separated from the target in the plane parallel to the holographic plane.

The enhancement method is based on (i) the use of the signal field for reconstruction and (ii) high-pass filtering of some of the information. This reconstruction method is most conveniently utilized by means of digital-computer reconstruction techniques.

Section II consists of a description of the proposed enhancement technique together with an evaluation of its usefulness. In Sec. III we present an account of a computer-simulated application of the enhancement technique to a geophysical holographic problem. Section IV

1-7

consists of a discussion of the simulation results and an evaluation of the method for actual field data.

II WEAK-SIGNAL ENHANCEMENT TECHNIQUE

The enhancement reconstruction technique is an extension of the conventional holographic reconstruction method.[1] It consists, in essence, of two successive reconstructions, the second using the strong return as the reconstruction signal.

In a conventional hologram the image information is stored as the product R^*S, where $S = S_1 + S_2$ is the total signal field at the hologram plane, S_1 is the strong unwanted signal, S_2 the weak signal of interest, and R is the reference field. Conventional reconstruction involves an additional multiplication by R', a reconstruction field at the hologram plane, followed by a transformation (e.g., a Fourier transform in the Fraunhofer case, a Fresnel transform in the Fresnel approximation) to the image plane. With a suitable R', this transformation yields, at the image plane, the field $\delta = \delta_1 + \delta_2$ which is the image corresponding to the holographic field.

The weak-signal enhancement technique involves the following steps: (a) recording of S, as in conventional holography; (b) the formation of $|S|^2 = |S_1 + S_2|^2$ from S, or directly; (c) high-pass filtering of $|S|^2$ (the result is denoted as $|\tilde{S}|^2$; (d) multiplication of $|\tilde{S}|^2$ by S and reconstruction. If $|S_1|^2$ is slowly varying, and S_1 and S_2 are spatially separated, we can carry out high-pass filtering [step (c)] to obtain the reduction

$$|S_1|^2 + |S_2|^2 + 2\,\mathrm{Re}(S_1S_2^*) - |S_2|^2 + 2\,\mathrm{Re}(S_1S_2^*) . \qquad (1)$$

Hence, step (d) yields

$$(S_1 + S_2)(|S_2|^2 + S_1 S_2^* + S_1^* S_2)$$
$$(|S_1|^2 + |S_2|^2) S_2 + 2|S_2|^2 S_1 + S_1^* S_2^2 + S_1^2 S_2^* . \qquad (2)$$

The last two terms give signals in the image plane which are spatially separated from the images of interest and will not be considered further. The third term yields essentially the image δ_1 but it is reduced by the small factor $2|S_2|^2$. The first term is the desired image term S_2 multiplied by the large factor $|S_1|^2$ (since $|S_1|^2 \gg |S_2|^2$). Thus, the weak image has been enhanced relative to the strong one by the large factor $\frac{1}{2}|S_1|^2/|S_2|^2$.

The condition that $|S_1|^2$ is a slowly varying intensity in the holographic plane is necessary so that (i) rejection of $|S_1|^2$ by high-pass filtering is effective; (ii) the final enhanced image δ_2 is not degraded. The condition that δ_1, δ_2 are spatially separated is necessary so that $S_1S_2^*$ is a term with high spatial frequencies and can be readily filtered from $|S|^2$.

It is instructive to consider the enhancement technique in the case of point objects and Fraunhofer holograms. In this case, S_1, S_2, and R are all sinusoidal functions, with spatial frequency determined by the angular positions $\vec{q} = [(\sin\theta)/\lambda](\cos\phi, \sin\phi)$ of the point sources, where θ and ϕ are the polar and azimuthal angles, respectively. For example, $S_1 = \exp(i\vec{q}_1 \cdot \vec{x})$, $S_2 = \exp(i\vec{q}_2 \cdot \vec{x})$ $(\alpha \ll 1)$, where $\vec{x}$ is the two-dimensional position vector in the hologram plane. Thus

$$|S|^2 = [1 + \alpha^2 + 2\alpha\cos(\vec{q}_1 - \vec{q}_2)\cdot x], \qquad (3)$$
$$|\tilde{S}|^2 = 2\alpha\cos(\vec{q}_1 - \vec{q}_2)\cdot\vec{x},$$

if the dc is rejected and $q_1 \neq q_2$. Hence

$$[2\alpha\{\exp(i\vec{q}_1\cdot\vec{x}) + \alpha\exp(i\vec{q}_2\cdot\vec{x})\}]\cos(\vec{q}_1 - \vec{q}_2)\cdot\vec{x}$$
$$= \alpha\{\exp(i\vec{q}_2\cdot\vec{x}) + \alpha\exp(i\vec{q}_1\cdot\vec{x}) + \exp[i(2\vec{q}_1 - \vec{q}_2)\cdot\vec{x}]$$
$$+ \alpha\exp[i(2\vec{q}_2 - \vec{q}_1)\cdot\vec{x}]\} . \qquad (4)$$

We thus obtain four point images. The amplitude of δ_2 is now larger than that of δ_1 by a factor of $1/\alpha$, instead of being smaller by a factor of α. The other two images occur at positions different from δ_1, δ_2, provided $q_1 \neq q_2$ (i.e., the images are not coincident), as already assumed. (We note that in this case $|S_2|^2$ is also filtered out so that the additional factor of 2 vanishes.)

Steps (a)–(d) necessary for the enhancement technique can be carried out with optical components, although not readily. They can, however, be very easily carried out on a digital computer, where effective filtering and large dynamic range are readily available.

In a problem where the equivalent source of the signal S_1 is a point, step (a) can be eliminated by using a synthetic point-source signal (instead of S as proposed) in step (d) to illuminate $|S|^2$. However, in cases where S_1 is not from a point source, as in the present study, it is preferable to retain step (a) and use this to reconstruct the image.

III COMPUTER SIMULATION OF WEAK-SIGNAL ENHANCEMENT TECHNIQUE

A Model and Computational Method

Since the experimental evaluation of the feasibility of the proposed holographic weak-signal enhancement technique in seismic or oceanographic holography would be expensive and time consuming, a simple (idealized) case of seismic holography was first simulated on a digital computer. In this simulation, it was desired to use a digital computer to reconstruct the image of a small acoustic scatterer buried below an interface between two acoustic media (as shown in Fig. 1); the source and linear detector array are above the interface. The scattering strength of the target was chosen such that the conventionally reconstructed holographic image δ_2 is not identifiable in the presence of the noise accompanying the strong image δ_1. In the computer simulation, we have used the following model:

(i) The transmitting (acoustic) source radiates coherent longitudinal waves (i.e., P waves). (ii) The interface between the two media is planar. (iii) Both media are homogeneous, isotropic, and lossless. (iv) Both media are solid, and hence mode transformation from P waves to S waves (i.e., shear waves) and vice versa takes place whenever propagating waves are either reflected, refracted, or scattered. (v) Either no surface waves reach the detector array or they can be discriminated against by, for example, gating. (vi) The holographic

7-8

fields are detected by a finite linear array of detectors located at many wavelengths away from the interface. (viii) The scatterer and virtual source are located many wavelengths away from the interface, yet they are in the near-field region of the receive aperture, as would be the usual case in seismic holography. Although ray-optics approximations to the solution of propagating spherical waves are valid in the far-field (and not the near-field) region of the aperture,[2] in our simulation study we shall for simplicity use the ray-optics approximations. (viii) There is sufficient angular separation between the scatterer and the unwanted strong-signal source so that low-frequency components can be readily filtered out from the $|S|^2$ signal.

Although the assumed two-layer model for the earth is not entirely realistic, the conclusion arrived at here will, however, be applicable to a seismic problem where the reflected signal S_1 is caused predominantly by a single interface. We note however that the inclusion of both S and P waves results in quite a stringent test of the method since the strong virtual source is a compound object and the interference between the S and P reflected waves must also be filtered out.

The computer simulation of such a problem is therefore expected to provide a reasonable evaluation of the proposed holographic weak-signal enhancement technique when applied to a practical problem.

The Rayleigh-Sommerfeld diffraction integral formula[3] [Eq. (5)] is used to reconstruct the original scene from the fields detected by the linear array. For the general configuration shown in Fig. 2, the diffraction integral formula calculates the field amplitude $f(x, y, z)$ at the point $P(x, y, z)$ from the known field distribution $f'(\xi, \eta)$ over the finite planar aperture $\Sigma(\xi, \eta)$.

The integral formula is[3]

$$f(x, y, z) = (1/i\lambda)\int_{\Sigma} K(r)\cos(\vec{n}\cdot\vec{r})\, f'(\xi, \eta)\, d\xi\, d\eta, \qquad (5)$$

where

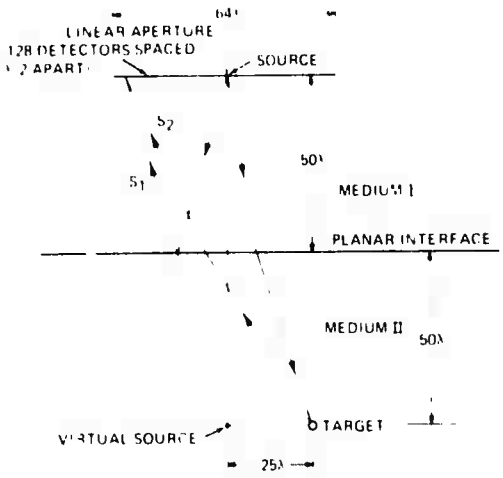

FIG. 1. Rayleigh-Sommerfeld formulation of diffraction by a planar aperture.

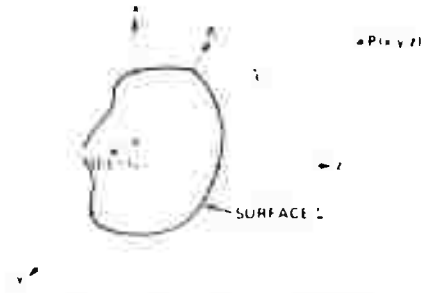

FIG. 2. Computer simulated model.

$$K(r) = e^{ikr}/r \text{ (three-dimensional kernel)}, \qquad (6)$$

$$r^2 = (x-\xi)^2 + (y-\eta)^2 + (z-\zeta)^2,$$

λ is the propagation wavelength of the detected fields, and $\cos(\vec{n}\cdot\vec{r})$ is the cosine of the angle between the outward normal $\vec{n}$ and the vector $\vec{r}$ joining Q to P. This formula assumes a scalar description of the acoustic fields. In our simulated problem this would yield reasonably accurate results since the signal at the receive aperture is mostly contributed by the longitudinal waves.

In the Fresnel (or Fraunhofer) zone, the image may be reconstructed using the simpler Fresnel (or Fraunhofer) diffraction formula, instead of the Rayleigh diffraction formula which should be used in the near-field zone. In our simulation work we are concerned with targets and virtual sources which are in the near field, as is the usual case with the long wavelengths utilized in seismic holography.

In order to uniquely determine fields in an unbounded space by using the diffraction integral formula, the field distribution must be specified over the two-dimensional aperture. In our simulated problem we have, for simplicity, computed fields only along a linear array. Therefore, for our near-field simulated problem, the three-dimensional kernel $K(r)$ used in diffraction integral Eq. (5) should be modified to reconstruct two-dimensional images from one-dimensional holograms. For simplicity, however, we have used the unmodified three-dimensional kernal [Eq. (6)]. This is expected to only slightly impair the "conventional" aperture-limited resolution of the reconstructed images.

Fast Fourier-transform techniques,[4-6] based on the Cooley-Tukey algorithm (known as FFT), have been used to digitally reconstruct the holographic images using the diffraction integral formula (5). The FFT is simply an efficient method for computing the discrete Fourier transform (DFT). The FFT can be used in place of continuous Fourier transform only to the extent DFT can be used, but with a substantial reduction in computer time. The FFT can be applied to operations such as computing a spectrogram, convolution, correlation, and filtering. In our problem the FFT algorithm is used (i) to evaluate the integral equation (5) via the convolution theorem methods and (ii) to filter out the low-frequency terms from a signal.

7-9

As discussed earlier, the low-spatial-frequency components have to be filtered out from the signal $|S|^2$. Since in our simulated problem we have *a priori* knowledge of the relative locations of the reflecting interface and scatterer, the spatial cutoff frequency is easily determined. These low-spatial-frequency components are then filtered out from the $|S|^2$ signal by a digital high-pass filter. Since in any practical imaging problem, the target locations are not known *a priori*, the appropriate cutoff frequency must be chosen by some alternative method. A filtering approach that may be followed in processing real field data is presented later.

B Model Parameters

Conventional holographic techniques as well as the holographic weak-signal enhancement technique are employed to reconstruct the original scene shown in the configuration of Fig. 1. The detectors in the linear array are assumed to be sensitive only to the vertical component of the force. The mathematical expressions for the pressure waves resulting from either reflection, refraction, or scattering of waves are available in the literature.[2,7,8]

The following reasonable values of model parameters have been chosen for the evaluation of the proposed WSET. Poisson's ratio for both media = 0.25; ratio of densities of medium I to medium II = 1; ratio of velocities of P waves in medium I to medium II = 1.5; ratio of the radius of scattering sphere to the wavelength $\lambda = 0.5$; reference wave $R = A\exp[(i/\sqrt{2})(x+z)]$; length of linear detector array = 64λ; number of detectors = 128. The size and the location of the detector array were selected such that no Head-type surface waves[2] would theoretically arrive at the detector array. The detectors in the linear are spaced at an interval of $\frac{1}{2}\lambda$, which is somewhat less than one-half of the smallest spatial wavelength λ_s in the signal S, so that the sampling rate is close to optimum. With the chosen parameter values, the scattered signal intensity $|S_2|^2$ was found to be 1.45×10^{-4} smaller than the reflected signal intensity $|S_1|^2$.

C Design Performance

The image resolution obtained is predominately aperture limited. [In addition (as discussed earlier), the use of the unmodified three-dimensional kernel in our calculations is expected to further impair the resolution.] In our example the images are reconstructed in the near-field region of the aperture, where the resolution calculations are difficult. Reasonable estimates for the image resolution can, however, be obtained from "far-field calculations" if the images are not reconstructed quite close to the aperture, as is the case in our problem.

Based on far-field calculations, the resolvable linear distance ΔL and the lateral distance ΔZ (depth of focus) between the two point-source objects for an aperture of width 2a at a distance z (normal to the aperture) are

$$\Delta L \approx \lambda\,(z/a),$$

$$\Delta Z \approx \lambda\,(z/a)^2. \tag{7}$$

In the process of signal enhancement we obtain the image of the target from the modulated signal $|S_1|^2 S_2$ and not the signal S_2. If $|S_1|^2$ is not constant over the holographic plane, an additional broadening is thus introduced into the enhanced image. However, since $|S_1|^2$ is a low frequency function, the additional loss of resolution is not expected to be too severe. Using Eq. (7), the expected half-widths of δ_1 and the enhanced image of δ_2 are roughly $\frac{1}{2}\lambda$, $\frac{1}{4}\lambda$, respectively; the depth of focus of the enhanced image is about 16λ.

In our case, a first-order estimate of the image degradation introduced by the usage of an unmodified kernel has indicated a rather insignificant contribution to the existing aperture-limited resolution of the image.

IV RESULT

A Simulated Example

Figure 3 shows the image intensity distribution obtained by a conventional holographic reconstruction of the total scene shown in Fig. 1. This reconstruction was done in the expected image plane of the virtual source δ_1. The image of δ_2 is not identifiable from the background noise. The image location and the resolution of the image of δ_1 are as expected; the ratio of the intensity of the weak signal to the strong signal is about 1.45×10^{-4}.

Figure 4 shows the image intensity obtained by another conventional reconstruction of the total scene—but now in the expected image plane of δ_2. The expected image plane of δ_2 is calculated to be at a distance of 125λ from the hologram plane. In this plane the target is located at a distance of 25λ away from the center of the hologram. The image from $|S_1|^2$ is out of focus and the image from $|S_2|^2$ is still unidentifiable from the background. In Fig. 5 we present an enlargement of part of Fig. 4 in the vicinity of the expected location of δ_2. There is no trace of the desired δ_2 image.

Figure 6 shows the weak-signal enhancement reconstruction in the expected image plane of δ_2 as would normally be of interest. Again intensities are plotted. The figure shows (i) the image of the weak target is at the

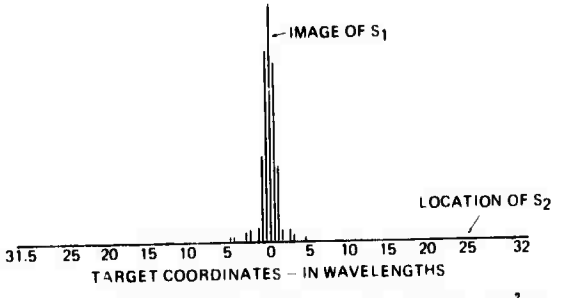

FIG. 3. Conventional holographic reconstruction $|S_1+S_2|^2$ in the image plane of S_1. The desired image $|S_2|^2$ is not observable in the presence of $|S_1|^2$.

7-10

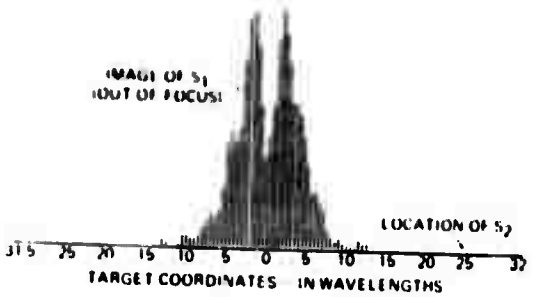

FIG. 4. Conventional holographic reconstruction $|S_1 + S_2|^2$ in the image plane of S_2. Again, $|S_2|^2$ is not visible.

expected location, 25λ, and considerably enhanced over the image of S_1, (ii) the half-width of the enhanced image is about 4λ (almost the same as theoretically predicted), and (iii) the weak-target intensity is enhanced by a factor of $|S_1|^4 \cdot |S_2|^4$. The theoretical improvement obtainable in the image intensities is expected to be on the order of 5×10^7. In actual fact, however, the effectiveness of the filtering of $|S_1|^2$ is likely to be the limiting process.

Comparison of Figs. 3 and 6 shows the considerable effectiveness of the weak-signal enhancement technique. It alters the situation from one in which the desired $|S_2|^2$ is unobservable in the presence of $|S_1|^2$ (Fig. 3) to one in which the unwanted intensity from S_1 is unobservable in the presence of the enhanced image of the S_2 target (Fig. 6).

D. Discussion

The results of the simulation study show that targets which scatter too weakly to be imaged in the presence of a strong reflected signal by conventional holographic methods can often be readily imaged by the proposed holographic weak-signal enhancement technique. The enhancement technique has been found to be able to image weak returns that are two to three orders of magnitude below the amplitude of those which are just discernible by conventional holographic techniques. A comparison of Figs. 3 and 6 shows the considerable enhancement which can be obtained (a factor of over 10^6 in intensities).

The effectiveness of the WSET depends upon the efficiency with which the high-pass filter can suppress the low-frequency part of $|S|^2$. The spatial frequency of the filtered signal increase with increasing angular separation between the weak image S_2 and strong unwanted image S_1. Thus the effectiveness of the filter, and hence the WSET, improves with increasing angular separation between the sources of the desired weak signals, and the undesired strong signals. For example, when S_1 is due to a strong reflection from a horizontal plane, the WSET is most effective when the receivers are not directly above the target[9].

C. Processing of Field Data

All processing steps involved in implementing the holographic WSET to field data are straightforward, except for the filtering of the low-frequency components. In the simulated case the filtering step was readily carried out because of *a priori* knowledge of the location of the reflecting interface. In any practical problem, the filtering step would, however, be somewhat more difficult, since the locations of reflecting interfaces will, in general, be unknown beforehand. In a practical imaging problem the following filtering procedure may be followed to implement the WSET.

(i) Conventionally reconstructed holographic images $S_1 + S_2$ are generated in a suitable number of adjacent image planes parallel to the holographic plane. These image planes should be spaced at roughly the depth of focus of the receive aperture. From these reconstructed images, the locations of the focused strong images S_1 are obtained, for comparison with the enhanced image fields obtained in step (iii).

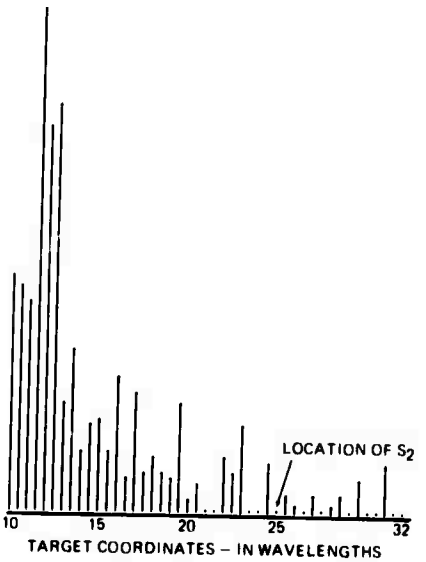

FIG. 5. Enlargement of part of Fig. 4 in the vicinity of the expected location of image S_2. $|S_2|^2$ is still undetectable.

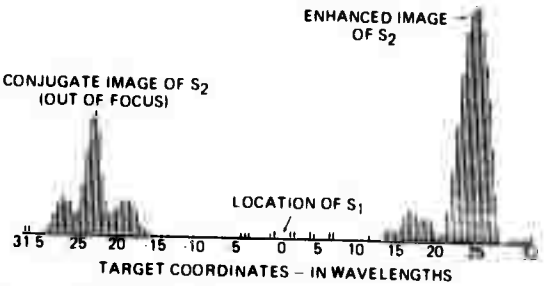

FIG. 6. Weak-signal enhancement reconstruction in the image plane of S_2. After enhancement, the desired image $|S_2|^2$ has become much larger than $|S_1|^2$. (The same model parameters have been used here as for Figs. 3–5.)

7-11

(ii) Several filtered signals $|S|^2$, each with a different filter cutoff frequency, are generated.

(iii) From each filtered signal $|S|^2$, enhanced images of weak targets are reconstructed in the several image planes by using the signal $s_1 + s_2$ for reconstruction. From the images so reconstructed, the optimum target reconstructions are chosen.

CONCLUSIONS

We have presented a technique which can enhance the image of a weak target in the presence of a strong (e.g., reflected) signal. By computer simulation we have shown that the proposed holographic enhancement technique can indeed provide considerable enhancement of the image of a weak signal accompanied by an undesired strong signal coherent with the target return signal. The WSET is feasible whenever (i) the strong-signal intensity is relatively slowly varying in the hologram plane and (ii) a sufficient angular separation exists between the target and the virtual source of the unwanted strong signal, so that effective filtering of the low-frequency terms can be achieved. To a great extent the effectiveness of this filter determines the weakest signal that can be imaged in this manner by the proposed WSET. Based on our computer simulation study we calculate that in a practical problem the proposed holographic WSET should readily image weak-scattering targets that would otherwise be lost in the background of the image of the accompanying undesired strong coherent signal.

ACKNOWLEDGMENTS

The authors are indebted to R. F. Steinberg and T. Sawatari for valuable discussions and J. Lindsay for numerical computations.

[1] J. W. Goodman, *Introduction to Fourier Optics* (McGraw-Hill, New York, 1968), Chap. 8.
[2] L. M. Brekhovskikh, *Waves in Layered Media* (Academic, New York, 1960), Chap. IV.
[3] A. Sommerfeld, *Optics*, Vol. IV of *Lectures on Theoretical Physics* (Academic, New York, 1954).
[4] G. D. Bergland, IEEE Spectrum, 41 (1969).
[5] J. W. Cooley and J. W. Tukey, Math. Comput. 19, 297 (1965).
[6] N. Brenner, IBM Corp. Contributed Program Library, Code No. 360, D-13, 4, 001 (unpublished).
[7] L. Knopoff, Geophysics 24, 30 (1959).
[8] L. Knopoff, Geophysics 24, 209 (1959).
[9] However, it must be pointed out that, while this is true, conventional imaging also becomes much more effective as the angular separation increases. In fact, conventional imaging improves more rapidly, other things being equal. Thus, the WSET is increasingly preferable *in comparison with other methods* as the angular separation is reduced.

DEPARTMENT OF THE INTERIOR
UNITED STATES GEOLOGICAL SURVEY

PRELIMINARY GEOLOGIC MAP OF THE CLIMAX STOCK AND VICINITY NYE COUNTY, NEVADA

By

F. N. Houser and F. G. Poole

MISCELLANEOUS GEOLOGIC INVESTIGATIONS
MAP I-328

PUBLISHED BY THE U. S. GEOLOGICAL SURVEY
WASHINGTON, D.C.
1960

35pp.

DEPARTMENT OF THE INTERIOR
UNITED STATES GEOLOGICAL SURVEY

A

WEST

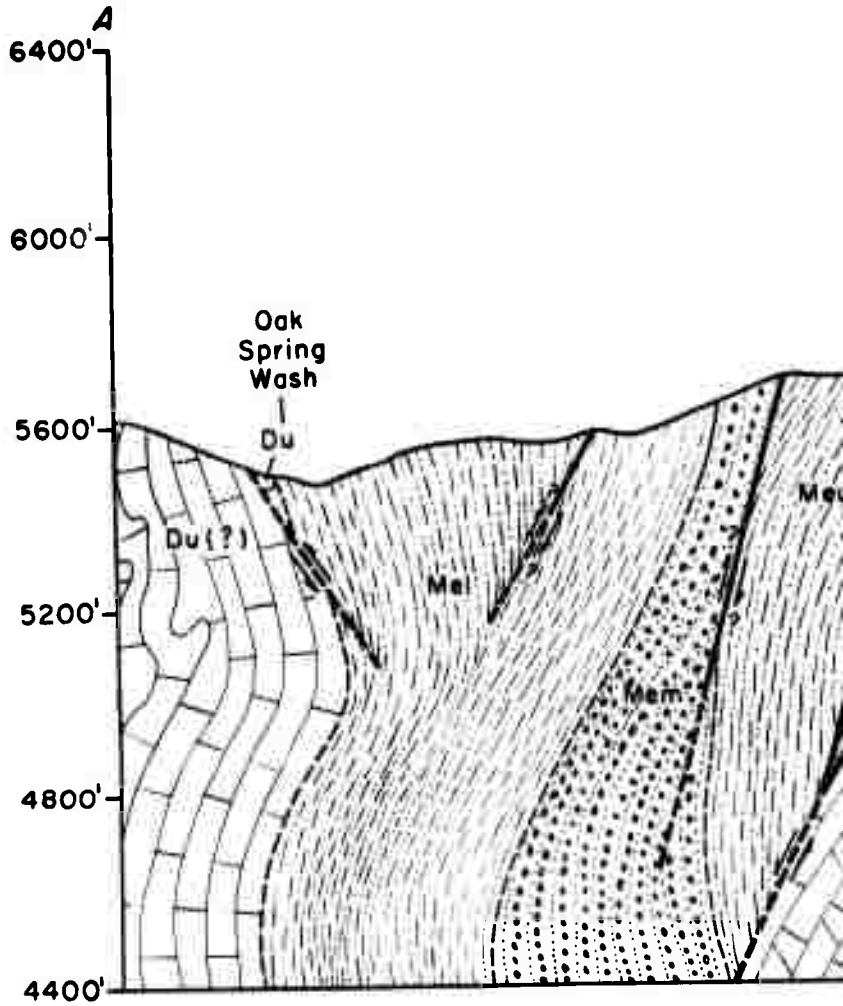

WEST

B

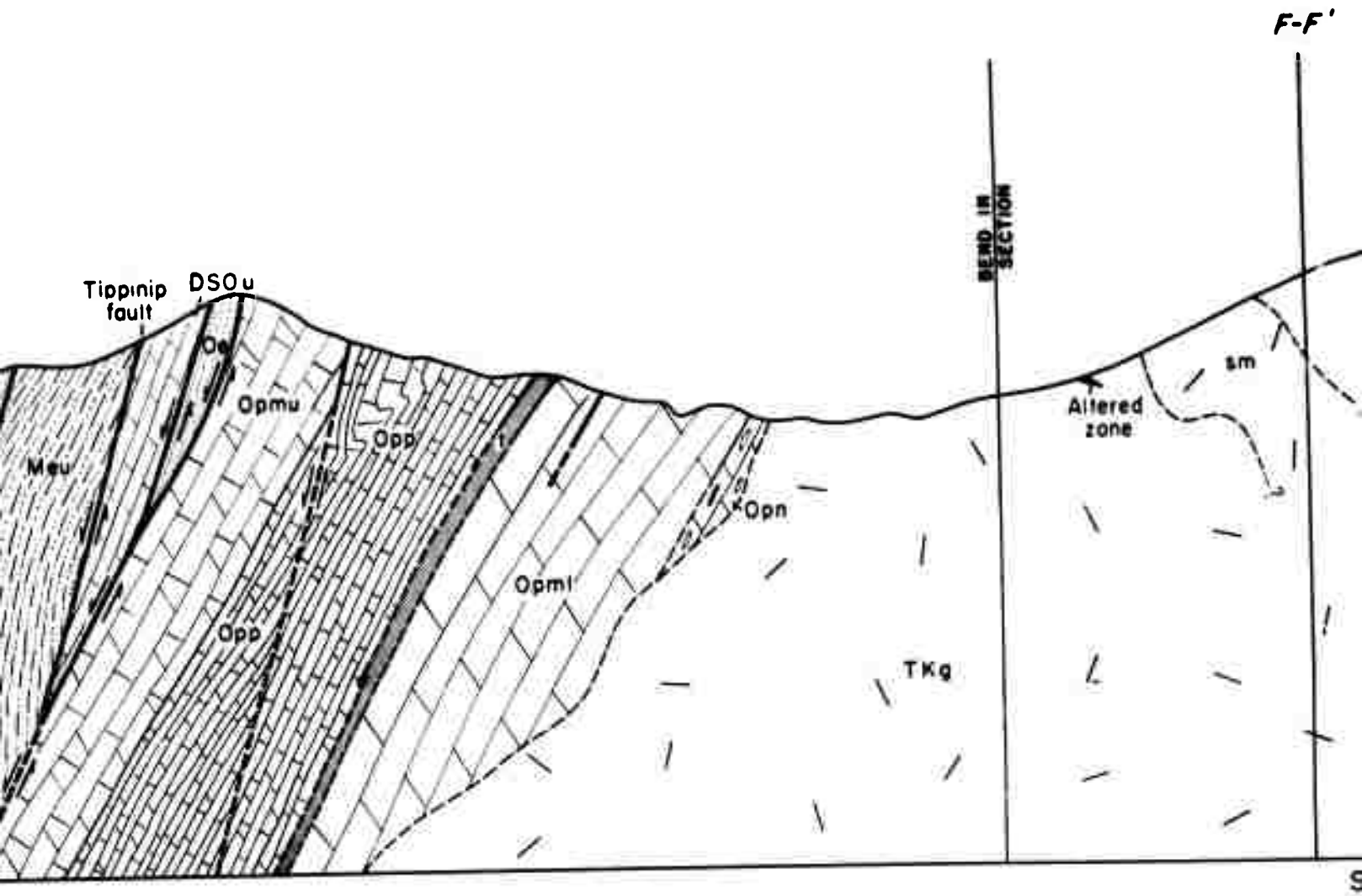
F-F'
BEND IN SECTION
Tippinip fault
DSOu
Opmu
Opp
Meu
Opn
Opml
Opp
TKg
Altered zone
sm


F-F'
Qalo
Altered
gd

PREPARED IN COOPERATION WITH THE
U. S. ATOMIC ENERGY COMMISSION

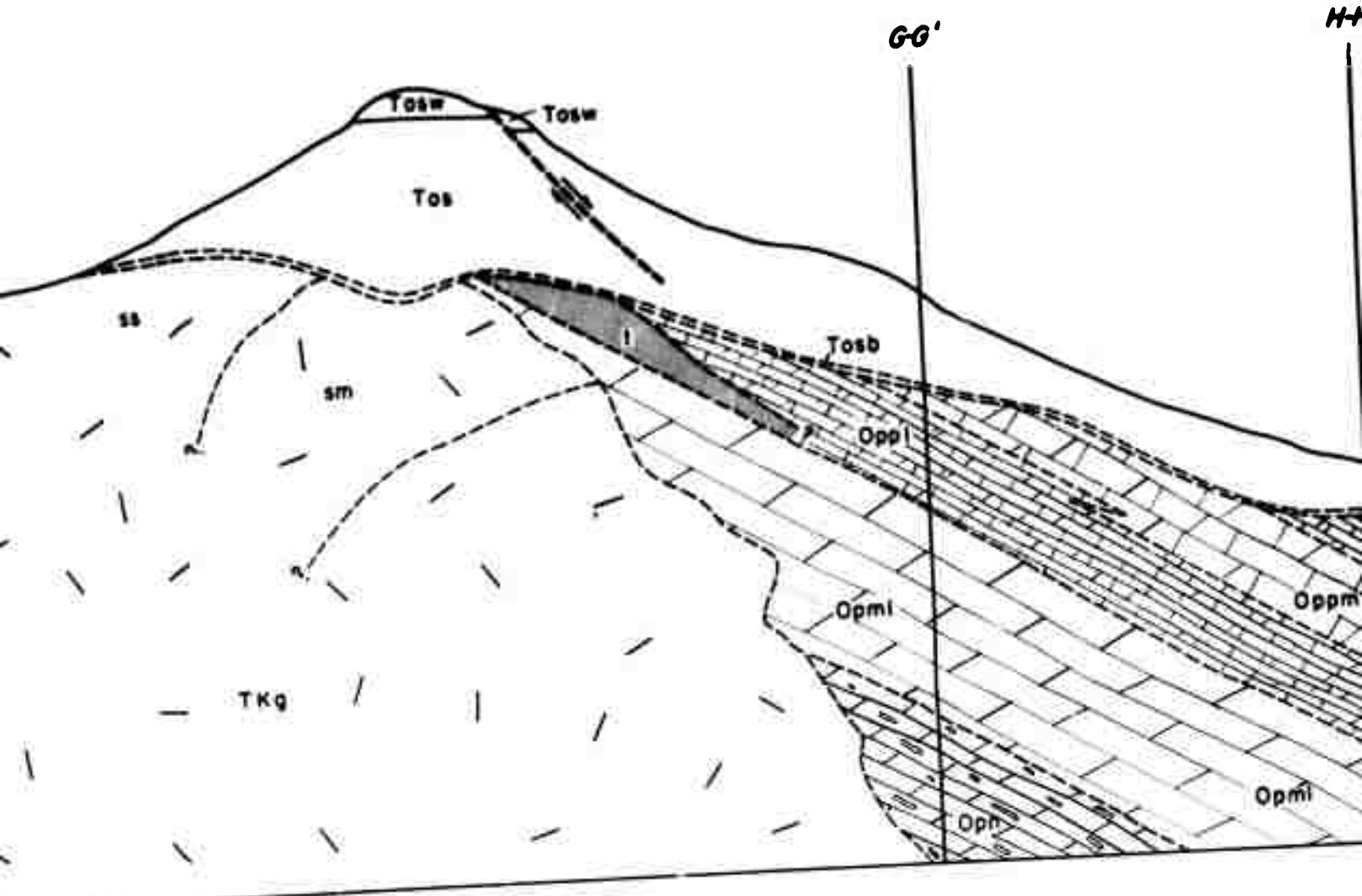

CTION A-A'

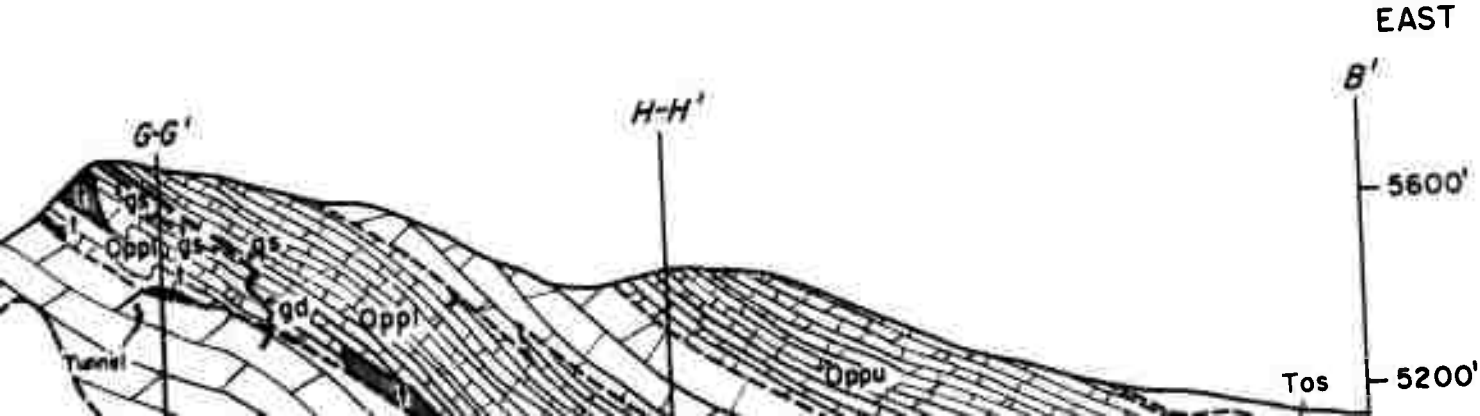

EAST

1

For detai

A'
6400'
6000'
5600'
5200'
4800'
4400'

Tos
Tosb
Opmu
Oppv
Oppl

Dolom

WEST

C
5600'

Oak
Spring
Wash

Tippipin

EAST

C'
5600'

1

EXPLANATION

For detailed descriptions of specific lithologic units see sheet 1

ROCK TYPES

Dolomite

Nodular dolomite

Dolomitic limestone or limy dolomite and tactite

Limestone

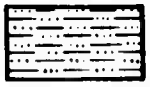

Argillite

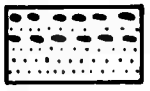

Quartzite and conglomerate

Sand and gravel

Porphyritic quartz monzonite

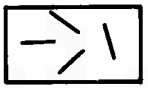

EAST

C'

5600'

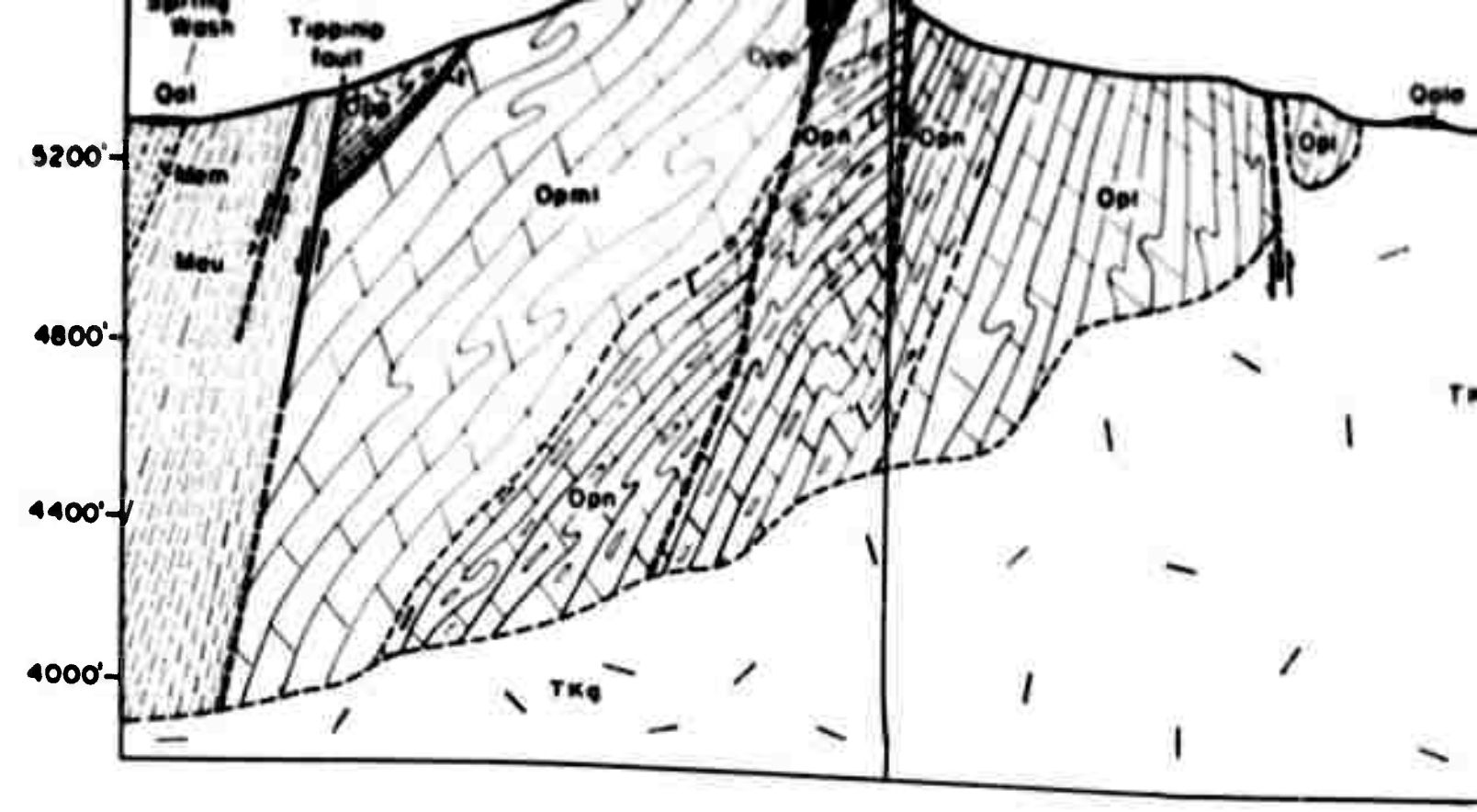
Tippinip fault
Qal
Opp
Oppl
Opn
Opl
Opla
Mbm
Mcu
Opmi
5200'
4800'
4400'
4000'
TKq

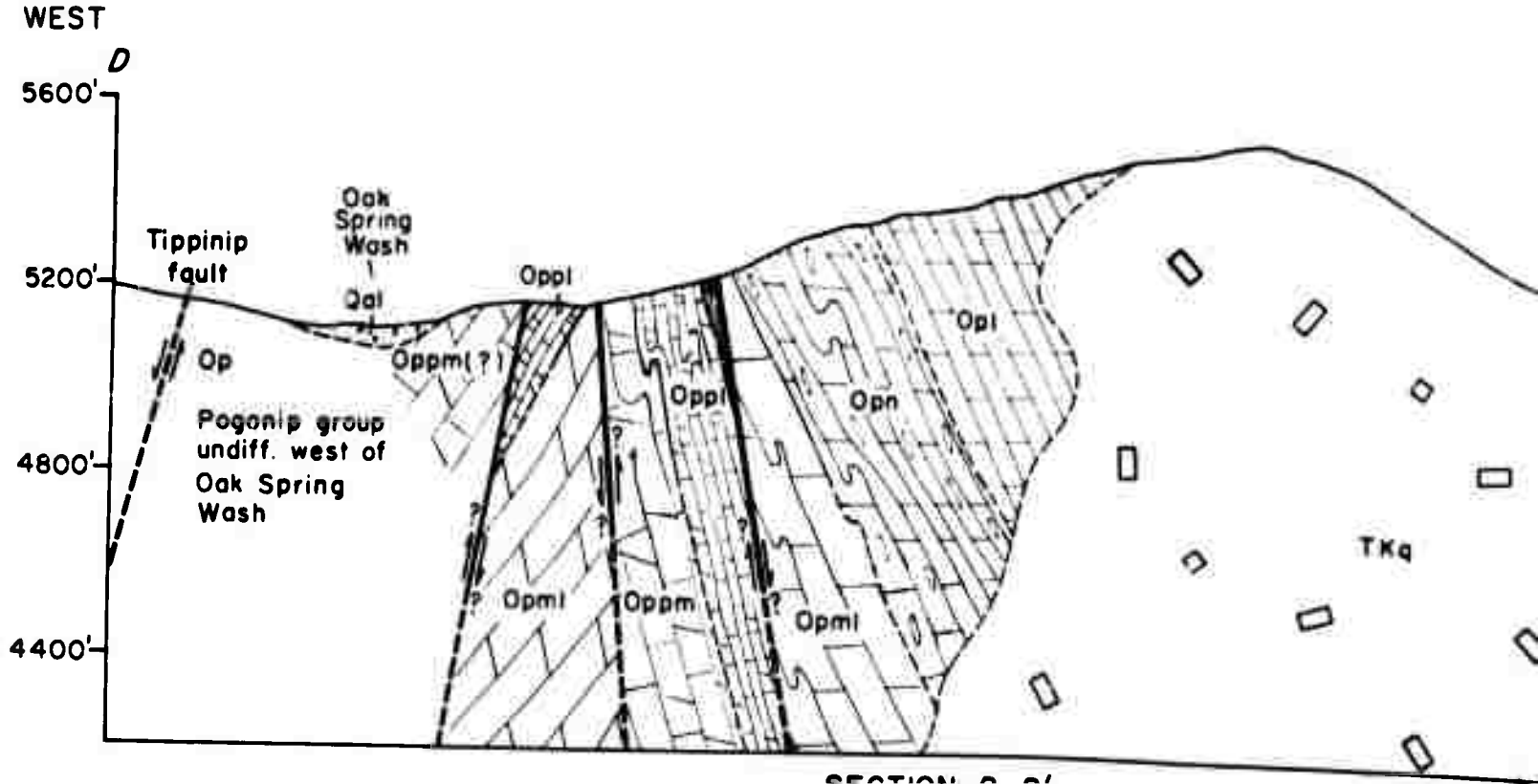
WEST
D
5600'
5200'
4800'
4400'
Tippinip fault
Oak Spring Wash
Qal
Op
Pogonip group undiff. west of Oak Spring Wash
Oppl
Oppm(?)
Opmi
Oppm
Opn
Opl
TKq

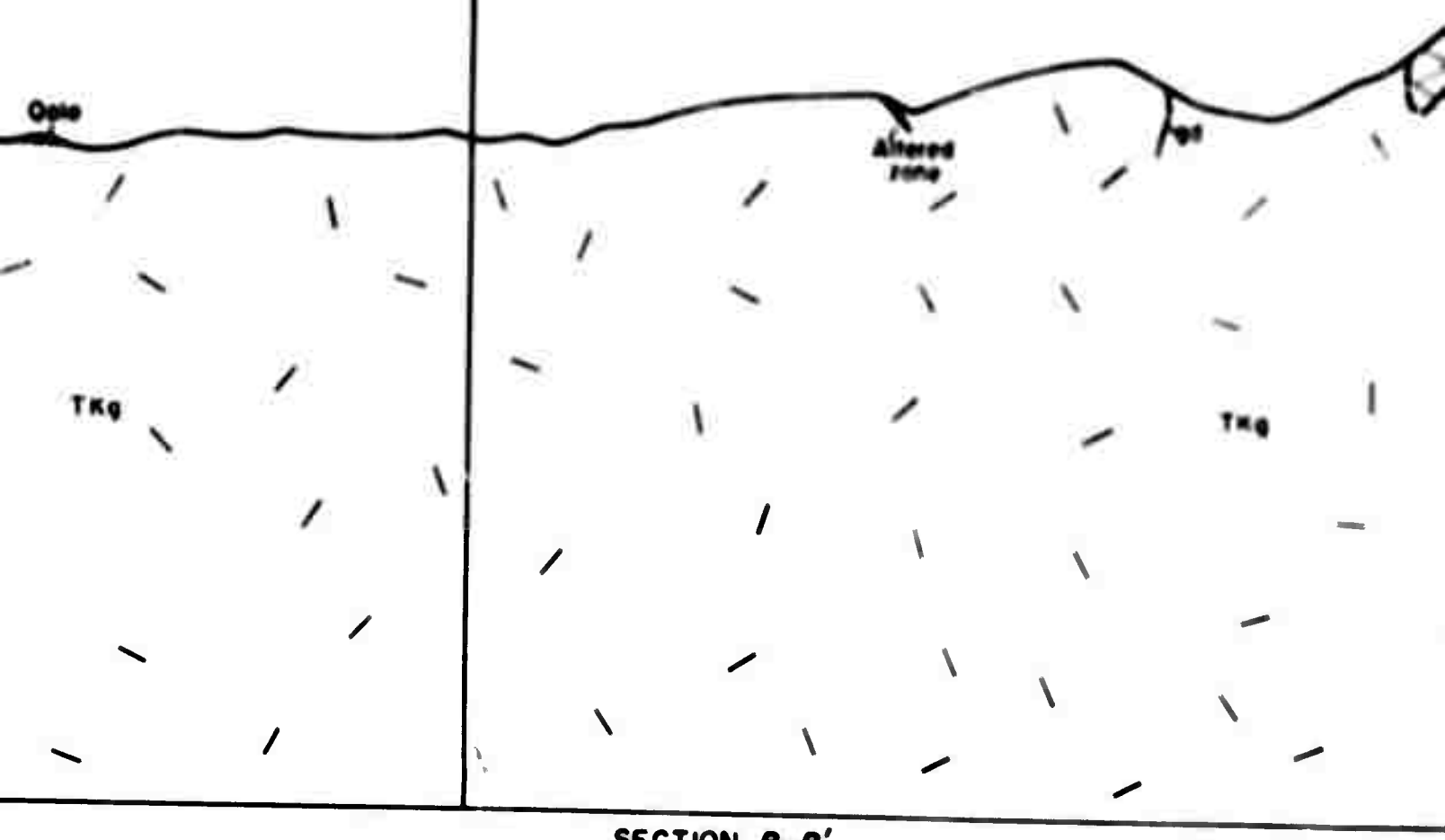

SECTION B-B'

NORTHWEST

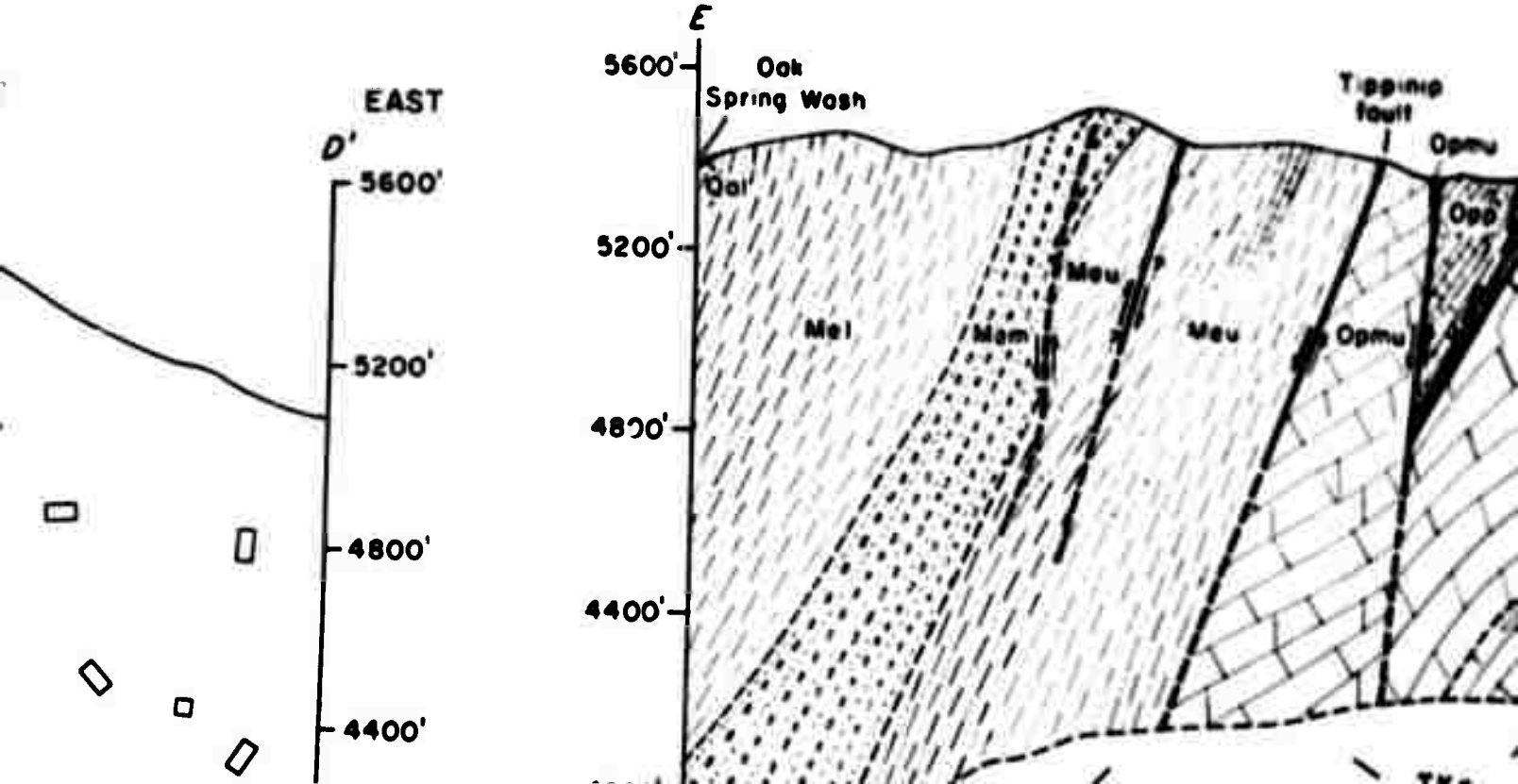

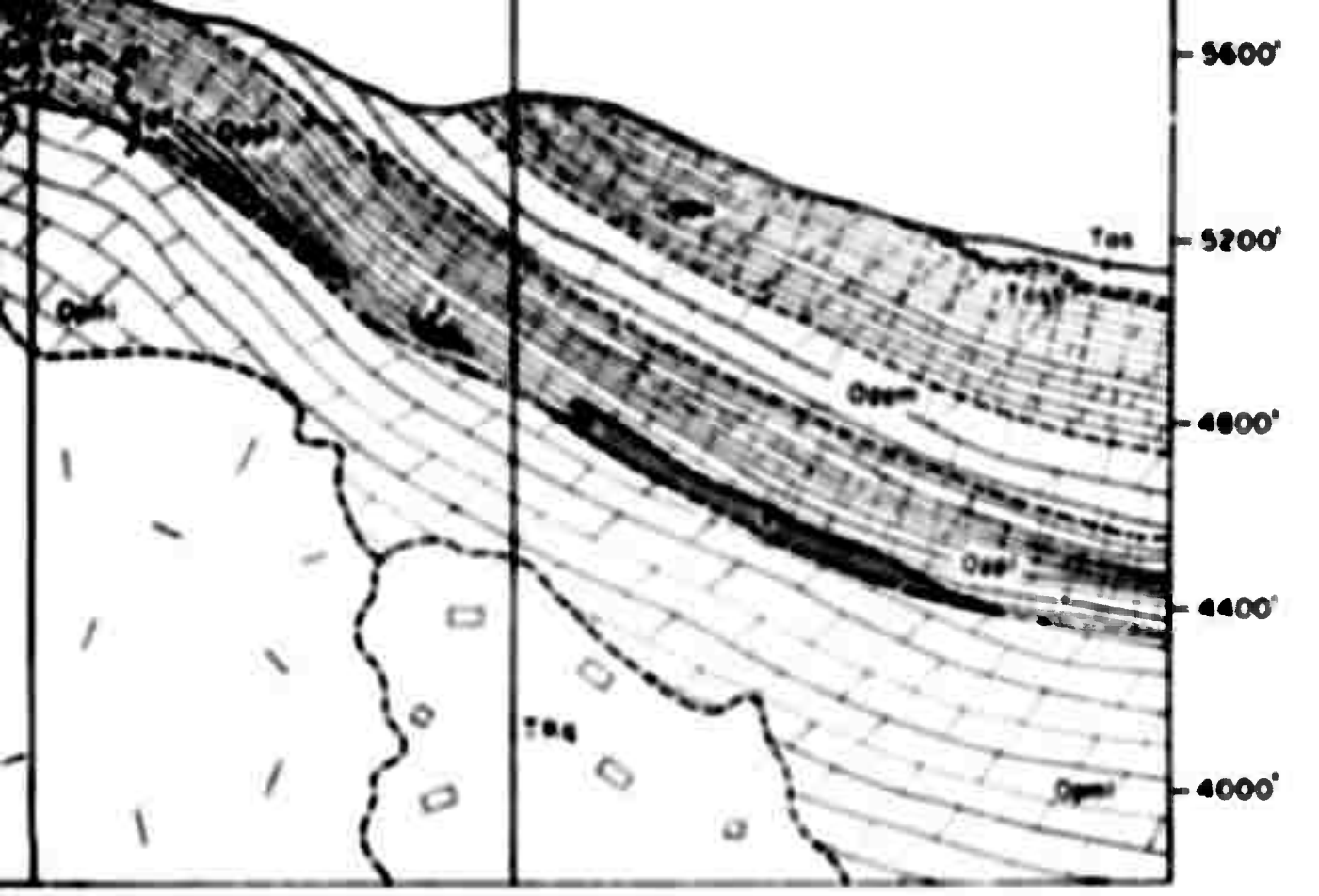
5600'
5200'
4800'
4400'
4000'
Tos
Opm
Tkq

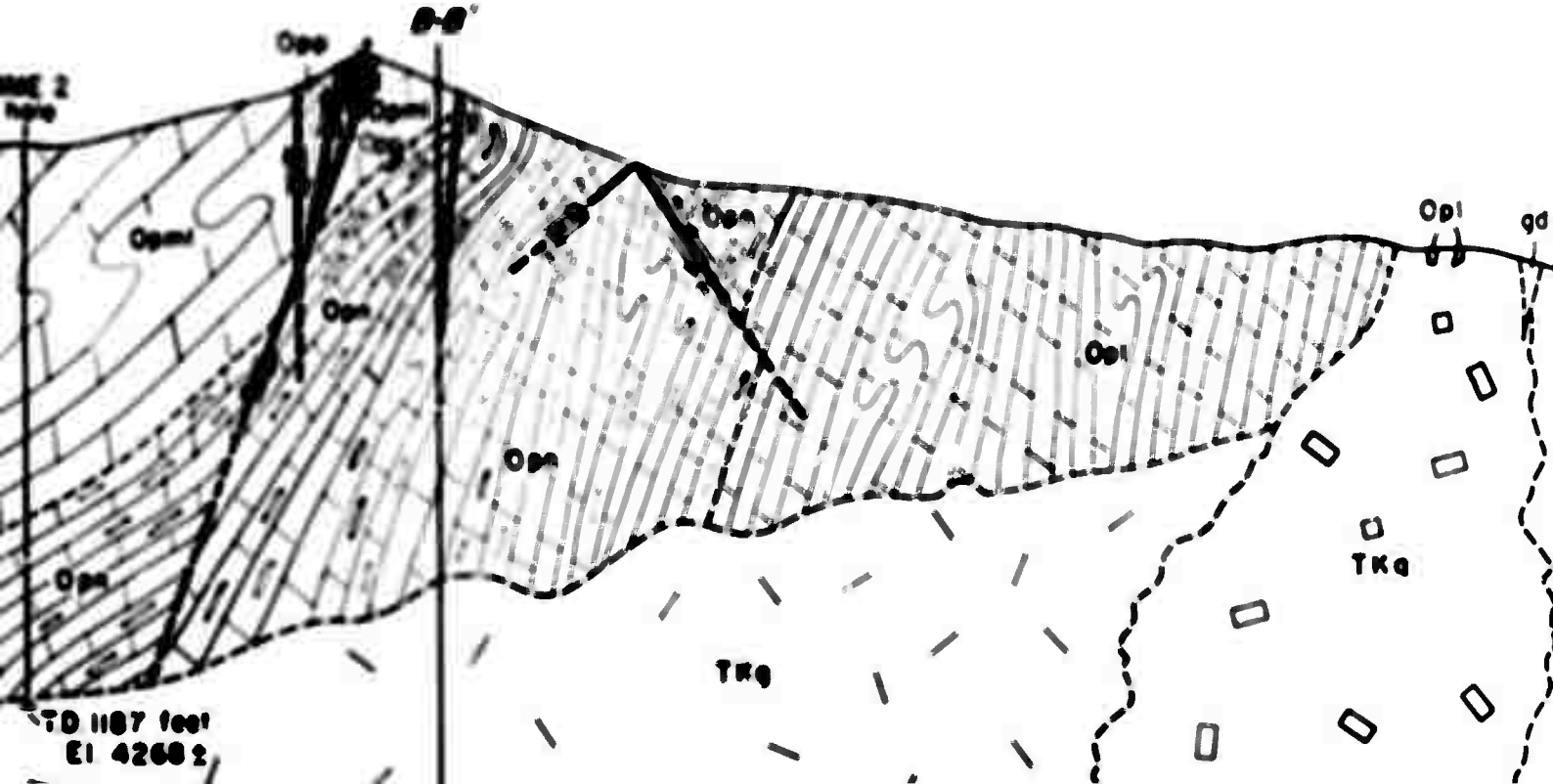
B-B'
Opo
Opm
Opl
TKq
TD 1187 feet
El 4268 ±

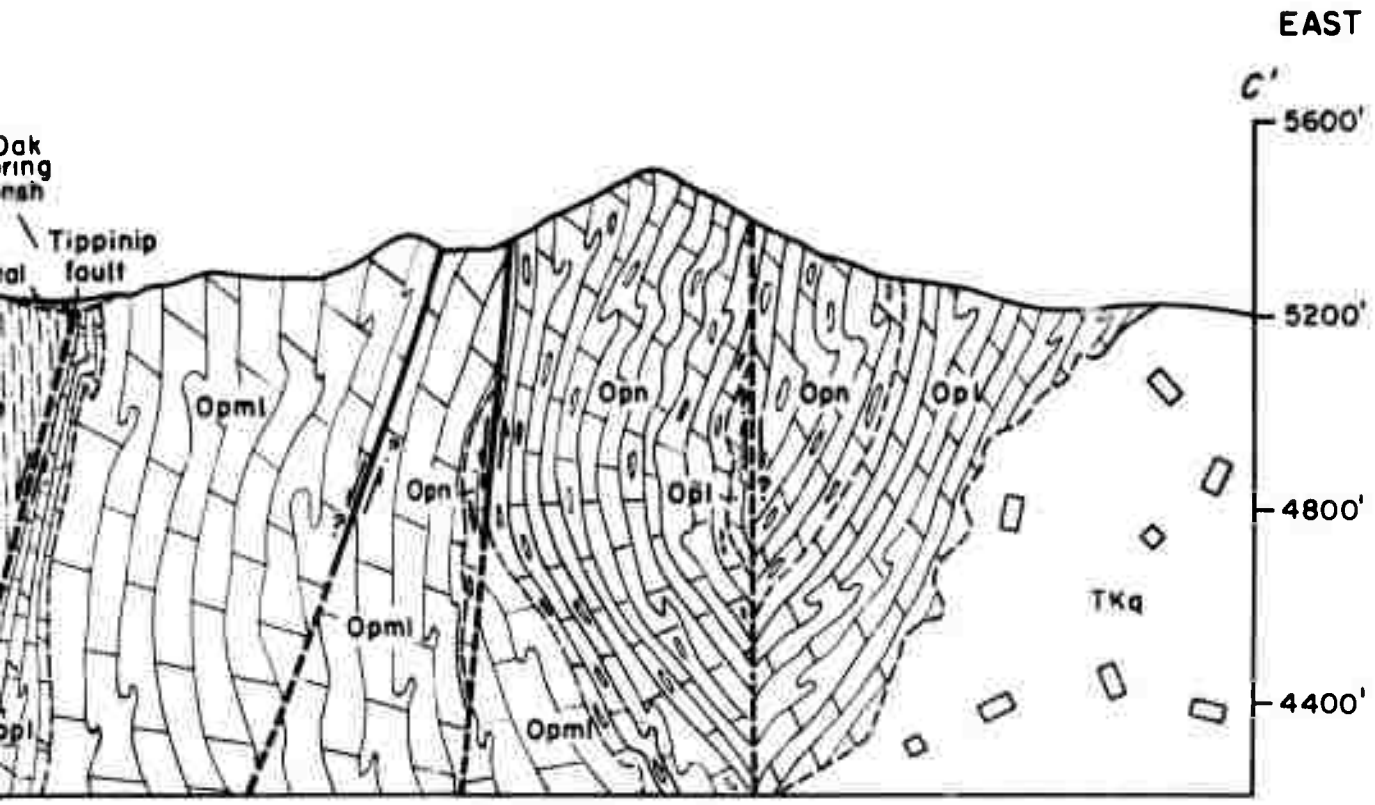
EAST
C'
5600'
5200'
4800'
4400'
Tippinip fault
Opml
Opn
Opl
TKq
SECTION C-C'

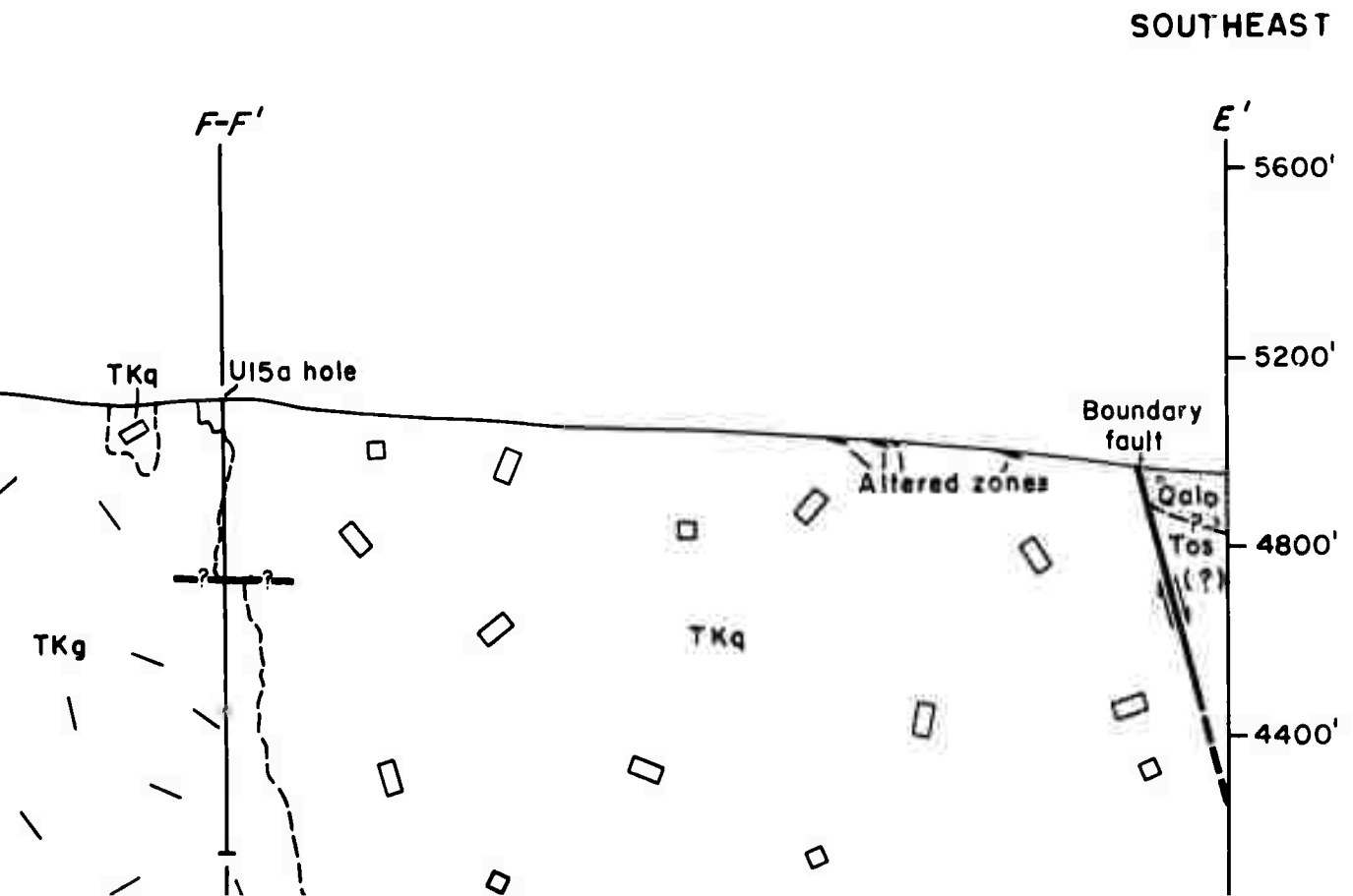
SOUTHEAST
F-F'
E'
5600'
5200'
4800'
4400'
TKq
U15a hole
Boundary fault
Altered zones
Qalo
Tos
(?)
TKg
TKq

EAST

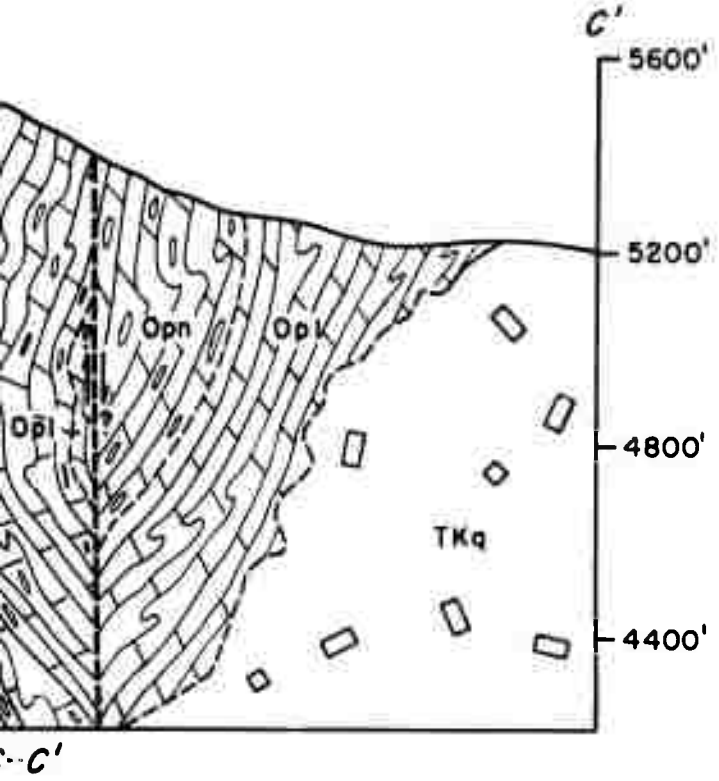

SOUTHEAST

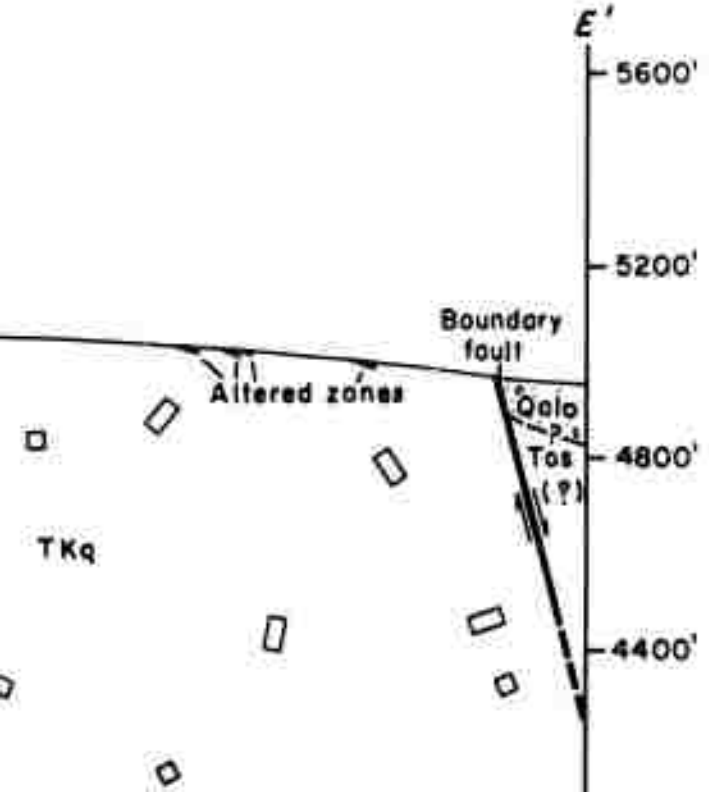

Porphyritic quartz manzonite

Granodiorite

Note: No zones of altered igneous rocks are shown below those exposed at the surface.

Tuff and related deposits

STRATIFICATION OR FOLIATION

Thick to very thick bedded

Thin to thick bedded

Laminated to thin bedded

Thinly laminated

SOUTH

K

F

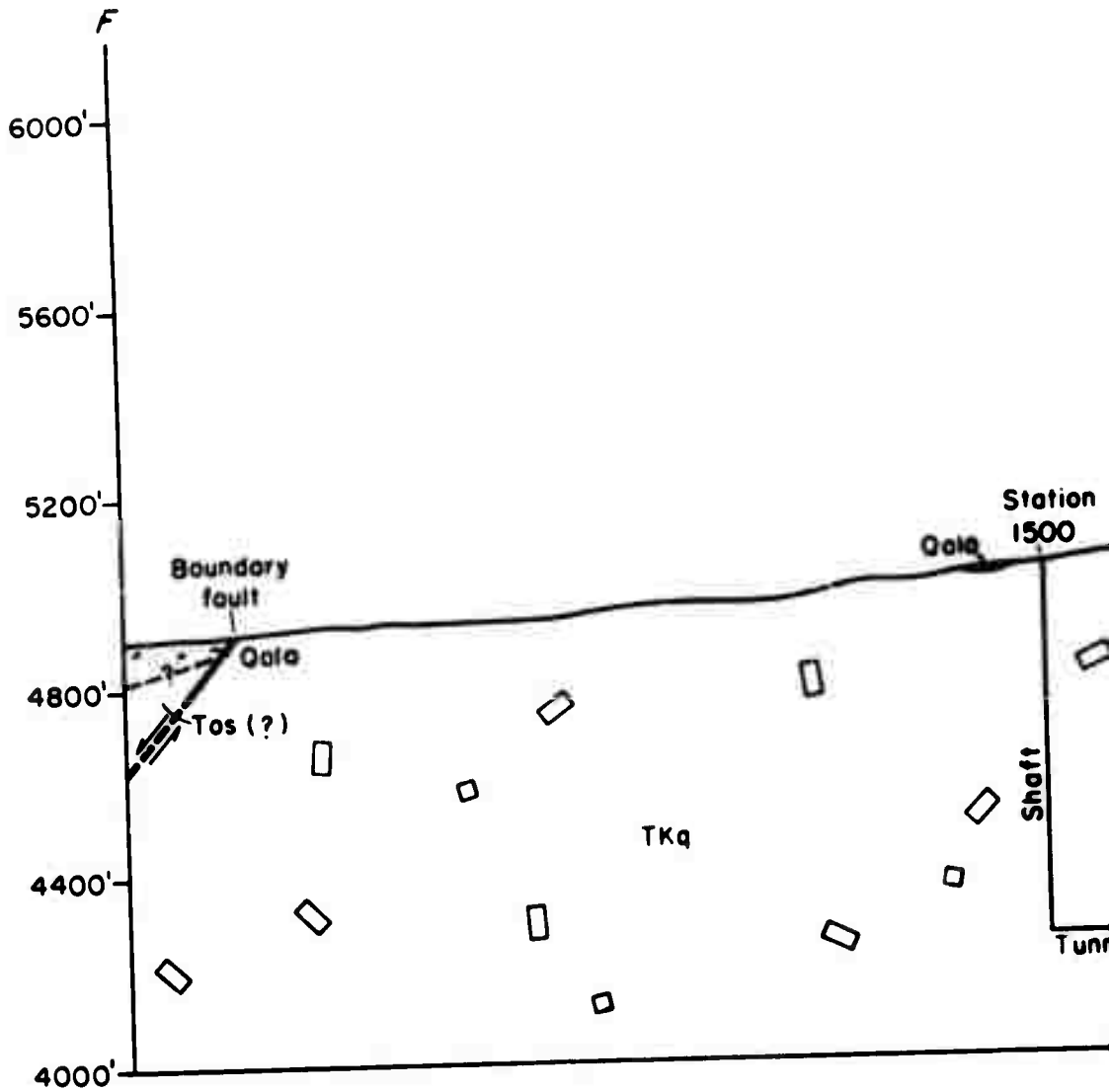
6000'
5600'
5200'
4800'
4400'
4000'
Station 1500
Qala
Boundary fault
Qala
Tos (?)
TKq
Shaft
Tunn

H

G

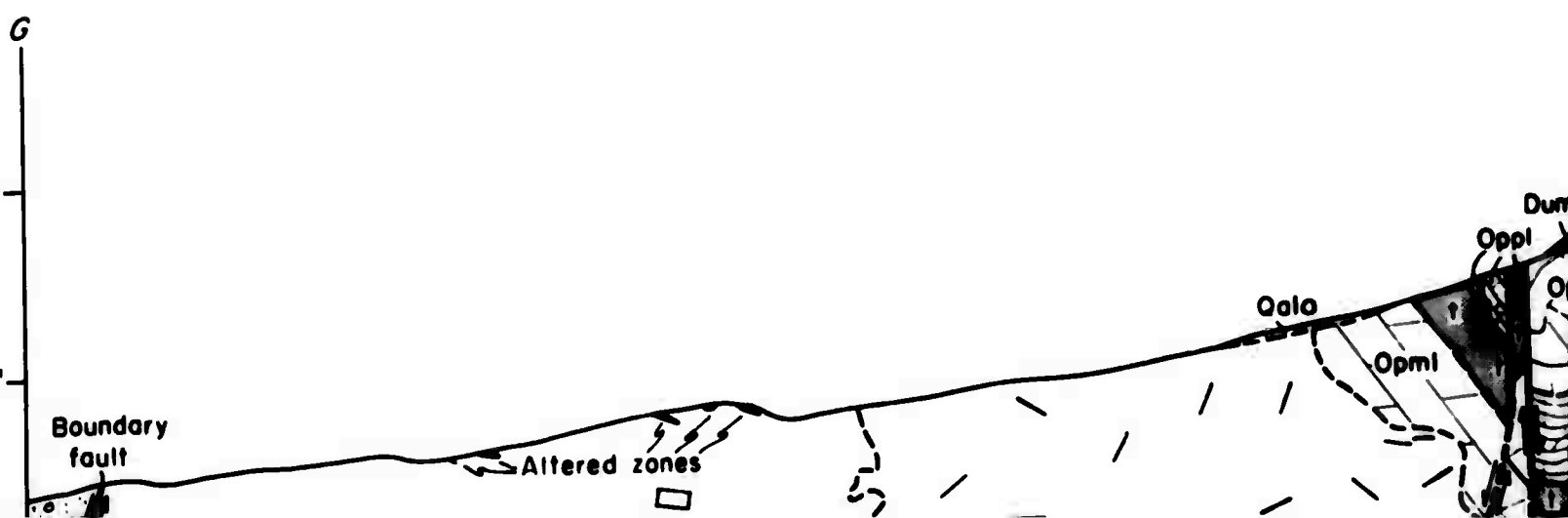
Dum
Oppl
Qala
Opml
Boundary fault
Altered zones

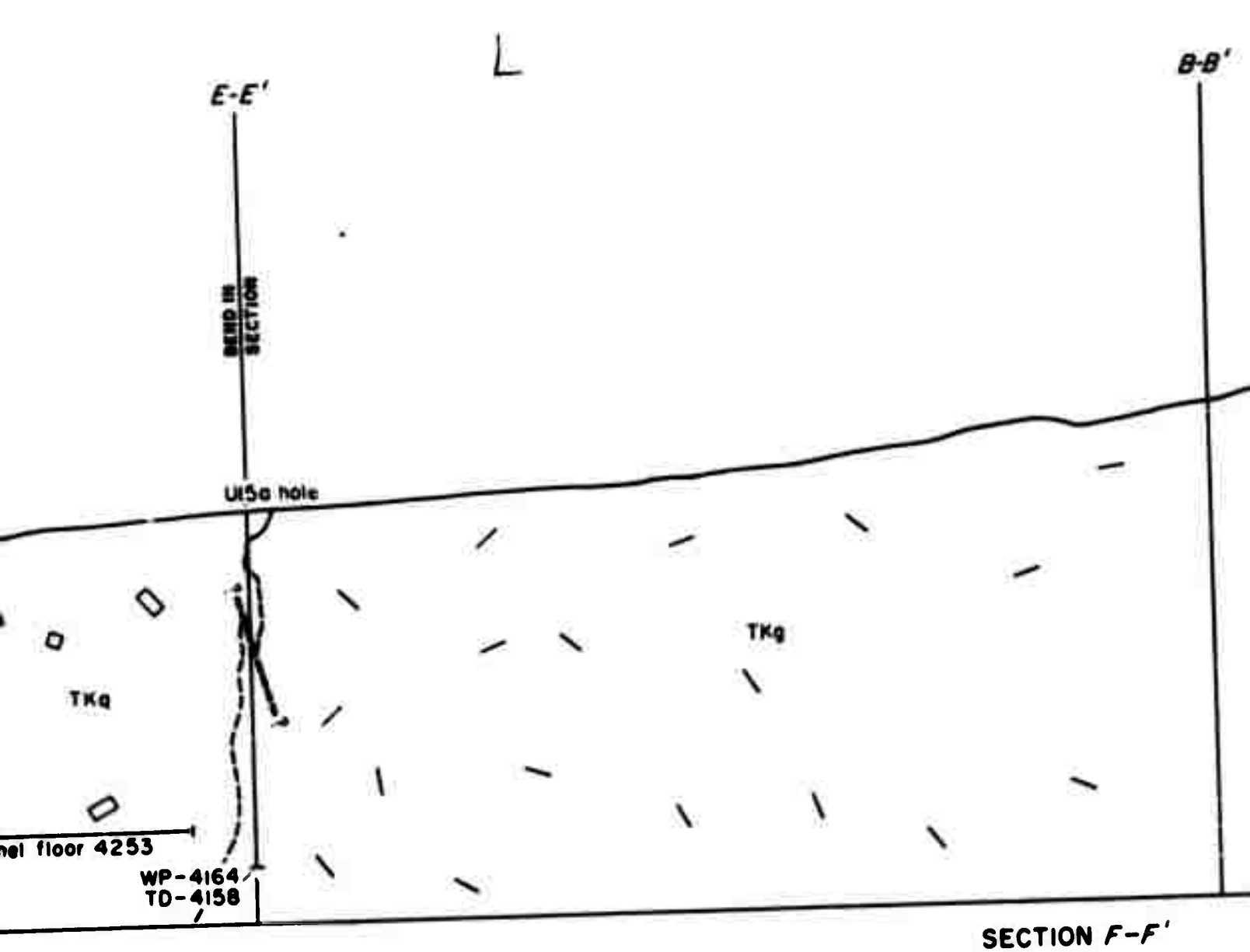
E-E'
B-B'
BEING IN SECTION
U15a hole
TKg
TKg
WP-4164
TD-4158

SECTION F-F'

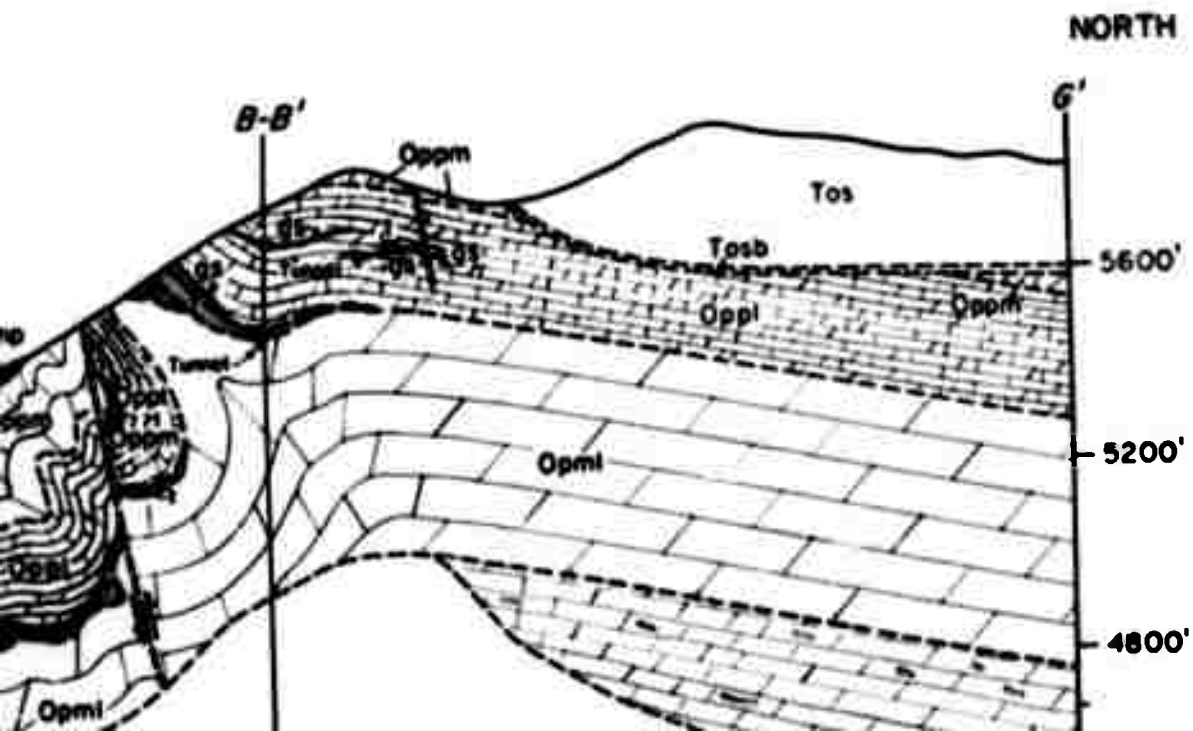
NORTH
B-B'
G'
Oppm
Tos
Tosb
Oppl
Opml
5600'
5200'
4800'

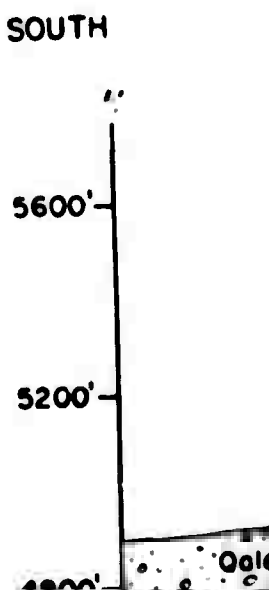
SOUTH
5600'
5200'

M

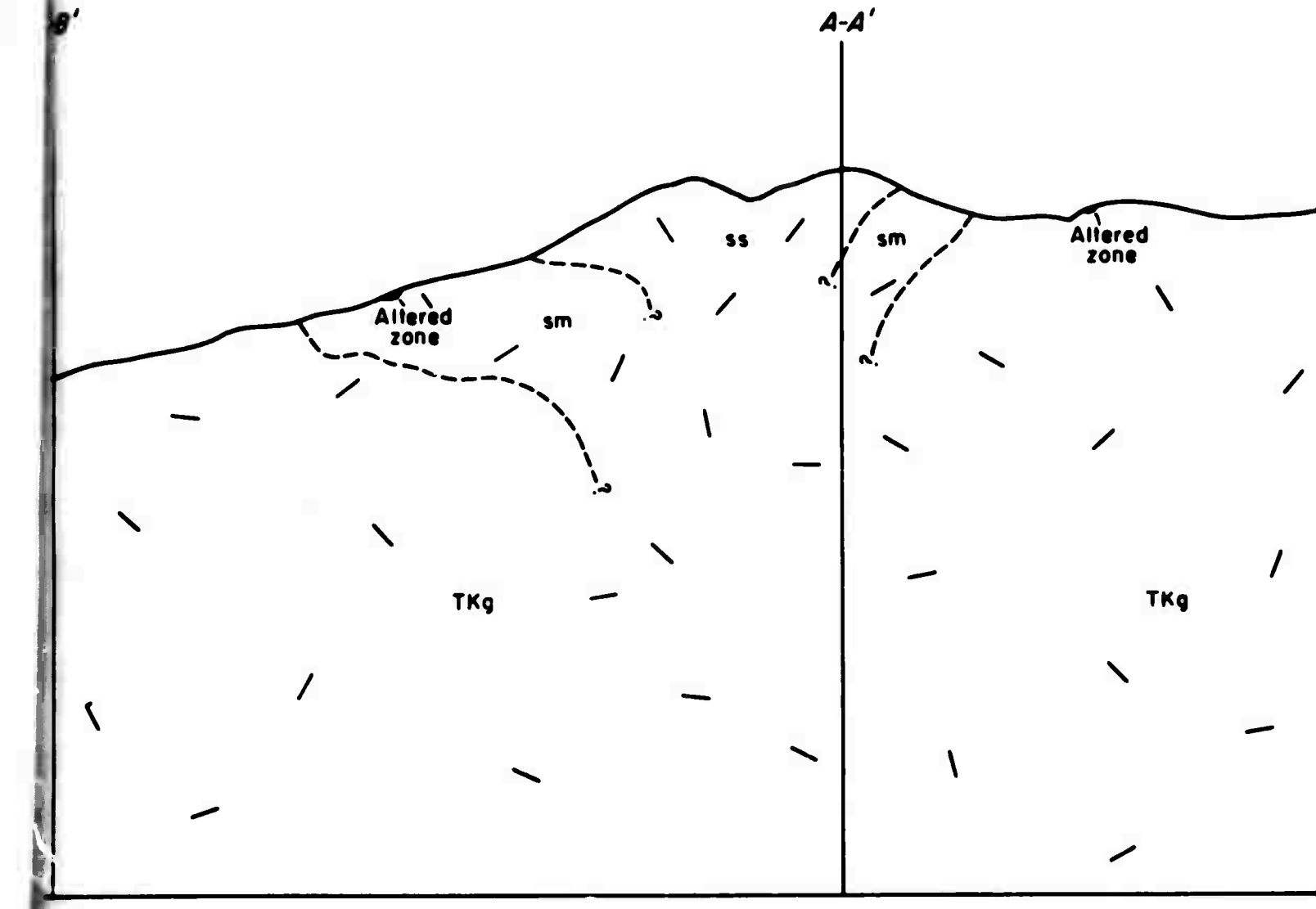

NORTH

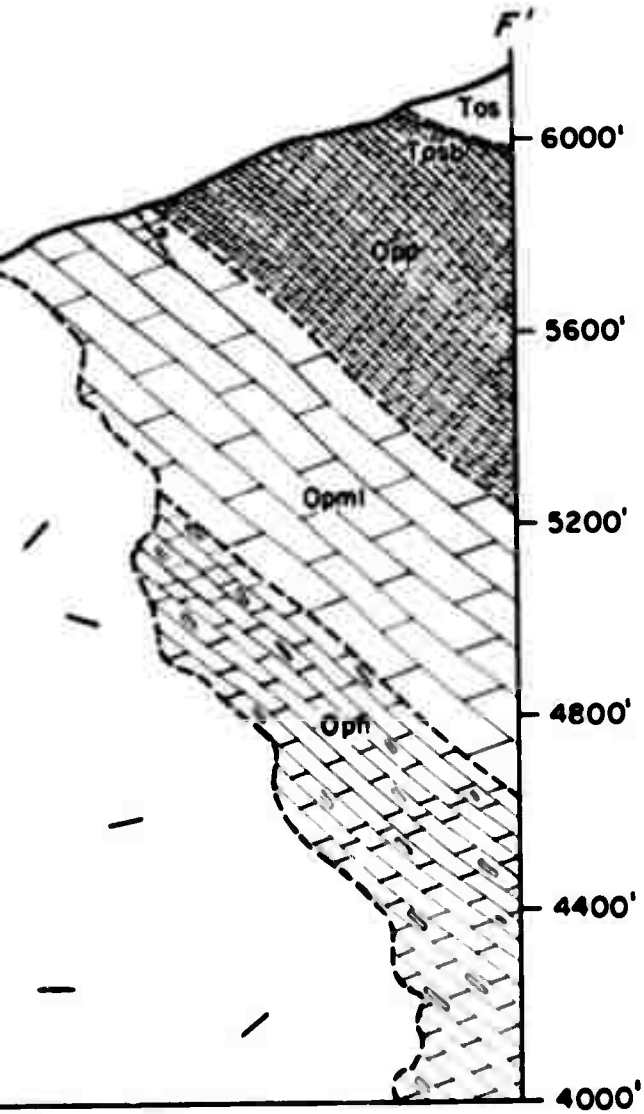

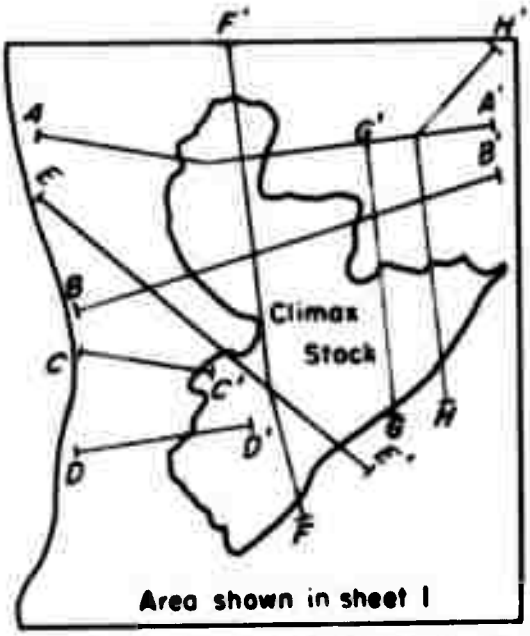

INDEX MAP OF CROSS SECTIONS
See sheet 1 for exact locations

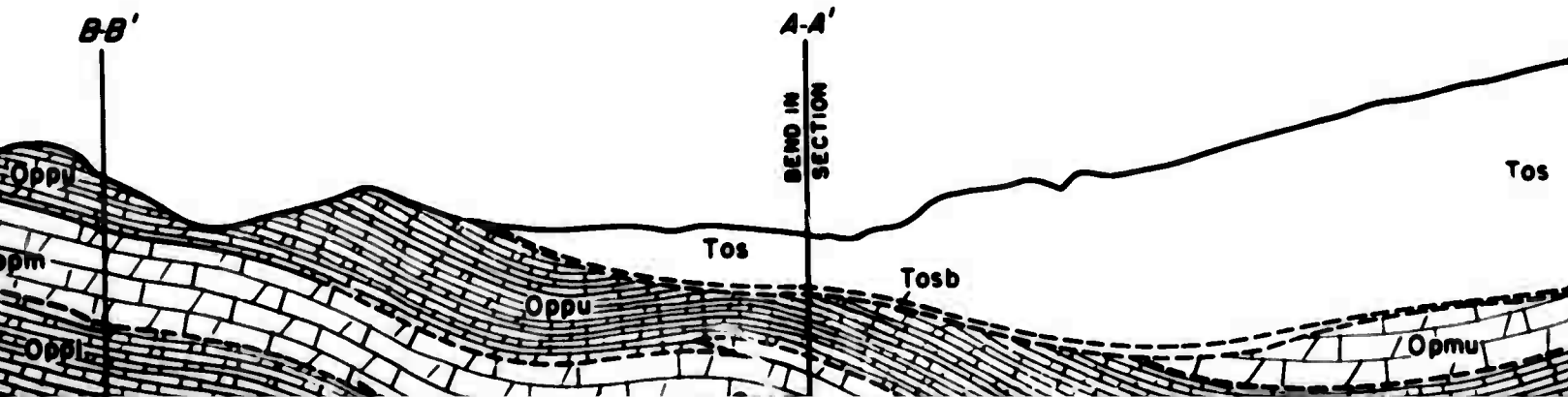

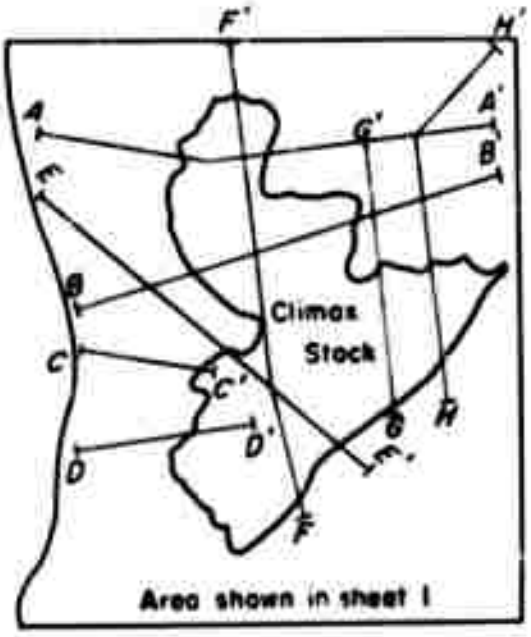

INDEX MAP OF CROSS SECTIONS
See sheet 1 for exact locations

NORTH

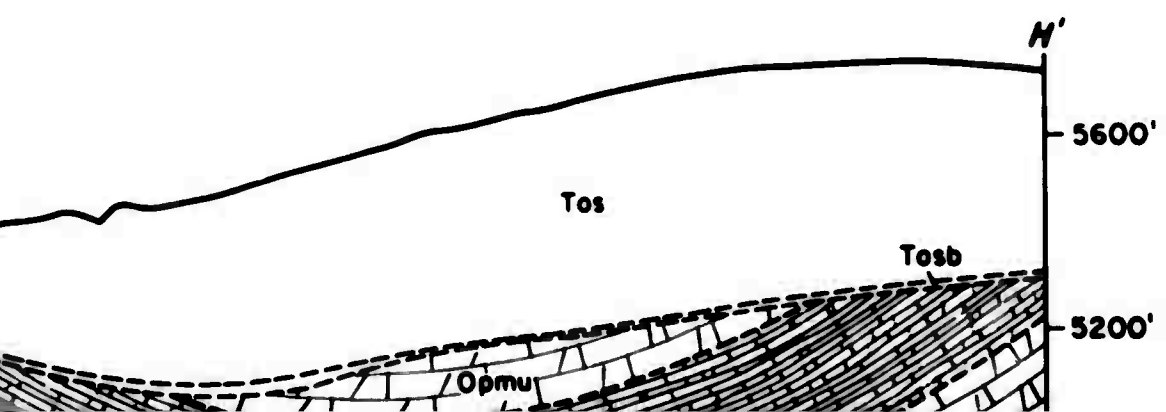

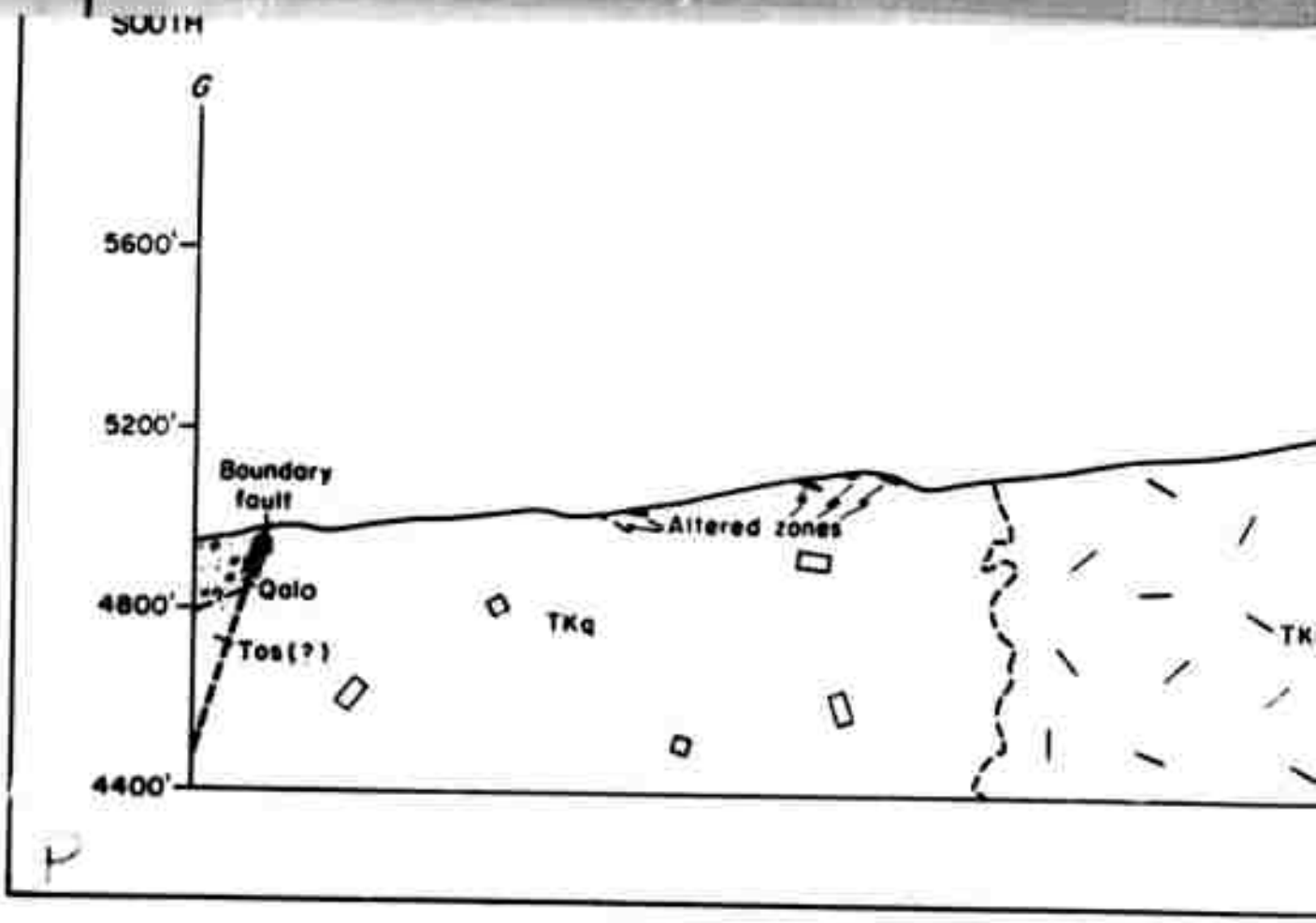

MISCELLANEOUS GEOLOGIC INVESTIGATIONS
MAP I-328 SHEET 2 OF 2

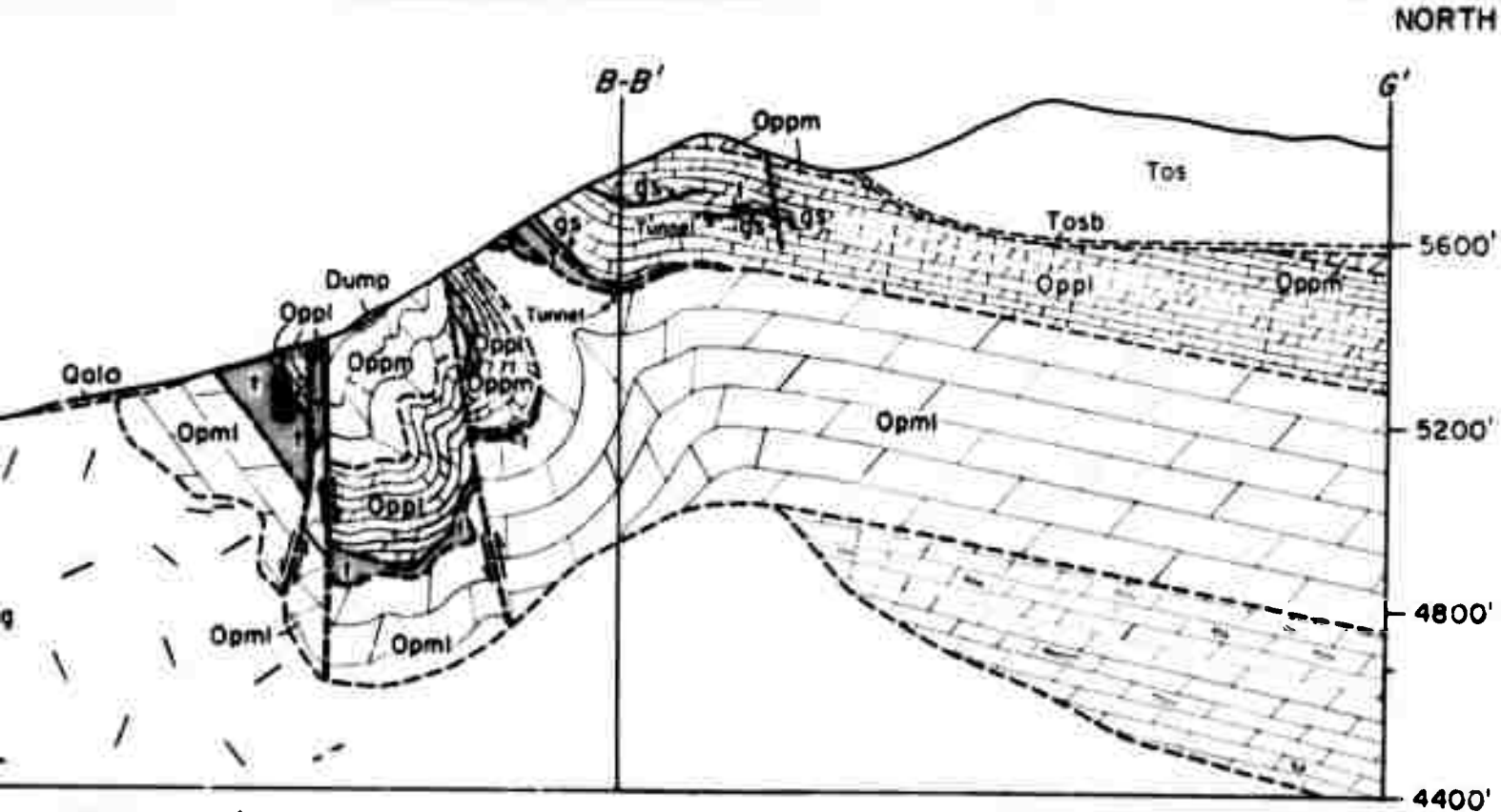

SECTION G-G'

SECTIONS THRO

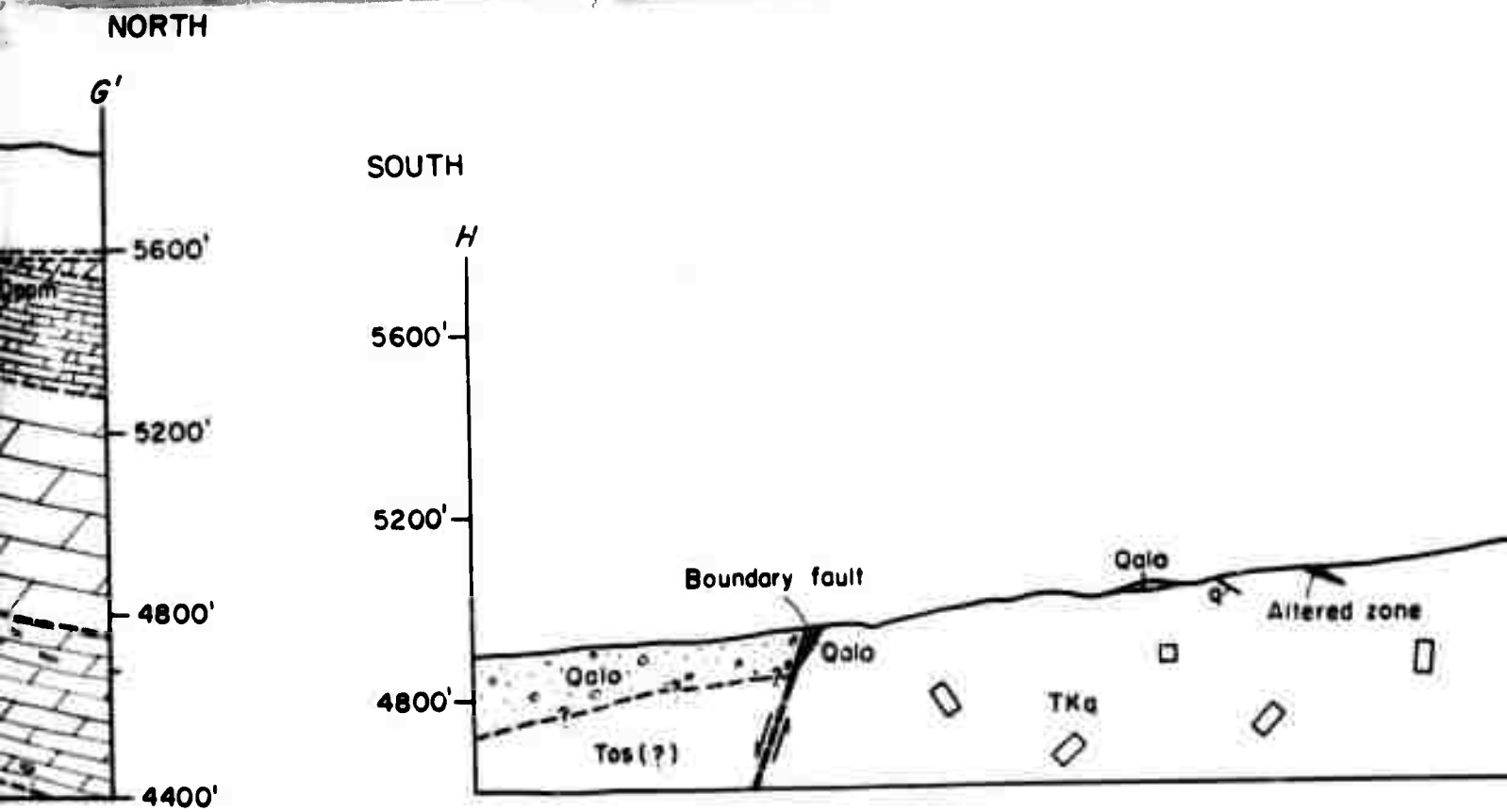

IONS THROUGH PARTS OF THE CLIMAX STOCK, NYE COU

By

F. N. Houser and F. G. Poole

400 0 400 800 1200 FEET

1960

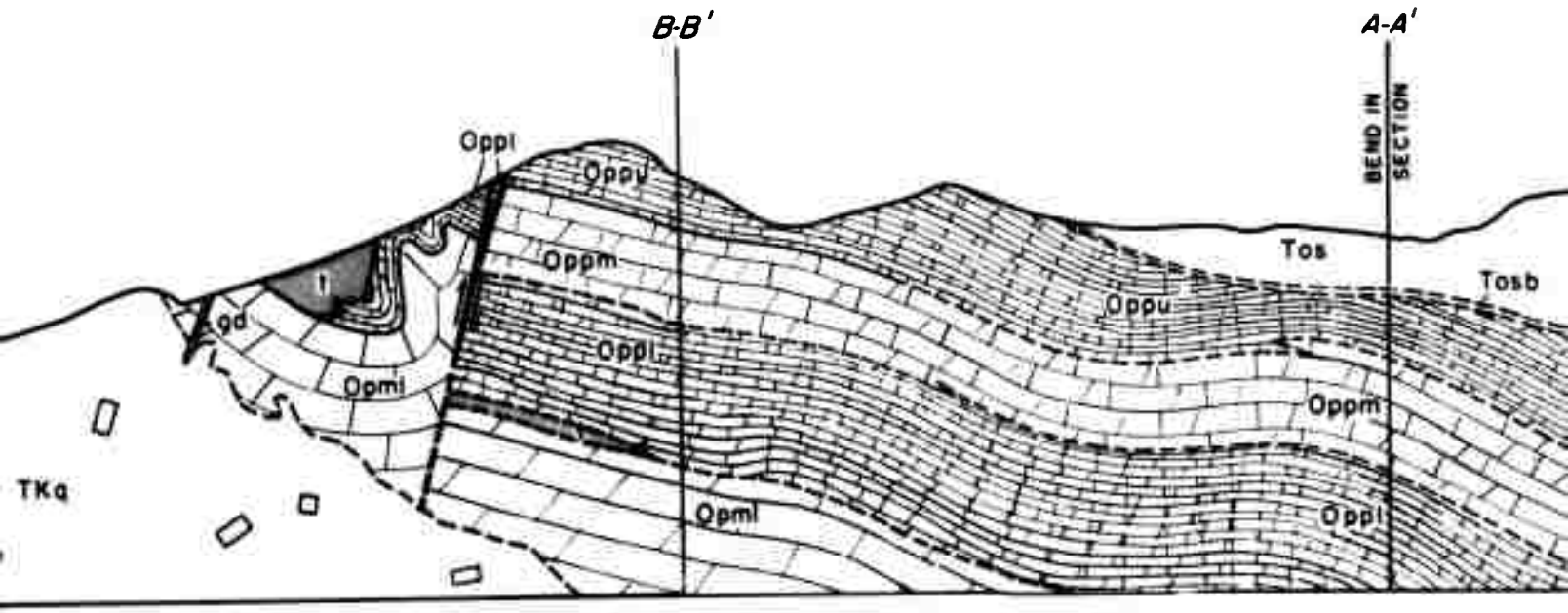

SECTION *H-H'*

Y, NEVADA

SOUTH

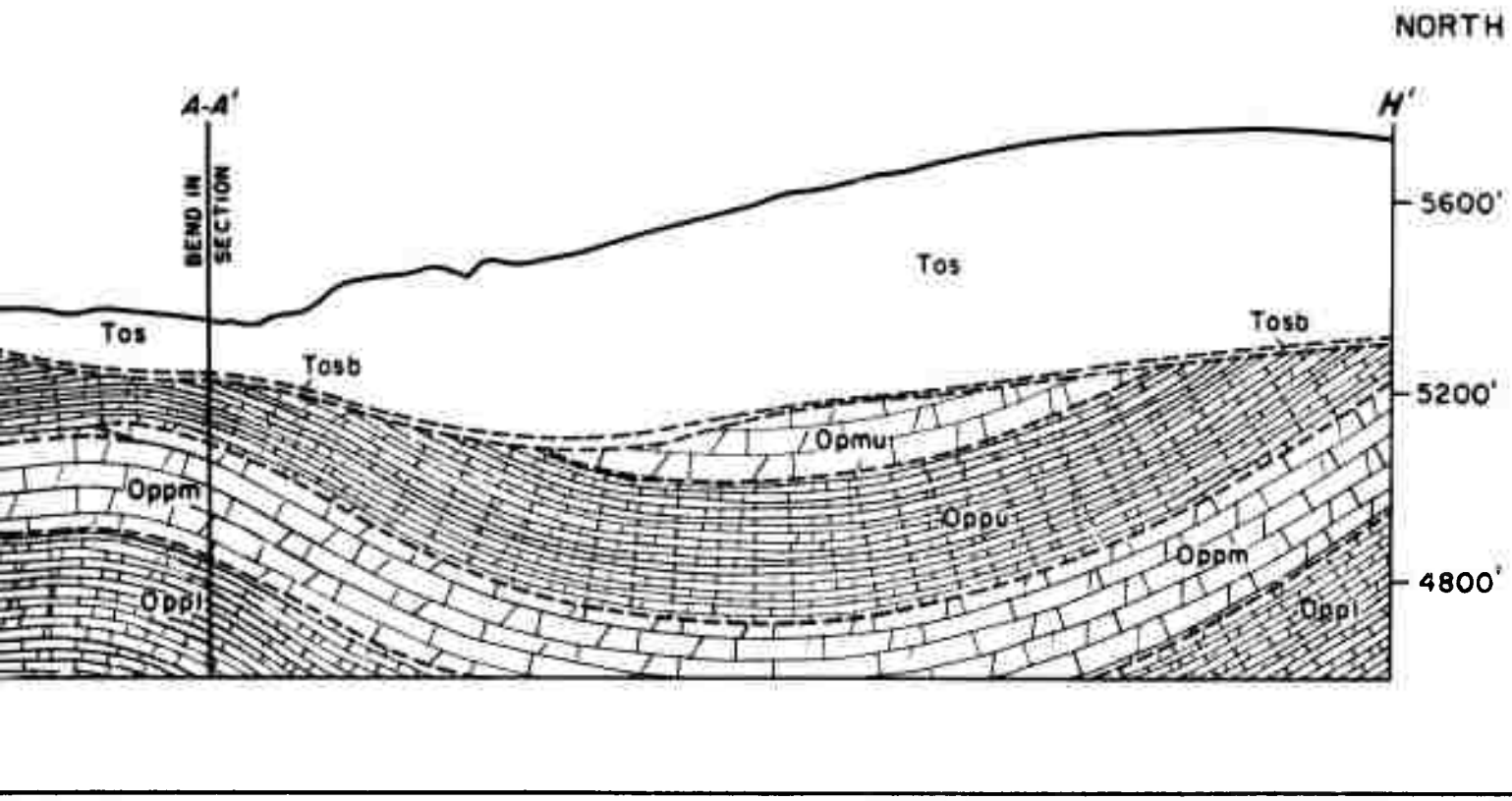

INTERIOR GEOLOGICAL SURVEY, WASHINGTON, D C., 61026

Geology mapped in 1959 and 1960

For sale by U. S. Geological Survey, price 1.50 per

DEPARTMENT OF THE INTERIOR
NITED STATES GEOLOGICAL SURVEY

PREPARED IN COOPERATION WITH THE
U S ATOMIC ENERGY COMMISSION

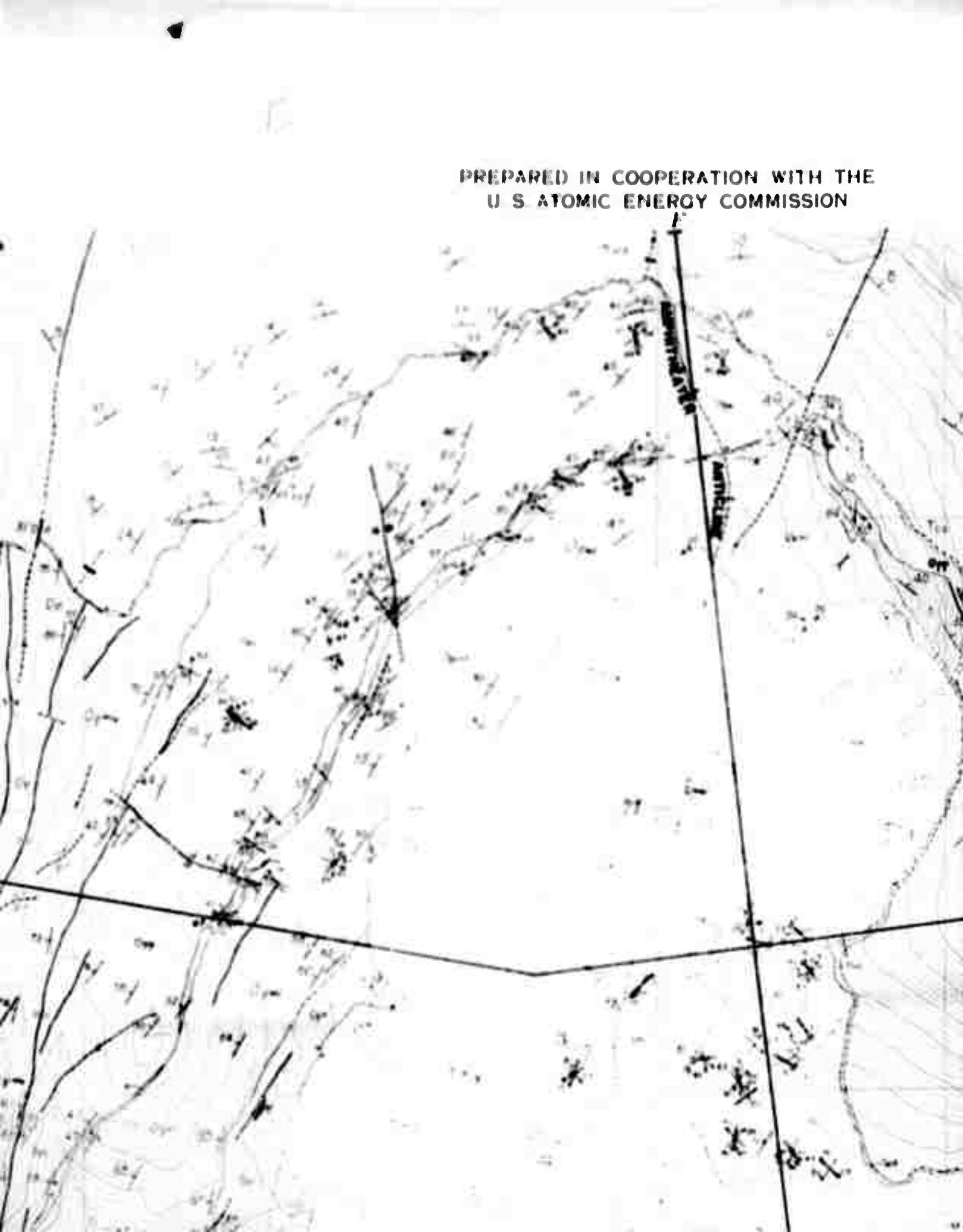

ION WITH THE
COMMISSION

C

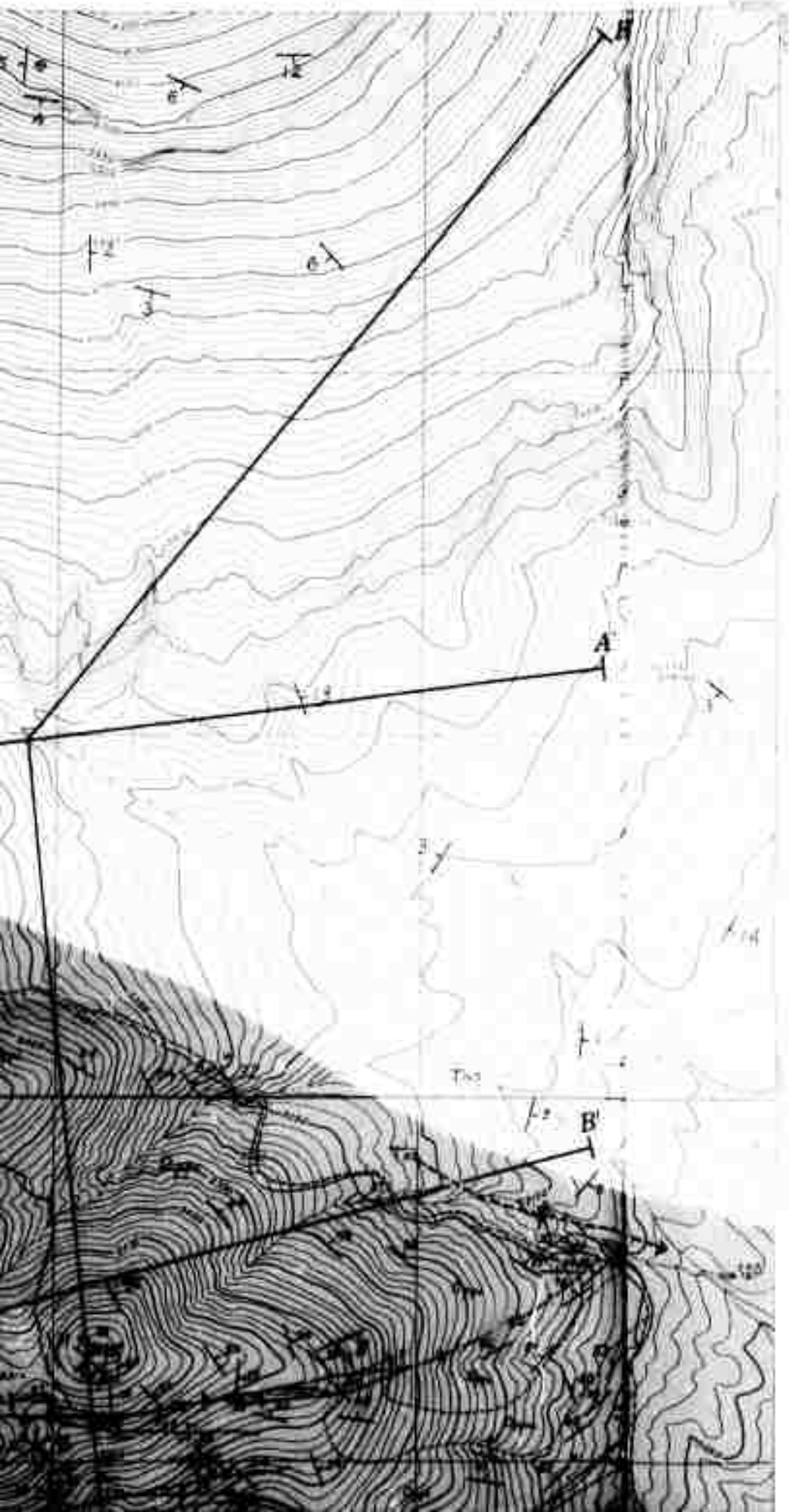

Younger
Unconsolidated grave
beds and la

Olde
Chiefly carbonate-
granu

O
Tosw, gray pumiceou
Tos, white, red, ye
crystal vitric tu
part.
Tosb, widespread ba
rubble breccia an
tuff

Granite, light-gray, e
aplite to pegmatite;
"a" prefixed to gd o
sericitic, or silici
sill

Granodiorite, light- t
grained, some fine-g

Quartz monzonite, light
to medium-g

Tipp
Dolomite, medium- to
line, thick- to very
timated minimum thi

E
Me, undifferentiated
Meu, argillite, chief

EXPLANATION

QUATERNARY

Qal

Younger alluvium and colluvium
Unconsolidated gravel, sand, silt, and clay in main stream beds and large talus deposits on slopes

Qalo

Older alluvium and colluvium
Chiefly carbonate-cemented or unconsolidated sand and granule and pebble conglomerate

TERTIARY

Tosw
Tos
Tosb

Oak Spring formation
Tosw, gray pumiceous crystal vitric welded tuff.
Tos, white, red, yellow, pink-gray pumiceous nonwelded crystal vitric tuff, zeolitized, especially in lower part.
Tosb, widespread basal unit; reddish-brown tuffaceous rubble breccia and conglomerate, and conglomeratic tuff

CRETACEOUS(?) OR TERTIARY(?)

Granite, light-gray, equigranular, fine- to coarse-grained; aplite to pegmatite; occurs as dikes (gd) and sills (gs); "a" prefixed to gd or gs indicates feldspathic, argillic, sericitic, or silicic alteration prominent in dike or sill

TKg

Granodiorite, light- to greenish-gray, predominantly medium grained, some fine-grained; occurs as a stock and sills

TKq

Quartz monzonite, light- to medium-gray, porphyritic, fine- to medium-grained; occurs as a stock

PENNSYLVANIAN AND PERMIAN(?)

PPt

Tippipah(?) limestone
Dolomite, medium- to dark-gray, aphanitic to finely crystalline, thick- to very thick bedded, nonfossiliferous. Estimated minimum thickness 200 feet

Me
Meu
Mem
Mel

Eleana formation
Me, undifferentiated
Meu, argillite, chiefly very dark gray, red-purple or buff, laminated to thin-bedded. Limestone, light- to very dark-gray, finely to coarsely crystalline, partly

PLANATION

QUATERNARY

TERTIARY

CRETACEOUS(?) OR TERTIARY(?)

PENNSYLVANIAN AND PERMIAN(?)

ALTERATION

Note: Not indicated specifically are broad areas of the stock that have undergone pervasive hydrothermal pyrite mineralization and argillic alteration of plagioclase and(or) chloritic alteration of biotite Also not specifically indicated is the extensive silication of the marble along fractures near the edges of the stock The following areas of alteration have been mapped mainly in the stock except as noted

Silicic alteration, strong(ss) and moderate (sm). Excludes individually mappable veins or groups of veins

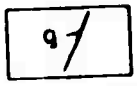

Quartz vein or group of veins

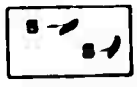

Sericitic

Sericite (white mica) is predominant or prominent mineral

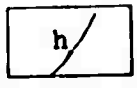

Hematitic

Hematite in prominent amounts. Generally associated with masses of altered igneous rock in which quartz is prominent or along siliceous or silicate veins in the marble

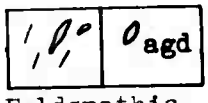

Feldspathic

(without letter symbol on map)

Lens-shaped feldspathized masses of igneous rock, commonly argillized and subordinately sericitized, silicified, and pyritized. The masses are commonly stained red, purple, yellow, and(or) brown by iron(?) oxides Because of the similarity of the size and shape at map scale, the granite dikes affected by the same alteration are indicated by "a"

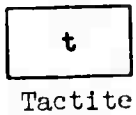

Tactite

Predominantly garnet with subordinate quartz, epidote, green mica(?), limonite, calcite, sulfide, tungstate, and copper carbonate minerals

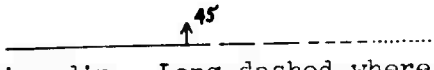

Contact, showing dip. Long dashed where approximately located, short dashed where gradational or inferred, dotted where concealed

and copper carbonate minerals

B

C

D U

IPPINIP FAULT

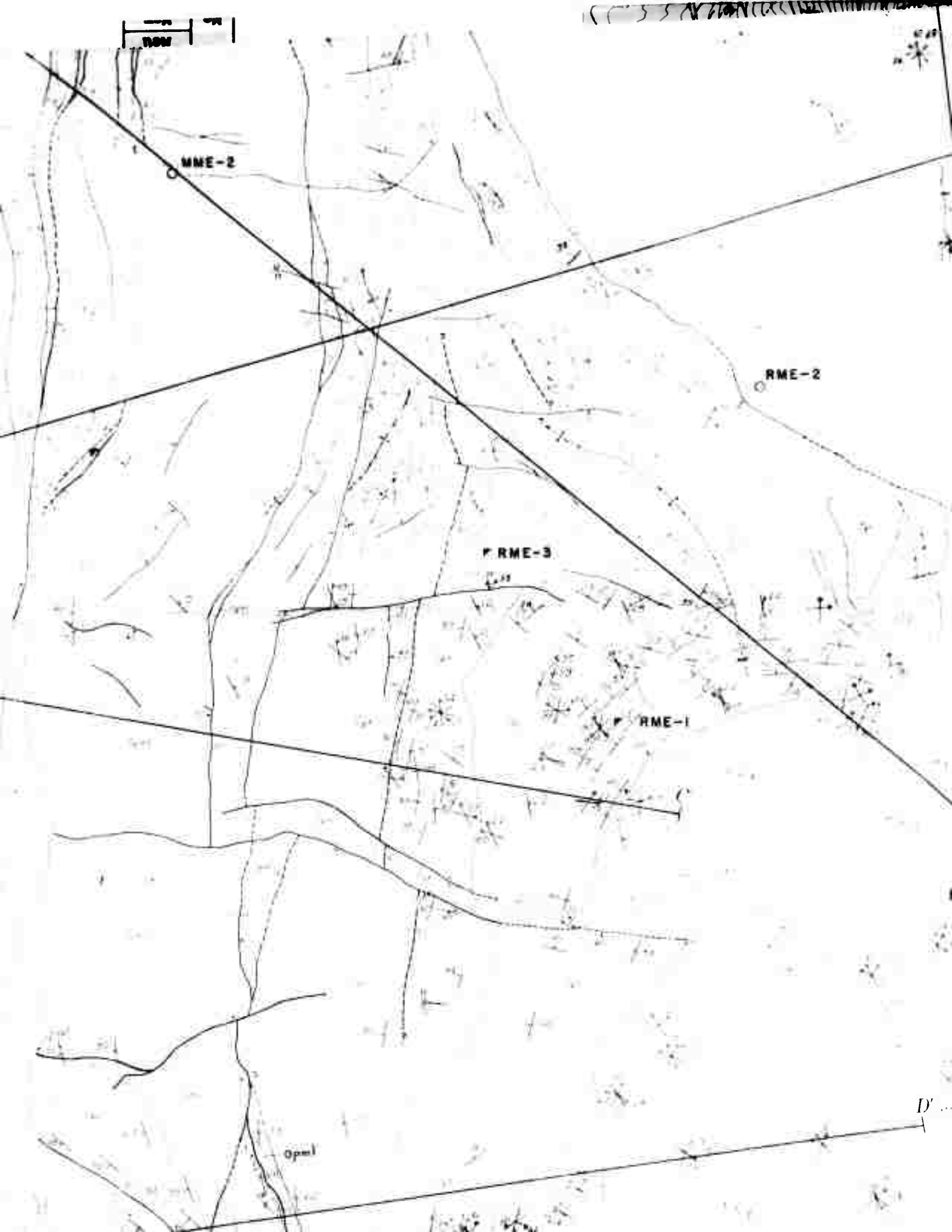
MME-2
RME-2
RME-3
RME-1
D'
Opml

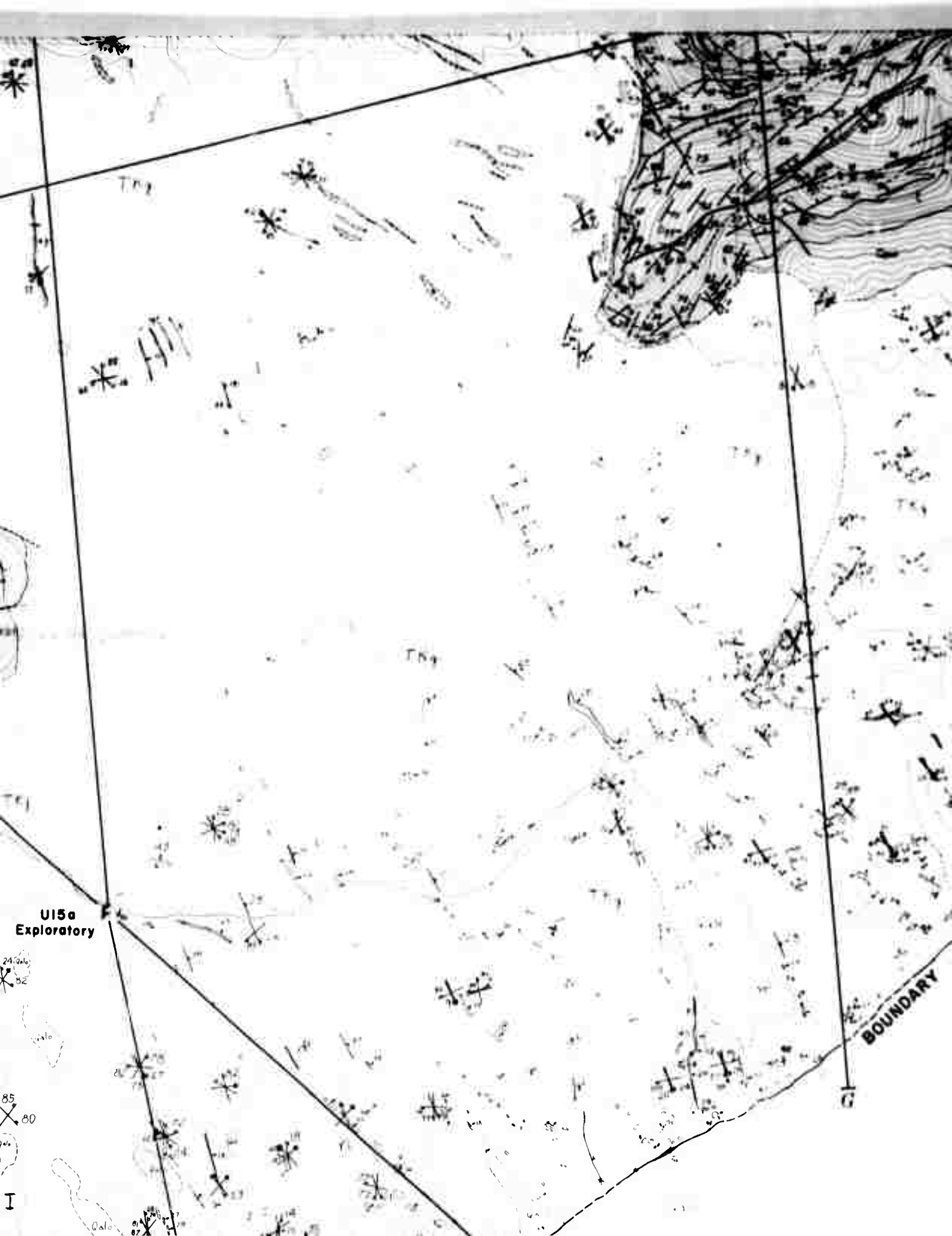
U15a
Exploratory
BOUNDARY

Ele

Me, undifferentiated

Meu, argillite, chiefly
buff, laminated to th
very dark-gray, finel
clastic, laminated to
abundant crinoids, in
argillite (80 percent
minerals east of Oak

Mem, quartzite, dar.. br
grained and silt, sub
and pebble conglomera
argillite, light-gray
700 to 1,200 feet.

Mel, predominantly argi
brownish-gray with su
plant remains and wor
excess of 2,400 feet

The Eleana formation as
Pennsylvanian age bec
Pennsylvanian corals
part of the formation

Devonian(?) r

Limestone and dolomitic
to dark-gray, very fi
part marble. Thickne
feet

Devonia

Ordovician r

Dolomite and limy dolom
to coarsely crystalli

Eu

Quartzite, white to ve
abundant locally, fi
vitreous, brittle, v
apparent

Op

Po

Dolomite to dolomitic li
bluish-gray, finely t
to thick-bedded, comm
cated). Partly to wh
places. Original str
cated by poor to mode
mainly by color bands
The map units differ

on

gray, red-purple or
Limestone, light- to
ly crystalline, partly
bedded, common to
n upper 400 feet with
s metamorphic silicate
. Thickness: 970 feet.
, very fine to fine-
rounded grains; granule
ray; and interbedded
brown Thickness:

lowish-brown to light
pale-red zones. Common
). Thickness: in

cludes the rocks of
e presence of Permian and
idium, in the uppermost

MISSISSIPPIAN

ifferentiated
e, buff, very light gray
oarsely crystalline, in
own but is at least 300

DEVONIAN(?)

urian, and
ifferentiated
ht- to medium-gray, finely
art marble

ORDOVICIAN, SILURIAN, AND DEVONIAN(?)

rtzite
gray, yellow iron stain
edium-grained, well-sorted,
, stratification is not

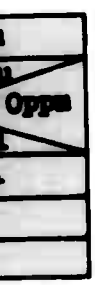

group
, very light gray to
ly crystalline, laminated
nodules (mostly sili-
nverted to marble in most
tion is absent or is indi-
good foliation defined
rtly by crystallinity.
e general description as

ORDOVICIAN

Contact, showing dip. Long dashed where approximately located, short dashed where gradational or inferred, dotted where concealed

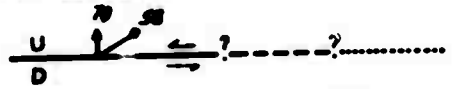

Fault, showing dip and plunge of slickensides. Dashed where inferred, dotted where concealed, queried where doubtful U, upthrown side; D, downthrown side. Arrows show relative movement

Anticline showing trace of axial plane and direction of plunge of axis. Dashed where inferred

Syncline showing trace of axial plane and direction of plunge of axis. Dashed where inferred

Overturned syncline showing trace of axial plane, direction of plunge and direction of dip of limbs. Dashed where inferred

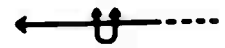

Overturned anticline showing trace of axial plane and direction of dip of limbs. Dashed where inferred

Axis and plunge of minor anticline

Strike and dip of beds

Strike of vertical beds

Horizontal beds

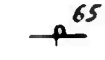

Strike and dip of overturned beds

Strike and dip of joint

Strike of vertical joint

Horizontal joint

Strike and dip of flow layers (Tosw unit only)

C

D

TIPPINIP FAULT

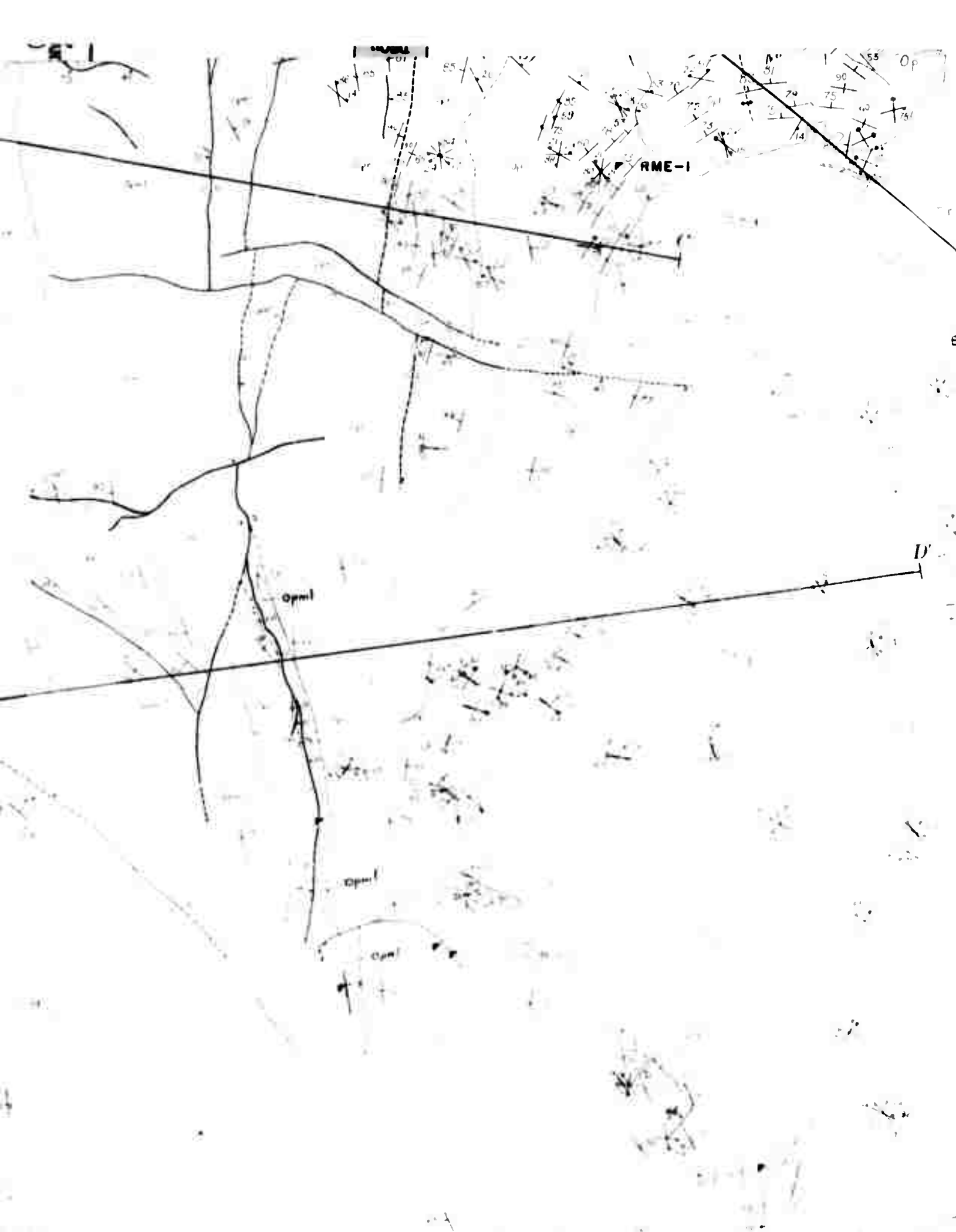
RME-1
D'
opml
opml
opml

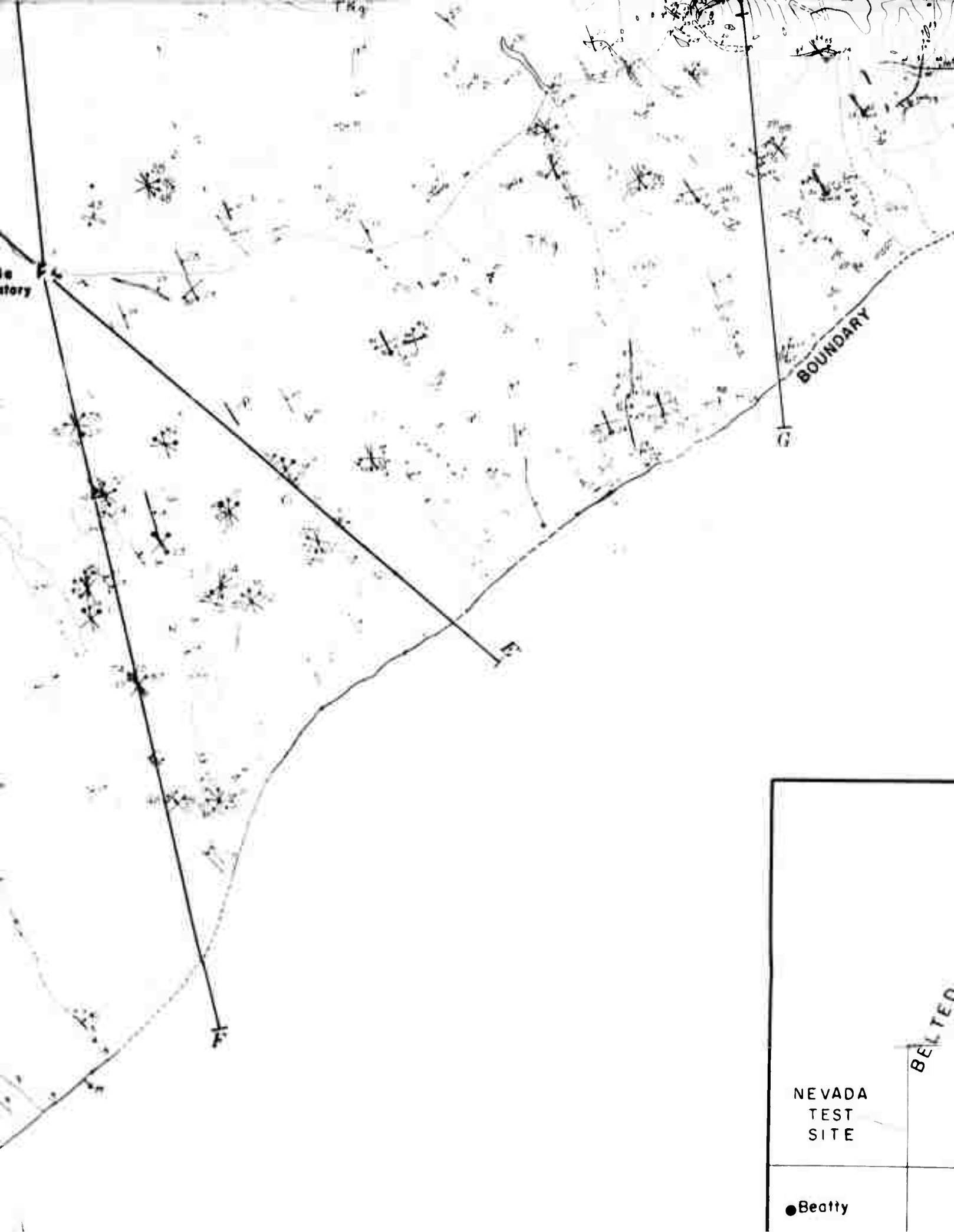
BOUNDARY
G
NEVADA
TEST
SITE
Beatty

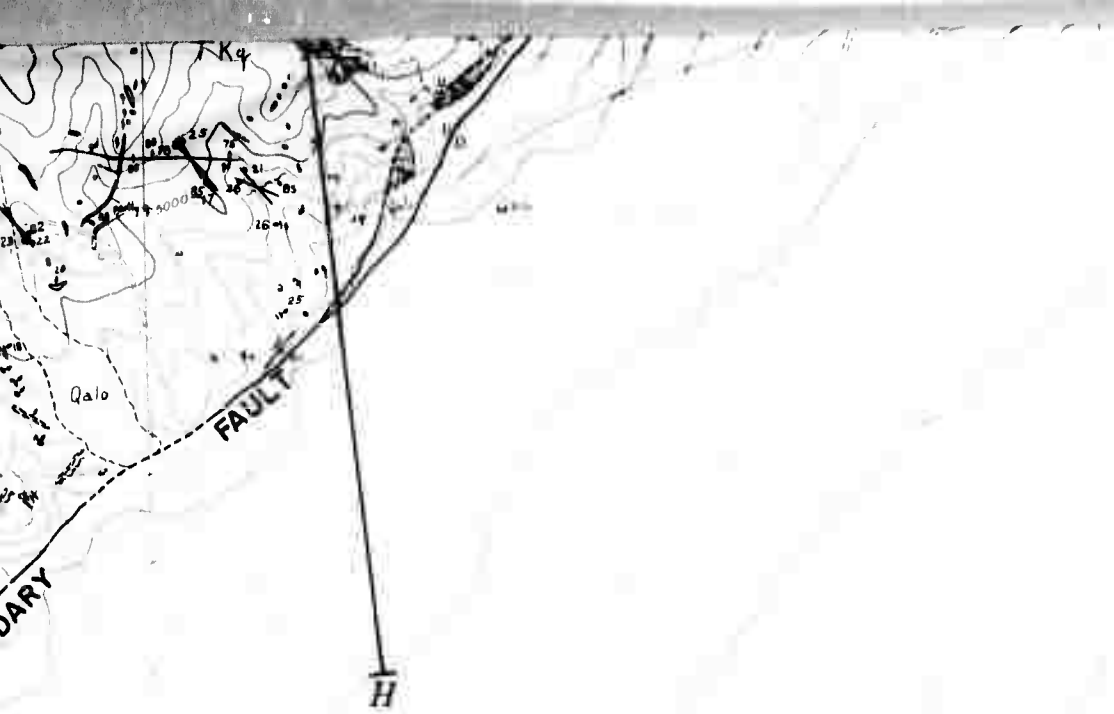

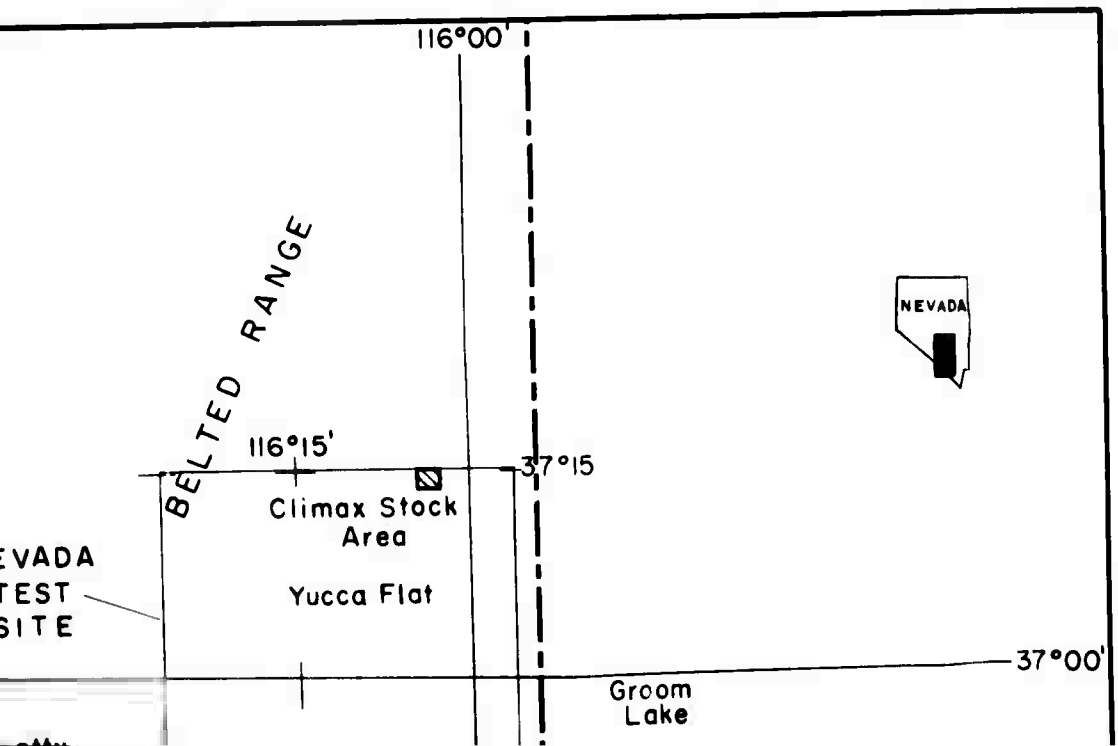

Ordovi

Dolomite and limy
to coarsely cry

Quartzite, whit
abundant loca
vitreous, bri
apparent

Dolomite to dolo
bluish-gray, f
to thick-bedde
cated). Partl
places. Origi
cated by poor
mainly by colo
The map units
noted:

Op, undifferenti

Opmu, limy dolom
bluish-gray to
thin- to very

Opp, dolomitic l
gray to dark-g
line, well-lam
marble) to ver
interbedded wi
very light gra
thin to very t

Opml, dolomite t
gray, some lig
indistinctly f
which is moder
absent in lowe
part.

Opn, dolomite an
abundant nodul

Opl, dolomite, w
moderately fol
interlayers up
nodules

Quartzite, lig
medium-grain
of dark- to

Devonian(?), Silurian, and
Ordovician rocks, undifferentiated

lomite and limy dolomite, light- to medium-gray, finely to coarsely crystalline; in part marble

ORDOVICIAN, SILURIAN, DEVONIAN(?)

Oe

Eureka quartzite

uartzite, white to very light gray, yellow iron stain abundant locally, fine- to medium-grained, well-sorted, vitreous, brittle, very hard, stratification is not apparent

Pogonip group

lomite to dolomitic limestone, very light gray to bluish-gray, finely to coarsely crystalline, laminated to thick-bedded, common chert nodules (mostly silicated). Partly to wholly converted to marble in most places. Original stratification is absent or is indicated by poor to moderately good foliation defined mainly by color bands but partly by crystallinity. The map units differ from the general description as noted:

, undifferentiated.

mu, limy dolomite to limestone, medium light bluish-gray to medium dark-gray, finely crystalline, thin- to very thick bedded.

p, dolomitic limestone, white and very light bluish gray to dark-gray, aphanitic to very finely crystalline, well-laminated (foliated where converted to marble) to very thin bedded, silty (Oppl and Oppu): interbedded with dolomitic limestone and dolomite, very light gray, finely to coarsely crystalline, thin to very thick bedded (Oppm).

l, dolomite to dolomitic limestone, gray to blue-gray, some light-gray, massive, nonfoliated to indistinctly foliated, except locally in upper part which is moderately foliated; nodules very rare to absent in lower part but common in places in upper part.

, dolomite and limy dolomite, white to bluish-gray, abundant nodules, moderately to well-foliated.

, dolomite, white to medium-gray, poorly to moderately foliated; contains some nonpersistent interlayers up to 75 feet thick with numerous nodules

ORDOVICIAN

CAMBRIAN

Cs

Stirling(?) quartzite

uartzite, light to medium pinkish-gray and dark-gray, medium-grained, poorly bedded with rare thin beds of dark- to medium-gray phyllite

Strike

Strike

Hori

Strike and di

Strike

Strike o

Horiz

Strike and dip of fl

Strike and

Strike and

RME

Dri

RME - Reynolds Electrical
ration hole; MME - Miner
exploration hole

Pro

Mi

ORDOVICIAN, SILURIAN, DEVONIAN(?)

ORDOVICIAN

CAMBRIAN

75

Strike and dip of beds

90

Strike of vertical beds

Horizontal beds

65

Strike and dip of overturned beds

56

Strike and dip of joint

Strike of vertical joint

Horizontal joint

7

Strike and dip of flow layers (Tosw unit only)

80

Strike and dip of cleavage

85

Strike and dip of shear zone

RME-2 MME-2

Drill hole

RME - Reynolds Electrical & Engineering Co. marble exploration hole; MME - Minerals Engineering Co. marble exploration hole

Adit

Prospect pit

Mine dump

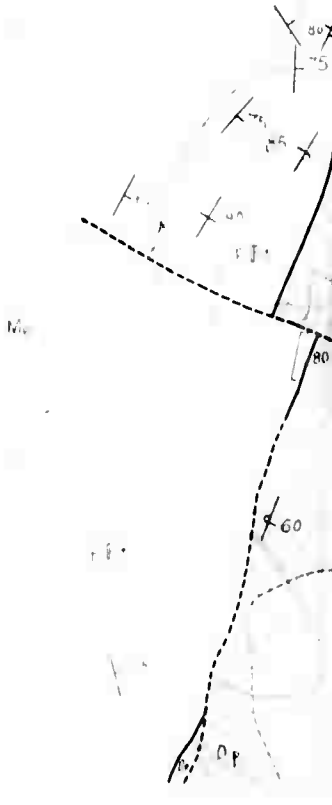

Topography by American Aerial Surveys Inc Covina California by stereophotogrammetric (Kelsh) methods from photographs taken in September 1959

Nevada State Coordinate grid interval 1000 feet

MISCELLANEOUS GEOLOGIC INVESTIGATIONS
MAP I-328 SHEET 1 OF 2

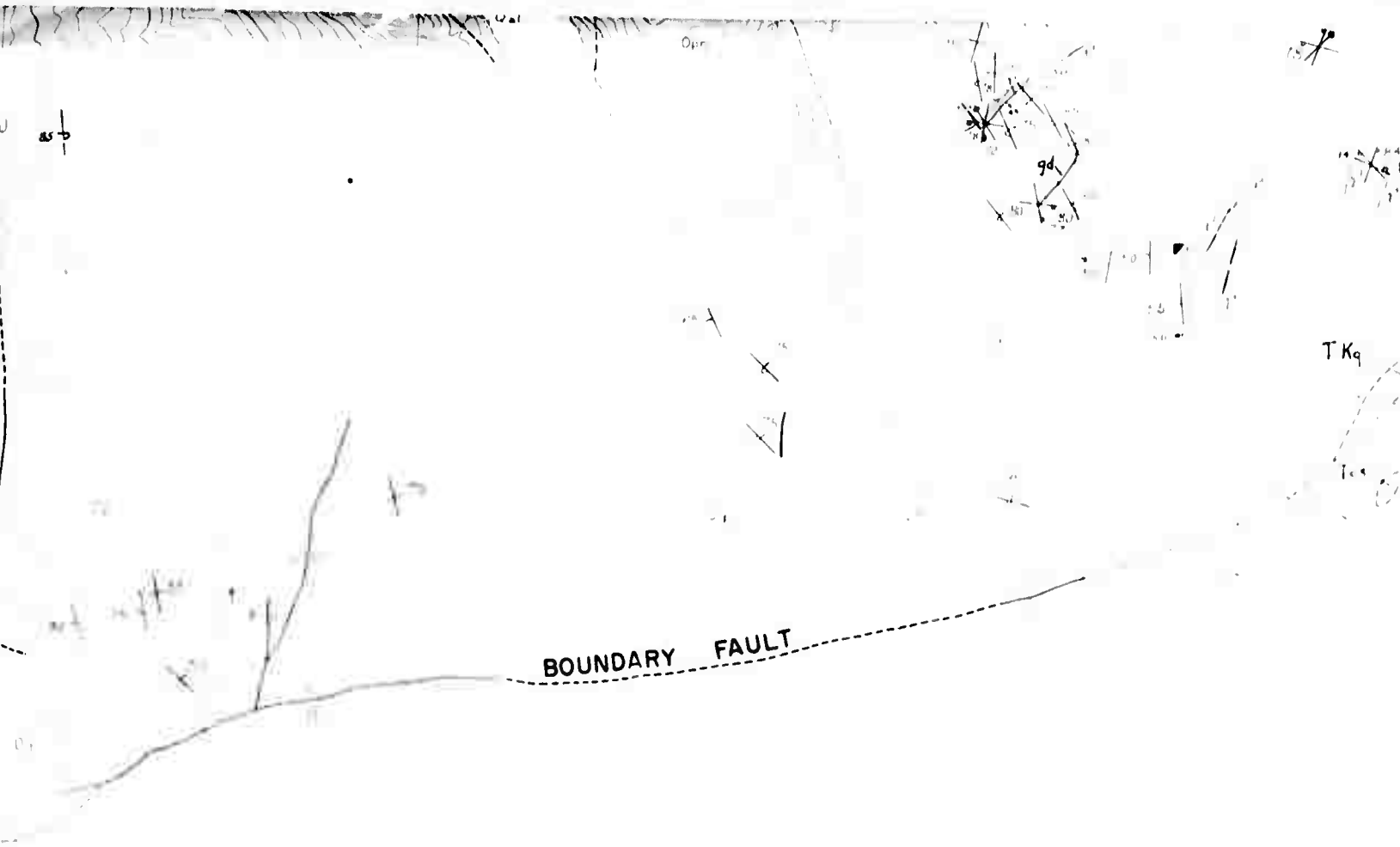

PRELIMINARY GEOLOGIC MAP OF THE CLIMAX STOCK

By

F. N. Houser and F. G. Po

400 0 400

1960

F

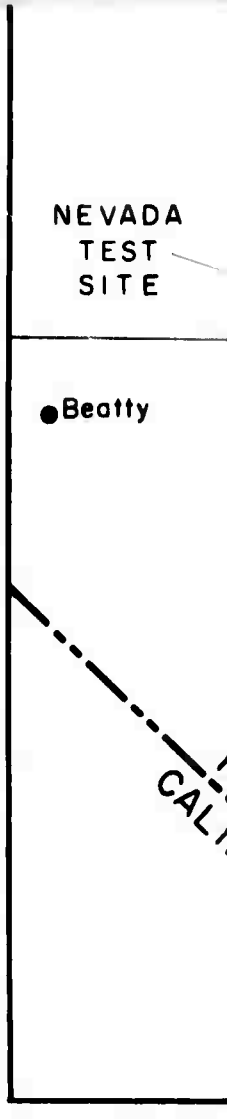

INDEX MAP

AND VICINITY, NYE COUNTY, NEVADA

le

120 FEET

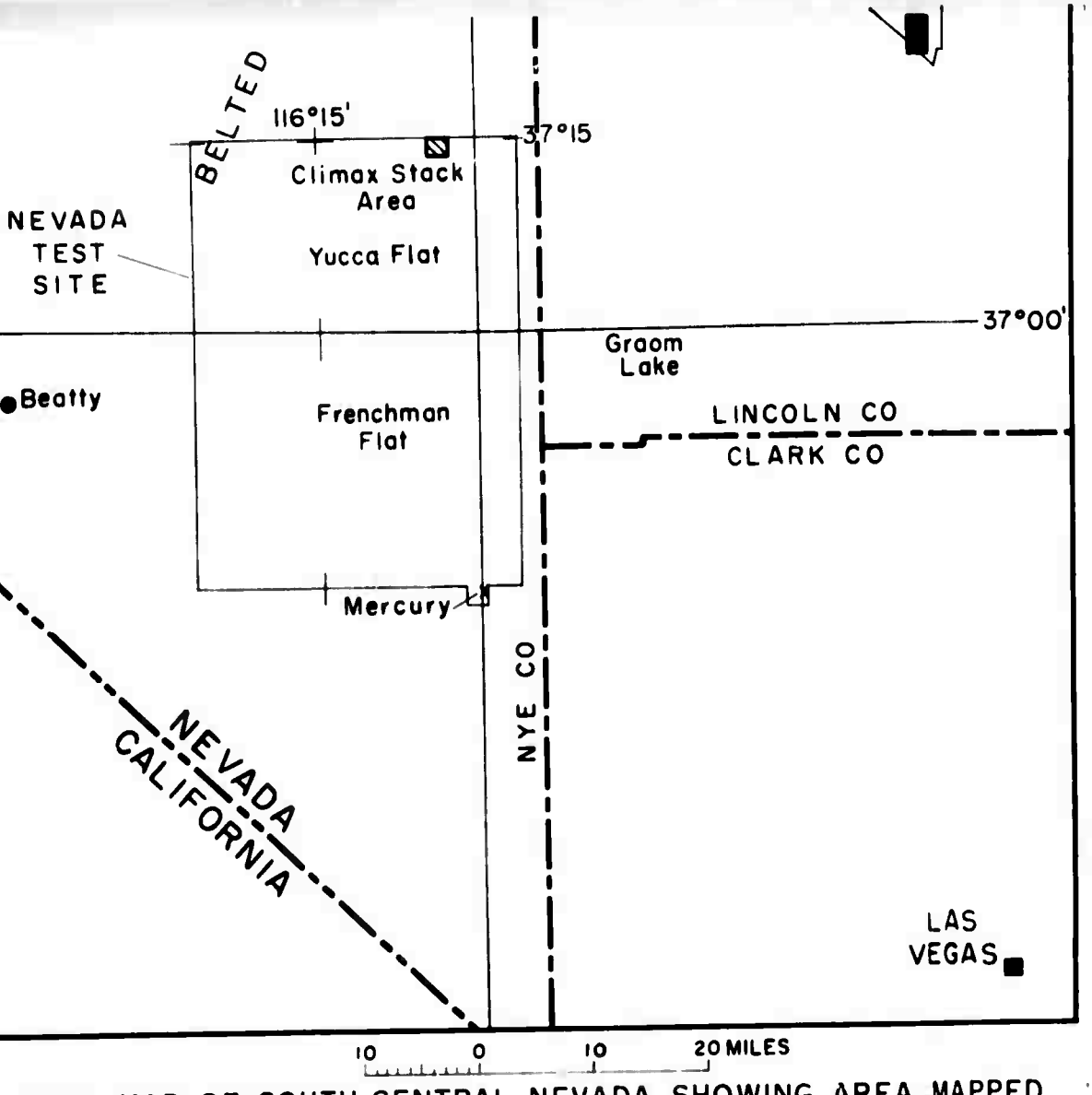

INDEX MAP OF SOUTH-CENTRAL NEVADA SHOWING AREA MAPPED

STERLING GEOLOGICAL SURVEY WASHINGTON D C 20242

Geology mapped in 1959 and 1960

For sale by U. S. Geological Survey, price 1.50 per set

Opl, dolomite,
moderately f
interlayers
nodules

Quartzite, l
medium-gra
of dark- t

In order to fa
this map, some
refinements ha

Opl, dolomite, white to medium-gray, poorly to moderately foliated; contains some nonpersistent interlayers up to 75 feet thick with numerous nodules

Cs

Stirling(?) quartzite

Quartzite, light to medium pinkish-gray and dark-gray, medium-grained, poorly bedded with rare thin beds of dark- to medium-gray phyllite

CAMBRIAN

In order to facilitate early publication of this map, some of the normal cartographic refinements have been omitted

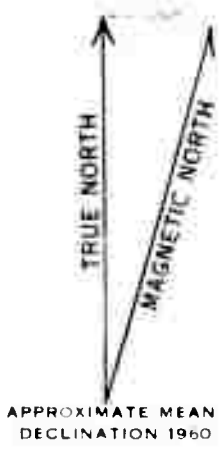

CAMBRIAN

ray,
s

× Prospect pit

Mine dump

MATE MEAN
ATION 1960